NAVAL POSTGRADUATE SCHOOL
Monterey, California

DISSERTATION

A COMPUTATIONALLY EFFICIENT ALGORITHM FOR DISTURBANCE CANCELLATION TO MEET THE REQUIREMENTS FOR OPTICAL PAYLOADS IN SATELLITES

by

Christian Giorgio Roberto Taranti

September 2001

Dissertation Supervisor:	Roberto Cristi
Dissertation Co-Supervisor:	Brij N. Agrawal

Report Documentation Page

Report Date	Report Type	Dates Covered (from... to)
30 Sep 2001	N/A	-

Title and Subtitle A COMPUTATIONALLY EFFICIENT ALGORITHM FOR DISTURBANCE CANCELLATION TO MEET THE REQUIREMENTS FOR OPTICAL PAYLOADS IN SATELLITES	**Contract Number**
	Grant Number
	Program Element Number
Author(s) Taranti, Christian Giorgio Roberto	**Project Number**
	Task Number
	Work Unit Number
Performing Organization Name(s) and Address(es) Research Office Naval Postgraduate School Monterey, Ca 93943-5138	**Performing Organization Report Number**
Sponsoring/Monitoring Agency Name(s) and Address(es)	**Sponsor/Monitor's Acronym(s)**
	Sponsor/Monitor's Report Number(s)
Distribution/Availability Statement Approved for public release, distribution unlimited	
Supplementary Notes	
Abstract	
Subject Terms	
Report Classification unclassified	**Classification of this page** unclassified
Classification of Abstract unclassified	**Limitation of Abstract** UU
Number of Pages 151	

REPORT DOCUMENTATION PAGE

Form Approved OMB No. 0704-0188

1. AGENCY USE ONLY (*Leave blank*)	2. REPORT DATE	3. REPORT TYPE AND DATES COVERED
	September 2001	Doctor's Dissertation

4. TITLE AND SUBTITLE
A COMPUTATIONALLY EFFICIENT ALGORITHM FOR DISTURBANCE CANCELLATION TO MEET THE REQUIREMENTS FOR OPTICAL PAYLOADS IN SATELLITES

5. FUNDING NUMBERS

6. AUTHORS Taranti, Christian Giorgio Roberto

7. PERFORMING ORGANIZATION NAME(S) AND ADDRESS(ES)
Naval Postgraduate School
Monterey CA 93943-5000

8. PERFORMING ORGANIZATION REPORT NUMBER

9. SPONSORING/MONITORING AGENCY NAME(S) AND ADDRESS(ES)

10. SPONSORING/MONITORING AGENCY REPORT NUMBER

11. SUPPLEMENTARY NOTES The views expressed in this thesis are those of the author and do not reflect the official policy or position of the Department of Defense or the U.S. Government.

12a. DISTRIBUTION/AVAILABILITY STATEMENT
Approved for public release; distribution is unlimited.

12b. DISTRIBUTION CODE

13. ABSTRACT(*maximum 200 words*)

Vibration control is a very important issue in satellites. The new high-resolution digital imaging devices are especially sensitive to vibrations. Antennas used in laser communications also require a very quiet environment so that their performance is not degraded. The Stewart platform is capable of isolating an optical payload from the noisy spacecraft bus. Until recently, only passive methods were used in all vibration isolation applications. Recent advances in Digital Signal Processing techniques made the development of vibration control algorithms possible, but these usually require large computational power. This work explores using a computationally efficient vibration-isolation method for optical payloads by using hexapods. The method suppresses the vibration at the assigned frequencies and does not affect unassigned frequencies if the plant is linear. The mathematical analysis includes convergence analysis and the effect of unassigned frequencies in the output. The computational requirements of the algorithm is evaluated and is compared to the Multiple-Error Least Mean Square. The method is very robust to nonlinearities; its performance is comparable to the Multiple-Error Least Mean Square with a fraction of the computational time and memory requirements. Also it requires very little plant knowledge. Theoretical results are verified through simulations using a Single-Input/Single-Output plant and a nonlinear hexapod model. The controller was also experimentally validated in two different hexapods and the performance was found to be similar to or better than the performance obtained with the Multiple-Error Least Mean Square method when a noisy reference signal is used.

14. SUBJECT TERMS
vibration, vibration suppression, vibration control, hexapod, Stewart

15. NUMBER OF PAGES

16. PRICE CODE

17. SECURITY CLASSIFICATION OF REPORT	18. SECURITY CLASSIFICATION OF THIS PAGE	19. SECURITY CLASSIFICATION OF ABSTRACT	20. LIMITATION OF ABSTRACT
Unclassified	Unclassified	Unclassified	UL

NSN 7540-01-280-5500

Standard Form 298 (Rev. 2-89)
Prescribed by ANSI Std. 239-18 298-102

Approved for public release; distribution is unlimited.

A COMPUTATIONALLY EFFICIENT ALGORITHM FOR DISTURBANCE CANCELLATION TO MEET THE REQUIREMENTS FOR OPTICAL PAYLOADS IN SATELLITES

Christian Giorgio Roberto Taranti
1st Lieutenant of the Brazilian Air Force
B.S., Technological Institute of Aeronautics (ITA, Brazil), 1994

Submitted in partial fullfilment of the
requirements for the degree of

DOCTOR OF PHILOSOPHY IN ELECTRICAL ENGINEERING

from the

NAVAL POSTGRADUATE SCHOOL
September 2001

Author: Christian Taranti.
Christian Giorgio Roberto Taranti

Approved by: Roberto Cristi.
Roberto Cristi
Associate Professor of Electrical Engineering
Dissertation Supervisor and Committee Chair

B.N. Agrawal.
Brij N. Agrawal
Professor of Aeronautics & Astronautics
Dissertation Co-Supervisor

Monique P. Fargues
Associate Professor of Electrical Engineering

Man-Tak Shing
Associate Professor of Computer Science

Xiaoping Yun
Professor of Electrical Engineering

Approved by:
Jeffrey B. Knorr, Chair of the Department of Electrical and Computer Engineering

Approved by: Carson K. Eoyang
Carson K. Eoyang, Associate Provost for Academic Affairs

ABSTRACT

Vibration control is a very important issue in satellites. The new high-resolution digital imaging devices are especially sensitive to vibrations. Antennas used in laser communications also require a very quiet environment so that their performance is not degraded. The Stewart platform is capable of isolating an optical payload from the noisy spacecraft bus. Until recently, only passive methods were used in all vibration isolation applications. Recent advances in Digital Signal Processing techniques made the development of vibration control algorithms possible, but these usually require large computational power. This work explores using a computationally efficient vibration-isolation method for optical payloads by using hexapods. The method suppresses the vibration at the assigned frequencies and does not affect unassigned frequencies if the plant is linear. The mathematical analysis includes convergence analysis and the effect of unassigned frequencies in the output. The computational requirements of the algorithm is evaluated and is compared to the Multiple-Error Least Mean Square. The method is very robust to nonlinearities; its performance is comparable to the Multiple-Error Least Mean Square with a fraction of the computational time and memory requirements. Also it requires very little plant knowledge. Theoretical results are verified through simulations using a Single-Input/Single-Output plant and a nonlinear hexapod model. The controller was also experimentally validated in two different hexapods and the performance was found to be similar to or better than the performance obtained with the Multiple-Error Least Mean Square method when a noisy reference signal is used.

TABLE OF CONTENTS

LIST OF FIGURES

LIST OF TABLES

LIST OF ABBREVIATIONS, ACRONYMS, AND SYMBOLS

Abbreviation, Symbol or Acronym	Meaning
NPS	Naval Postgraduate School
PPH	Precision Pointing Hexapod
SRDC	Satellite Research and Design Center
UQP	Ultra-Quiet Platform
LMS	Least Mean Square
ME-LMS	Multiple-Error LMS
SISO	Single-Input/Single Output
MIMO	Multiple-Input/Multiple-Output
SIMO	Single-Input/Multiple-Output
DSP	Digital Signal Processing/ Digital Signal Processor
PSD	Position Sensing Device
CMG	Control Moment Gyro
TMD	Tunned Mass Device
LQG	Linear-Quadratic Gaussian
ADC	Adaptive Disturbance Canceller
DOF	Degree-of-Freedom
PZT	Piezoelectric Stack Actuator
RAM	Random Access Memory
PC	Personal Computer, IBM or Compatible
FIR	Finite Impulse Response

DFT	Discrete Fourier Transform
SNR	Signal to Noise Ratio
CPU	Central Processing Unit
A/D	Analog to Digital Converter
D/A	Digital to Analog Converter
I/O	Input/Output

ACKNOWLEDGMENTS

I would like to thank my advisor, Prof. Roberto Cristi, for all his help and patience, and for directing the path of this research while allowing me the freedom to employ my own personal approaches. He stood at my side at the darkest moments showing me possible options and solutions. Professor Brij Agrawal also greatly influenced my work. His insightful advice and example were important not only for completing this research but also for influencing my entire life.

Initiating my research would have been much harder if it had not been for professors Monique Fargues, Man-Tak Shing and Xiaoping Yun who were on my committee. I have had the pleasure of being in their classes and each has had a profound impact on me as a student and as a researcher. Dr. Breno Castro, a dear friend stood by me whenever I reached a dead-end. The countless chats with him gave me insight into various phases of this research. Dr. Jong-Jen Chen was also crucial to this research. Questioning each step in every phase of this work, he helped me to make sure that each step was based on a solid foundation. I also appreciate Ron Russell's assistance in editing this dissertation and polishing my English.

The folks at the Satellite Research and Design Center were also instrumental. The interaction among the students is intense and beneficial to all. These students, from a wide range of backgrounds and curriculums, support one another and exchange knowledge freely, which vastly improves the quality of the research they generate. It was an honor to be among them.

Of course, I cannot thank my wife, Ursula, enough. First, I thank her for helping me keep my promise to never say, "Sorry, we can't go out because I have a test tomorrow." Secondly, I must thank her for all the times she altered her schedule to help me, and for the time she spent helping me revise my dissertation. Beyond this, she was most of the time understanding and created

an environment in which I could be productive and achieve my goals, although she still deserve the nickname I have given her, ”Cactus Flower.” Finally, I wish to thank my family and friends for all the help, which eventually led to my being here in the United States studying at the Naval Postgraduate School.

I. INTRODUCTION

A. THE VIBRATION ISOLATION PROBLEM

Although the vibration control problem has been studied for a long time, it received increasing attention after the advent of submarines. The main purpose of a submarine is to travel unnoticed and the noise generated by its several subsystems can defeat its purpose, making its localization and identification easier. As a result, the study of noise and vibration received much attention, especially during the Cold War when several techniques for noise and vibration isolation were developed.

During the sixties, space started being considered as a very strategic area and imaging was among the many applications that found their way to the military spacecraft. During the first decades of space imaging, vibration was not as important as it is today because of the limitations of the imaging sensors available at that time. Nowadays satellites are larger and have much more rotating machinery than in recent past. Among the vibration-generating devices present in the recent satellites are large appendages, which snap when entering or emerging from an eclipse, solar panels that rotate to track the sun, cryocoolers, pumps, reaction wheels, control momentum gyros (CMG), reaction jets and magnetic torquers. The vibrations produced by these elements, if transmitted to the imaging device, can degrade its performance appreciably. Figure 1.1 shows an example of such degradation.

At the same time, the electronic industry has made astonishing advances in imaging devices. Resolution is now much higher than it was a few years ago, and new optical techniques produce lenses and mirrors with less distortion, generating sharper images. Even when distortions are present, the images can be post-processed on the ground, using the latest advances in image-

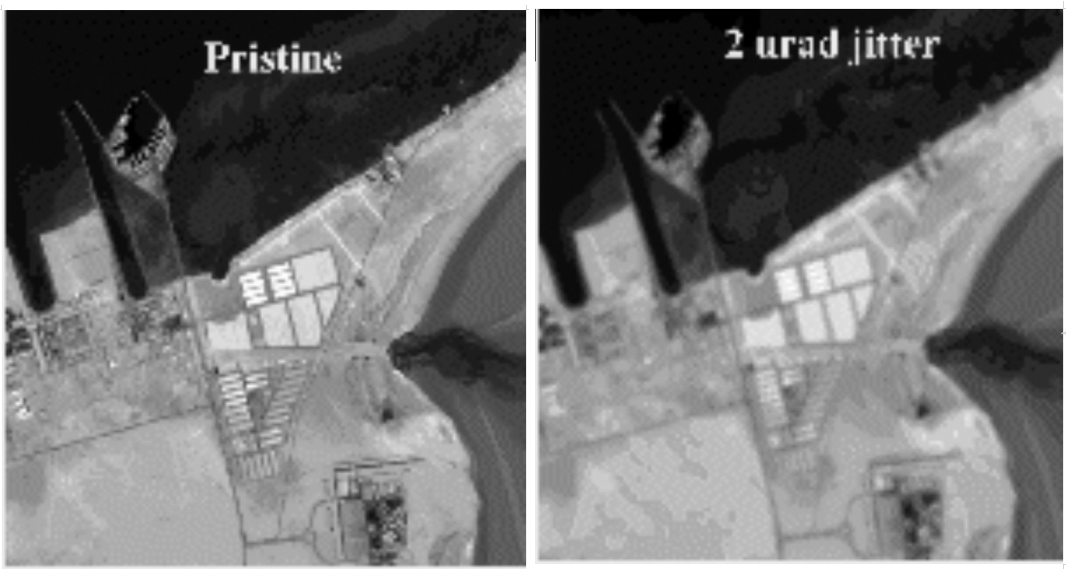

(a) Jitter free (b) Jitter present ($2\mu rad$)

Figure 1.1. Jitter Effect on an Imaging Device (From [1]).

processing techniques to enhance them. One famous example is the spherical aberration on the Hubble telescope's original primary mirror. Using image processing techniques, the telescope could still be used while the mirror was being upgraded[6].

The most common cause for vibration-induced image degradation is due to vibrations produced elsewhere and transmitted through the satellite bus to the imaging device. Isolating the noisy environment, dampening the structure or isolating the instrument itself by using an isolating mount (see Figure 1.2) can reduce this type of vibration. The vibration can also be produced on the quiet side when moving parts, such as cryocoolers, must be mounted as closely as possible to the sensor.

Passive methods are used in most vibration-control and vibration-isolation implementations for several reasons: they are robust; they do not consume electrical power; they are very reliable and the technology is mature. Passive approaches can be applied to mounts that prevent the vibra-

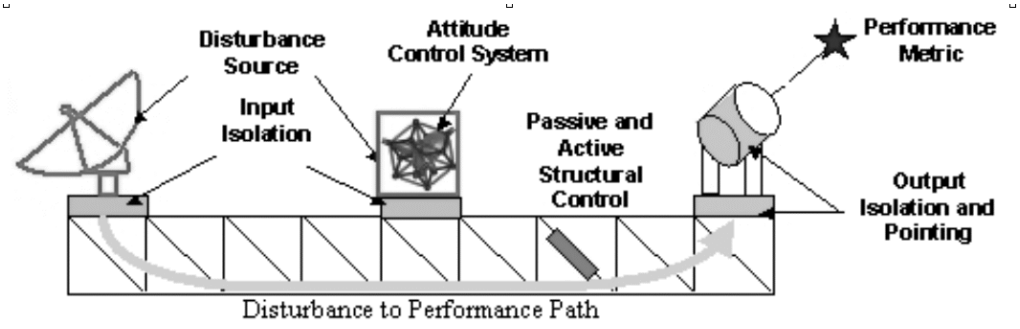

Figure 1.2. The Vibration Isolation Problem (From [1]).

tions to propagate to or from the spacecraft bus or to increase the dampening of a larger structure. Unfortunately, passive approaches do not solve all vibration problems.

When a vibration isolation mount is used, the vibration has two main paths to migrate from the noisy to the quiet side: the vibration isolation medium and the umbilical. Even though it is possible to design very soft passive mounts to preventing the vibration to propagate through the mount, prevent the vibration from propagating through the umbilical is impossible. In the same way, passive isolation approaches are incapable of suppressing the vibration generated on the quiet side. This is especially important for infrared imaging for which the sensor must be cooled and a cryocooler must be placed as closely as possible to the sensor in order to increase its performance. Passive solutions can only perform vibration cancellation in certain cases.

Disturbance isolation, also called “vibration suppression,” is the suppression of periodic disturbances. These disturbances are usually generated by rotating machinery and appear as lines in the frequency spectrum. These lines have a power content much higher than the background vibration noise. If the frequency is known and fixed, TMDs (tuned-mass devices) can be used, but their placement on the structure is critical. Thus TMDs are not usually suited for isolation mounts. Active methods can deal with frequencies not known *a priory* or with frequencies fluctuating, and the placement of the actuators is not as critical as when using passive methods.

B. ACTIVE VIBRATION SUPPRESSION

Since meeting the requirements using passive-only solutions is becoming increasingly difficult, active solutions have been pursued. Current research indicates that the most viable solution is the use of a generic local vibration isolator that combines both passive and active isolation. Among the several approaches tested, the most promising is the Stewart Platform [7], which can generate force and torque in any direction. It also exhibits good stiffness properties [2] with actuators much smaller than those needed with serial manipulators. The need for localized vibration isolation prompted the development of the Vibration Isolation and Suppression System (VISS) [8, 9, 3] and the Satellite Ultraquiet Isolation Technology Experiment (SUITE) [10].

A hexapod has complex dynamics and a detailed model can be quite complicated. Even if a perfect model is developed, space missions usually do not allow the opportunity for scheduled maintenance in order to repair aging or failed systems and thus system identification may be needed. For this reason, all vibration control work found in the reviewed literature uses some sort of adaptive method. This approach makes it possible to compensate for model imperfections and aging.

Since the hexapods are multiple-input/multiple-output (MIMO) systems strongly coupled [11], expecting that the best performance can be obtained by using MIMO controllers is reasonable. Some methods are available for MIMO plants, such as Multiple-Error LMS[12], Clear Box [13, 4] and Repetitive Control [14, 15]. Unfortunately, the computational resources available in satellites, limit the use of these methods for vibration isolation of optical payloads.

One important characteristic common to all hexapods used for vibration isolation as described in the literature is the use of smart struts. All of them have six identical struts with an actuator and a vibration sensor embedded (geophone or accelerometer), meaning that using one

independent single-input/single-output (SISO) controller for each strut is possible. This approach, while simple, has limitations for a system as strongly coupled as a hexapod, and mixed results have been achieved [11, 16].

Eliminating the requirement of having a MIMO controller does allow more choices since several vibration-suppression algorithms were never extended to the MIMO case. In 2000, Kuo and Morgan [17] presented an interesting review of some of the vibration isolation algorithms available and, then classified them into “reference-based” and “synthetic reference.” The first group uses a reference signal correlated with the disturbance while the second one uses some other information to generate an internal reference signal. The “synthetic reference” group contains is one set of controllers called “notch filters.”

Notch filters have several properties that are very attractive for vibration isolation in satellites. First, no external signal is used as a reference. Since extra information about the frequency is given or generated on-the-fly, the frequency information can be used to generate a synthetic reference. This eliminates the requirement of having an additional sensor, at the expense of requiring additional information to generate the reference signal. Another characteristic of this class of controllers is that excellent results can be achieved for suppressing vibrations generated by rotating machinery, also called tonal disturbances.

Among the controllers found in the reviewed literature, the one used in 1998 by Bertran and Montoro in [18] (based on the work presented by Kuo and Min in 1995 [19]) required the least amount of computational effort is

This controller is quite simple and does not use the model of the plant explicitly. Although this controller is very simple, the reviewed literature did not mention this controller being applied to MIMO systems, especially on hexapods. In addition, no extension of Montoro and Bertran’s work for MIMO plants was found. More important, no stability analysis was found in the literature that

considers a generic plant. However, such analysis is essential to meet the high-reliability requirements of space applications. Another drawback is that the method requires the knowledge of the frequency to be suppressed. Other frequencies could be present on the error signal and some interference can occur. This possibility must be addressed if this controller is to be implemented in an actual space system. However, this problem has not yet been addressed in the literature reviewed.

Although much effort has been spent on developing vibration control and isolation methods, our examination of the literature revealed that no one has evaluated the computational effort that each method requires. Consequently, a cost analysis must be developed and the vibration-isolation method selected must be compared to the Multiple-Error LMS implementation.

Finally, most modeling work done on hexapods was from a robotics perspective, using direct and inverse kinematics. Li and Salcudean presented a model for a hexapod, but assumed that the dynamics of the actuators are negligible [20]. Lebret, Liu and Lewis derived a very complete model for a hexapod starting from the energy approach, but unfortunately the geometry assumed in their work does not apply to the hexapods available at the *Satellite Research and Design Center*: each pair of actuators was connected to the top plate through a single joint. In 1991, Fujimoto, Kinoshita et al. derived a model from the robotics perspective [21], but assumed that "the joint does not move in high speed," preventing its application from being used for vibration-isolation purposes. A complete model of the hexapod suitable for simulations is needed in order to study the effects of the multiple-input/multiple-output (MIMO) nature of the hexapod without the interference of actual hardware imperfections.

C. PROBLEM STATEMENT

The goal of this research is to study a computationally efficient algorithm that meets the vibration-isolation requirements of optical payloads using hexapods. The method needs to be tolerant to nonlinearities, must require significantly less computational resources than the Multiple-Error LMS implementation, and the method must perform comparably to the Multiple-Error LMS method. Additionally, the method must be able to deal with multiple frequencies.

A stability analysis and a study of the effect of uncontrolled frequencies must be performed. The results must be validated on simulations and experimentally.

Finally, the computational cost of both the proposed method and the Multiple-Error LMS approach must be derived and must be compared in order to verify if the proposed method achieves the desired goal of significantly reducing the computational cost over the reference method (Multiple-Error LMS).

D. OVERVIEW

Chapter I presents the vibration-isolation problem, reviews the literature and states the research objectives.

Chapter II describes the two different hexapods used to perform the experiments.

Chapter III provides a detailed state-space model of the Precision Pointing Hexapod. This model allows the designer to derive some important properties of the plant and is used to implement a detailed simulation program.

Chapter IV presents the Adaptive Disturbance Canceller method, derives the stability criterion, and studies the method's performance when multiple frequencies are present. Simulations

are used to validate the mathematical results using both a SISO plant and the model developed in Chapter III.

Chapter V derives and compares the computational requirements for both the Adaptive Disturbance Canceller and the Multiple-Error LMS approach, as well as derives and compares the corresponding memory requirements.

Chapter VI validates the results experimentally by using the two hexapods available at the *Satellite Research and Design Center*, at the Naval Postgraduate School. A comparison between the Adaptive Disturbance Canceller and Multiple-Error LMS is also presented.

Finally, Chapter VII presents a summary of the work and conclusions and some suggestions to overcome the main weaknesses of the Adaptive Disturbance Canceller.

II. HARDWARE DESCRIPTION

A. OVERVIEW

The Stewart platform, also known as a “parallel manipulator,” was introduced by Stewart in 1965[7] and is composed of two plates connected by some (passive or active) links. One of the plates is considered to be the reference (base) and the other (top) is the one for which the attitude and position are to be controlled. A diagram of such a platform is shown in Figure 2.1. The platform can be controlled by changing the length of the links. It can be shown that in order to get six degrees of freedom, one needs at least six actuated struts. One can also verify that more than six actuators will not increase the number of the DOF of the manipulator (differently from the serial-linked case). The hexapods have several interesting characteristics, namely, high stiffness and reduced size and weight when compared to serial-link manipulators. A comprehensive study of hexapods and their characteristics can be found in [2, 22, 23, 24, 25, 26].

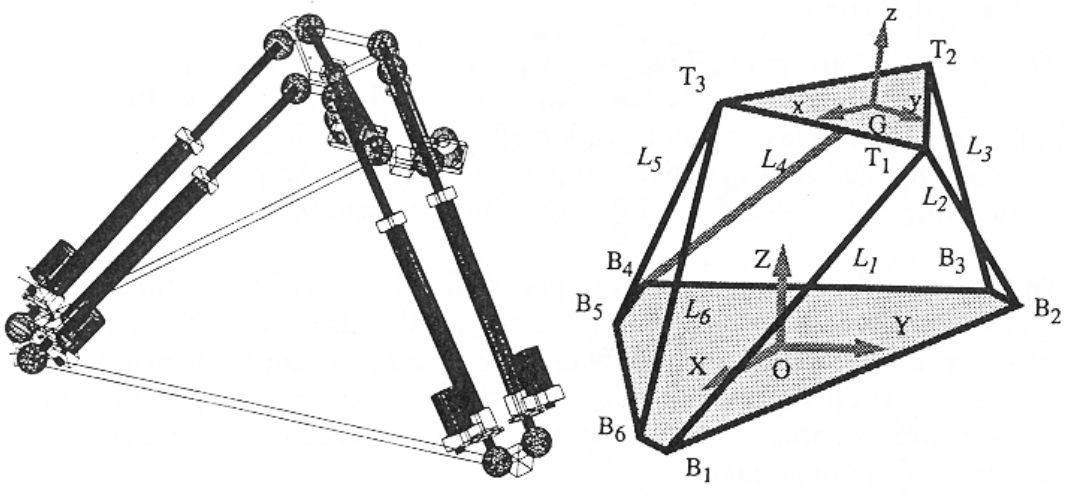

Figure 2.1. Hexapod View in 3D (From[2]).

Section B describes the first hexapod available at the *Satellite Research and Design Center*, the Ultra-Quiet Platform. This hexapod is equipped with high bandwidth piezoelectric and sensitive geophone sensors on each strut.

Section C details the Precision Pointing Hexapod, which has long stroke actuators and is capable of pointing and can simultaneously isolate vibration. Since this hexapod is modeled in Chapter III, it is described in more detail.

B. ULTRA-QUIET PLATFORM

This Ultra-Quiet Platform, shown in Figure 2.2, was conceived for vibration-isolation purposes. It follows a cubic configuration (see Figure 2.3) in order to minimize the cross-coupling among the struts [27]. The hexapod rests on a satellite bus mockup (Figure 2.4) where the disturbance source is mounted. The whole structure is mounted, with rubber vibration suppressors, on a Newport RS4000 floating table in order to provide isolation from the ambient vibration noise.

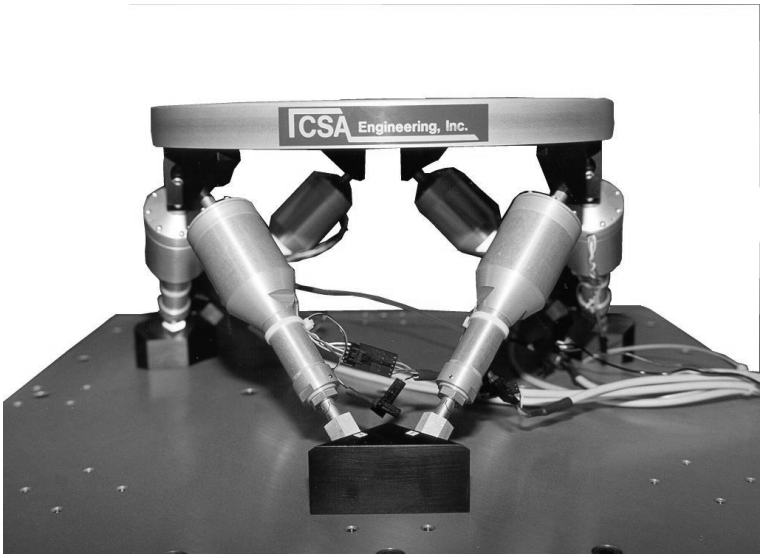

Figure 2.2. Ultra-Quiet Platform.

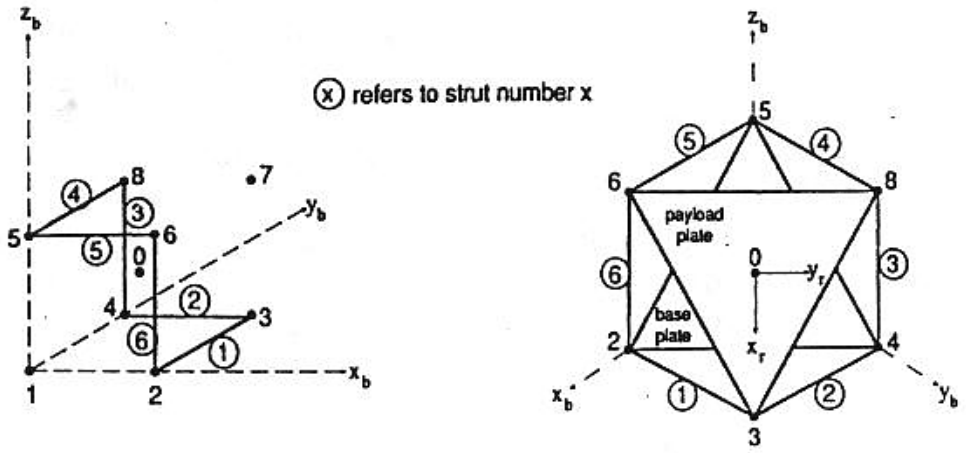

Figure 2.3. Cubic Configuration (From [3]).

The Ultra-Quiet Platform struts are equipped with piezoceramic stack actuators (PZT). These actuators have a very large bandwidth (resonance peak around $1.2KHz$) and a displacement of $\pm 50\mu m$, which is adequate for vibration control. The power to the actuators is provided by a *PCB Piezotronics* 790A06 amplifier ($\pm 200V$ at $\pm 100mA$). Each smart strut is also equipped with a *Geospace* GS-11D geophone, which measures linear velocity. These sensors have a natural frequency of $14Hz$ with a damping ratio of 0.8. The signal conditioning is provided by the *CSA Engineering Active Vibration Control System* (AVCS). The fixtures have passive isolation built-in, which provides damping in series with the actuators.

The disturbance source produces acceleration parallel to the z-axis, as defined in Figure 2.1. It uses an *Aura Bass Shaker* (AST-1B-4, $25W$), and it is mounted on top of the mockup, below the bottom plate of the hexapod. The shaker signal is produced by a DSP board and is amplified by a DC power amplifier (*Kepco BOP* 20-10M).

The implementation of the algorithm is made on a *dSpace Alpha Combo*. This system comprises a *DS1103* and an *Alpha Board*. The *Alpha Board* is powered by a *DEC Alpha* $500MHz$ processor with $2MB$ of RAM. The *DS1003* board acts as a slave I/O board and contains a *Texas*

Instruments TM320C40 processor running at $50MHz$ and $512Kb$ of memory. The setup is shown in Figure 2.4. The controller runs on the *Alpha Board*, while all the I/O functions are executed on the *DS1003* board.

All the I/O are performed at $10^4\, samples/s$ while the controller and disturbance generator run at $10^3\, samples/s$. Since there is not appreciable power contents on the measurements above $2KHz$, anti-aliasing filters were implemented by oversampling the measurements ($10KHz$), passing them through a Chebychev (type I, corner at $200Hz$, 3^{rd} order) and finally down-sampling the output of the filters to $10^3\, samples/s$.

The outputs of the controller are up-sampled to $10^4\, samples/s$ and then low-pass filtered by a type I Chebychev filter in order to smooth the output sent to the actuators. The disturbance signal received the same treatment. Filtering, A/D sampling, D/A conversions and communication between the controller and the host PC occur in the DS1003 board.

The code is implemented, compiled and downloaded to both boards through the dSpace/Matlab Real-Time Workshop environment. The actual controller, as well as the disturbance generator, is custom-coded in *C*. These tasks are accomplished by using a host PC, an Intel-based P-III Dell Dimension XPS $600MHz$. The same host PC is also used to collect all the relevant data produced during the experiment. The data are then converted into Matlab's proprietary format for storage.

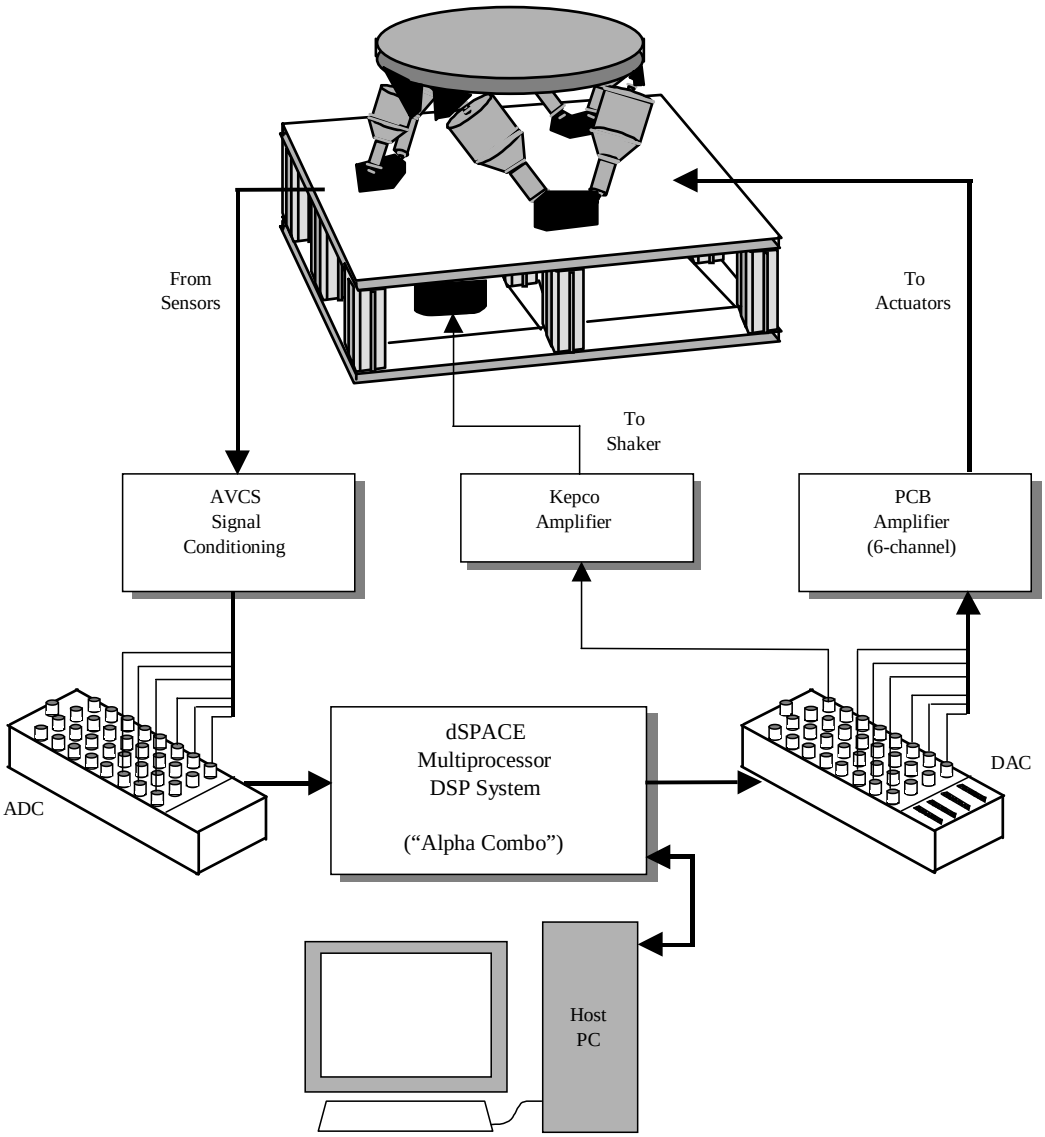

Figure 2.4. UQP Experimental Setup (From [4]).

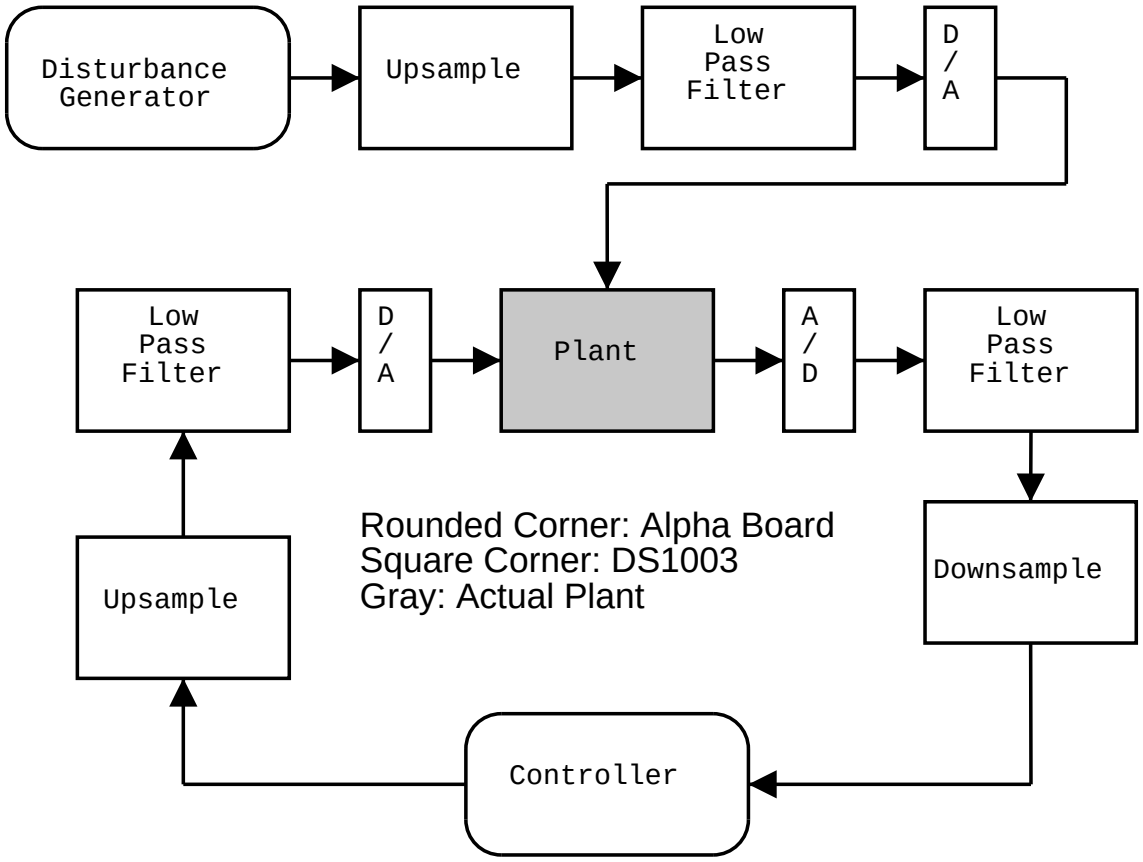

Figure 2.5. Ultra-Quiet Platform Controller.

C. PRECISION POINTING HEXAPOD

The main limitation of the Ultra-Quiet Platform is its small stroke, which prevents it from being used for steering. In order to evaluate the possibility of performing both pointing and vibration isolation, a hexapod with a longer stroke is needed. To address this need, the *Satellite Research and Design Center* acquired a new hexapod: the Precision Pointing Hexapod, from CSA Engineering, Inc.. The platform is designed to allow both vibration control and pointing. In order to achieve the large stroke required, the Precision Pointing Hexapod uses voice-coil actuators, which provide $\pm 5mm$ travel. Accelerometers are mounted inline to provide vibration information. The platform, as delivered by CSA Engineering, Inc., is depicted in Figure 2.6.

This hexapod was selected for modeling because it has a larger stroke. This hexapod will be used for pointing research as for well as vibration-isolation research and thus an accurate model is needed. A complete state-state model is an invaluable tool for testing new algorithms before implementing them on the actual hardware. In order to have the model developed, a deep understanding of the hardware is needed and therefore the description of the Precision Pointing Hexapod hardware is more detailed than the understanding needed to simply operate it.

1. Actuators

This platform is well suited for position and vibration control. The actuators, manufactured by Moltran Industries, Inc. (model *AFX 70N*), have a stroke of more than $\pm 5mm$ and can provide more than 2.5^o of tilting and 10^o of twisting. The actuators can deliver up to $40N$ of dynamic force and up to $70N$ of static force, being adequate to control large levels of vibration. The most important characteristics, from Moltran's datasheet, are shown on Table 2.1 and a picture of one of the actuators, as mounted, can be seen in Figure 2.7.

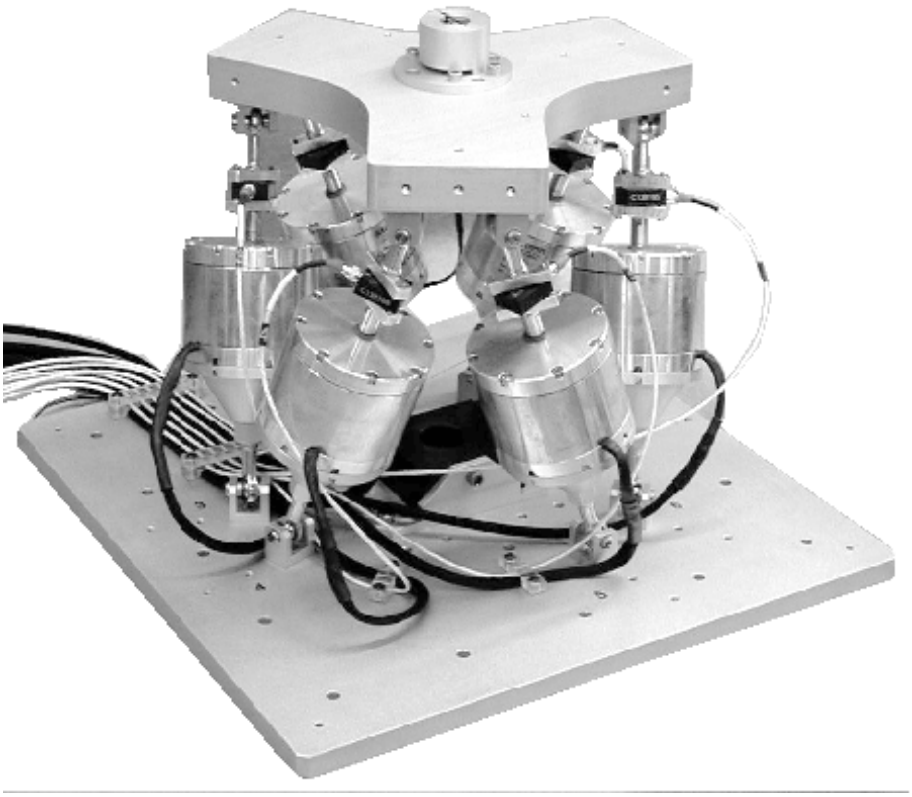

Figure 2.6. Precision Pointing Hexapod.

Figure 2.7. Actuator and Accelerometer.

	Value	Units
Model	Axial Force Transducer AFX 70N	-
Force at $40W_{DC}$, coil at 25^oC	100	N
Force at $40W_{rms,sine}$, coil at 25^oC	70	N
Force at $40W_{DC}$, coil at 140^oC	70	N
Force at $40W_{rms,sine}$, coil at 140^oC	50	N
Gain at the Origin	17.5	$\frac{N}{A}$
Gain at $\pm 5mm$	15	$\frac{N}{A}$

Table 2.1. Actuator Specifications.

The actuators are powered by a custom power supply provided by CSA Engineering, Inc, composed by six independent switching inverting amplifiers (switching frequency of 29KHz). The amplifier has negative gain (-1) and accepts a voltage in the range $\pm 4V$ on the inputs through coaxial cables. The outputs of the individual amplifiers are directly connected to the actuators.

2. Accelerometers

The Precision Pointing Hexapod is equipped with six accelerometers (*Kistler, 8304B2 K-Beam*) mounted inline with the strut's axis, as seen in Figure 2.7. These accelerometers have a range of $\pm 2g$ and are linear over the range 0 to $200Hz$. The main specifications are shown in Table 2.2.

3. Disturbance Generator

A vibration source is provided in order to simulate periodic disturbances. This is accomplished by using an *Aura Bass Shaker AST-2B-4* mounted on a custom adapter. The shaker charac-

	Value	Unit
Range	± 2	g
Sensitivity	1000	mV/g
Frequency Response $\pm 5\%$	300	Hz
Resolution	0.1	mg_{rms}

Table 2.2. Accelerometer Specifications.

teristics are shown in Table 2.3. The shaker adapter, shown in Figure 2.8, allows vibrations along the z-axis, *x-y axis* (as defined in Figure 2.1), twist, tip and combinations of the previous. The shaker can also be mounted on the top plate, producing vibration along the z-axis.

The signal that drives the shaker is produced by the DSP controller and sent to an AC power amplifier *Sony STR-D Amplifier*. The output of the amplifier is connected to the shaker.

4. Floating Table and Environment Isolation

The whole platform is soft-mounted on a Newport Stabilizer^{TM} laminar flow isolator, preventing the ground vibration from interfering with the experiment. In order to maximize the shaker's

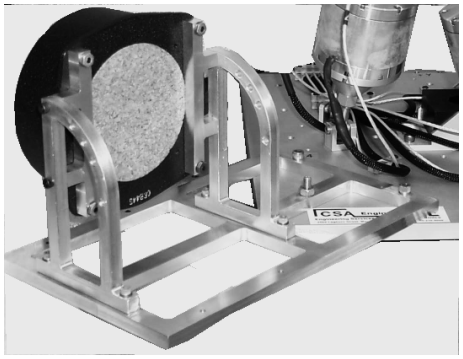

Figure 2.8. Base Shaker Adapter.

	Value	Unit
Model	AST-2B-4	
Magnet Type	ceramic	
Power Rating	50	W
Force, Nominal, at Resonance	132	N
Weight	1.125	Kg
Resonance Frequency	42	Hz
Frequency Range	20-100	Hz

Table 2.3. Shaker Specifications.

efficiency, the lower plate is mounted on the NewPort table using very soft rubber pads. Since these pads flatten due to the hexapod's weight, they are replaced before each set of experiments to ensure the highest degree of isolation.

5. Electronic Support

Both the power supply and the anti-aliasing filters are implemented in the "Control Box." This box accumulates the functions of power supply for sensors, shock detector, emergency shut-down, signal conditioning and anti-aliasing filter and noise suppressor. Figure 2.9 shows the main functions implemented in the Control Box.

Power is provided by a custom off-the-shelf power supply that provides $\pm 5V$ and $\pm 12V$, which are the voltages that both the box's electronics and the sensors need.

The accelerometers are connected by a standard DB25 connector that provides them with $+12V$ and ground. It also receives the accelerometer's signals ($\approx 1V/g$), which are sent to the anti-aliasing filters.

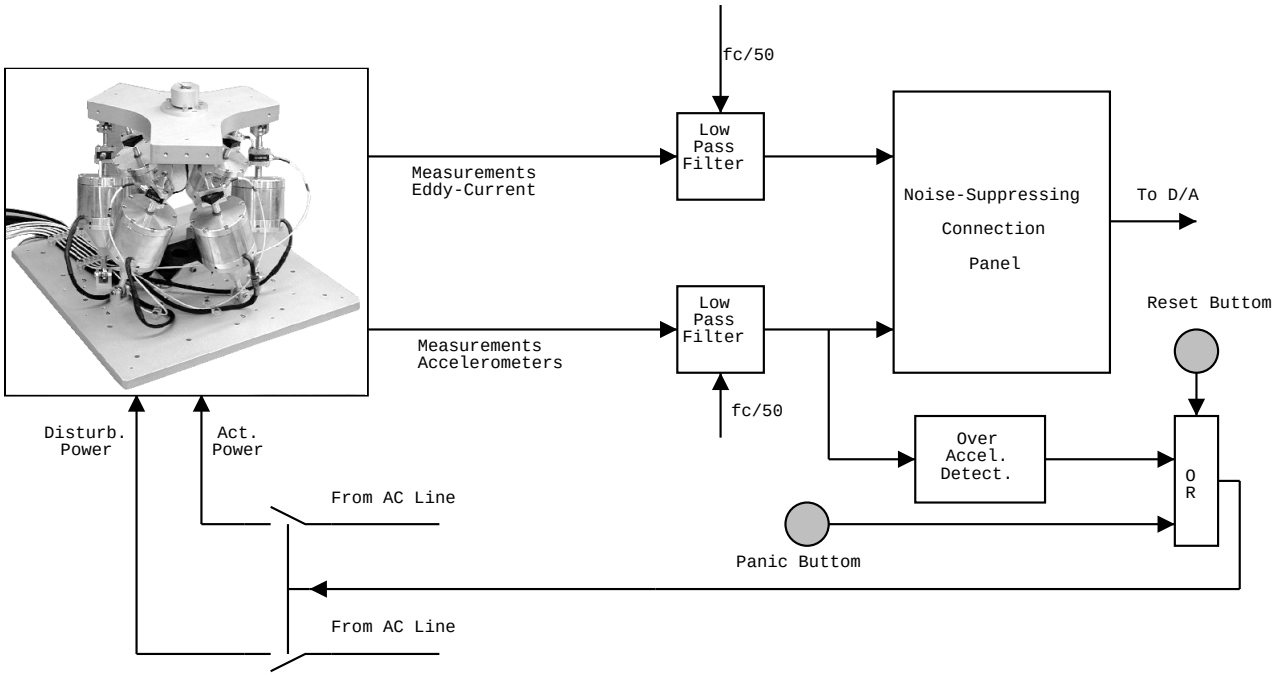

Figure 2.9. Control Box Main Functions.

A sample from the signal from the accelerometer #1 is sent to a window comparator. The normal operation of the hexapod should not exceed $\pm 2g$, which is the range of the accelerometers. If the top plate of the hexapod exceeds $\pm 2g$, the accelerometer's output voltage will be either smaller than $0.5V$ or larger than $4.5V$ and thus a shock is considered to have occurred. In response to this condition, a dedicated circuit will disconnect the actuator and disturbance amplifiers from the 110V rail, cutting their power supply. The power can only be restored by pressing the *reset* button. The same effect can be obtained by pressing the *panic* button. This mechanism is essential to preserve the hexapod integrity if the controller becomes unstable, especially at lower frequencies.

The anti-aliasing filters are implemented as fourth-order switched-capacitor Butterworth filters. The corner frequency can be adjusted by changing the frequency of the oscillator by means of a potentiometer. The corner frequency is defined as $f_c = f_{osc}/50$. Since this is actually a digital filter (although it is implemented with analog components), one must ensure that there are no

frequencies above $f_c/2$ when selecting f_{osc}. The cutoff frequency was selected at $50Hz$ due to the strong nonlinearities. The filtered measurement signals are then sent to a connection panel where $10nF$ capacitors are used to reduce the noise even further. Those capacitors are needed to prevent the environment noise from corrupting the measurements.

6. Controller and Host Computer

The hexapod is controlled by a dedicated *PowerPC*-based board (*dSpace DS1103*), which is installed inside the host PC. A connection panel is attached to the board and provides all the external communication with the board. The relevant interactions are shown in Figure 2.10.

The host computer is a *PC Dell Dimension XPS T500*. The controller is implemented by using *dSpace* and *Mathworks*' *Real Time Workshop.* All filtering, disturbance generation and I/O operations are implemented with *Simulink* block diagrams. The actual control laws are implemented in either *C* or *Simulink.* All the data logging is performed using *dSpace*'s *Control Desk*, which allows the desired variables to be streamed to disk and then converted to *Matlab*'s proprietary format.

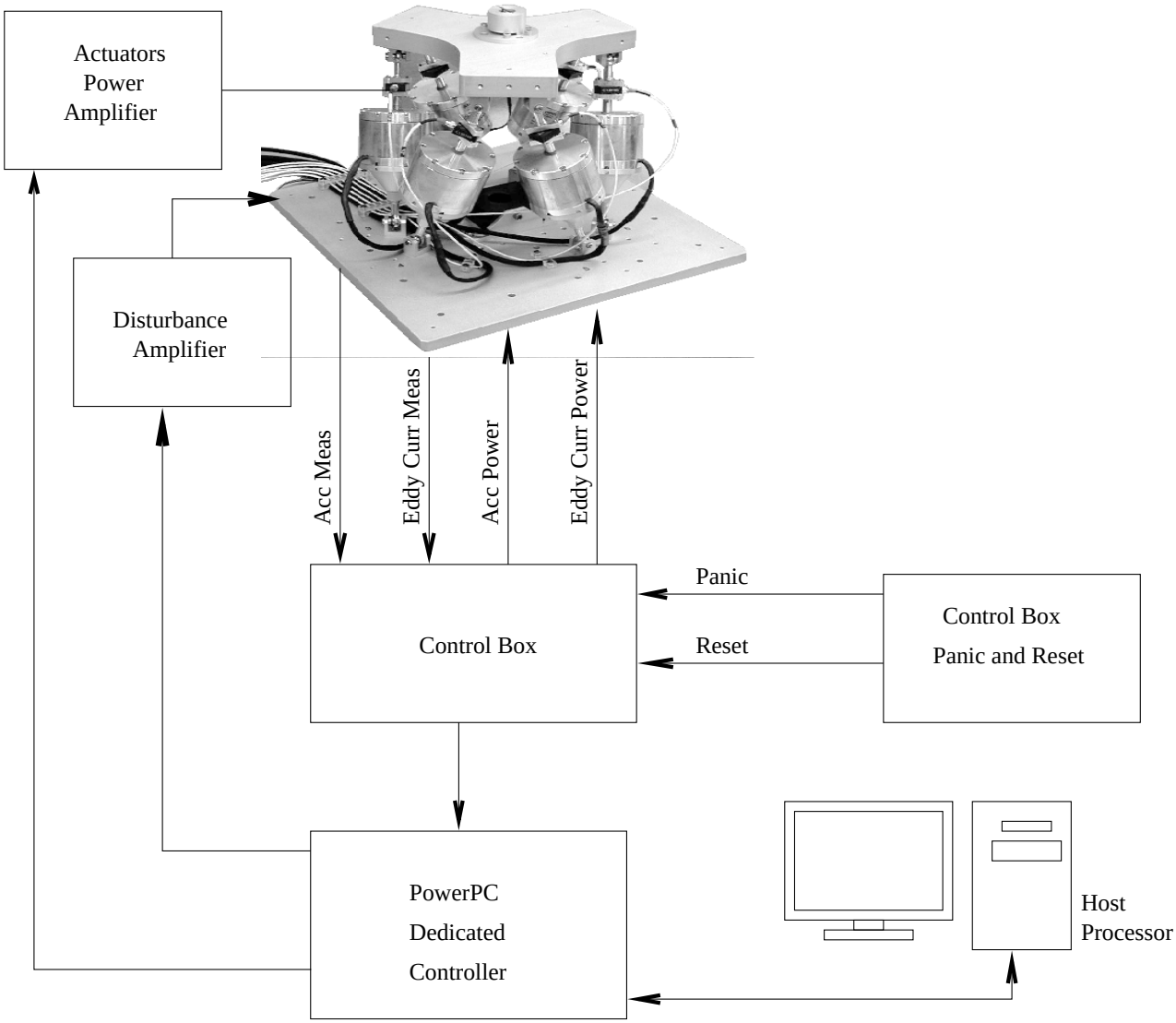

Figure 2.10. Precision Pointing Hexapod Experiment Setup.

III. MATHEMATICAL MODEL

A. OVERVIEW

This chapter presents the development of a mathematical model for the Precision Pointing Hexapod suitable for vibration simulation and control. This model enables testing of different control laws without having to implement them in the actual hardware, and thus enables the engineer to evaluate the actual influence of each parameter on the controller performance.

- Section C lists the symbols used in the derivation.
- Section D derives the equations used by the model starting from the momentum conservation equations, according to the Newtonian formulation.
- Section E describes the Euler angles and Euler Parameters, explaining why the Euler angles were selected for the hexapod's model.
- Section F modifies the free-body equations to take into account the fact that the forces acting on the top plate are assumed to act only on the joints.
- Section G incorporates the actual actuator's model.
- Section H provides the measurement equations and thus completes the model.

B. INTRODUCTION

Controlling a system requires knowledge of its behavior. A control system may even operate without *a priori* knowledge of the system, but it must build this information over time to perform successfully, as in the adaptive case. Even for adaptive controllers, a good model of the plant is

important in order to provide adequate parametrization. Another reason for a mathematical model is given by the nature of the measurements, since they are usually not the quantities directly involved in the requirements. In fact, the desired measurements for the platform are roll, pitch, yaw and the angular and linear accelerations. None of these quantities are measured directly by the sensors: they are related to the sensors by a mapping, which can be static or dynamic.

For the particular problem of the hexapod subject of this research, linear and angular accelerations can be statically derived from the acceleration of each joint of the moving plate as a linear transformation. However, angular positions ϕ, θ and ψ (roll, pitch and yaw) are related to the accelerations by differential equations. To provide estimates of the desired variables, a model-based technique, such as the Kalman Filter, has to be implemented. The performance and reliability of its results are as good as the reliability of the mathematical model of the system.

The rest of this section describes in detail all the steps involved in the model construction and presents the results. A detailed description of how the equations were derived is very important so that the same methodology can be applied to derive models of other hexapods.

C. LIST OF SYMBOLS, NOMENCLATURE AND DIMENSIONS

The Precision Pointing Hexapod was presented in Section II.C and only relevant details are included in this section. The basic geometry of the platform is shown in Figures 3.1 and 3.2. A hexapod is geometrically defined by its 12 joints (six upper joints and six lower joints). The origin is defined as the geometric center of the six upper joints when the platform is at rest with the actuators at mid-course (Figure 3.1). The axes of the coordinated system are also depicted in Figure 3.1.

The physical quantities used to define the system in the formulation are shown in Table 3.1. The definition of the symbols used in the derivation are in Table 3.2.

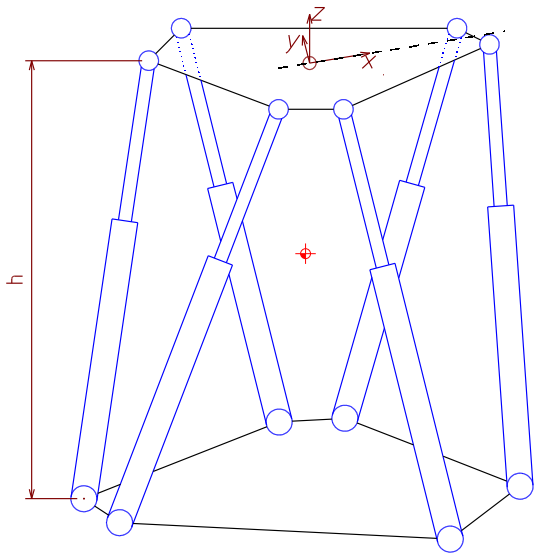

Figure 3.1. Hexapod—3D.

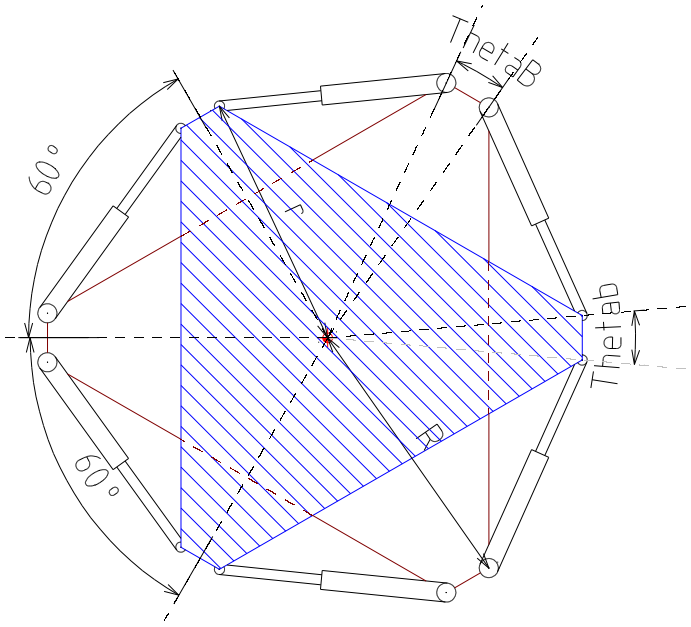

Figure 3.2. Hexapod—Top View.

Symbol	*Value*	*Unit*	*Description*
r	.25	m	Radius of the circle that contains all the upper joints (see Fig. 3.2)
R	.40	m	Radius of the circle that contains all the lower joints (see Fig. 3.2)
θ_B	$\frac{5\pi}{180}$	rad	Angular separation of the closest lower joints, measured from the center of the lower joints (see Fig. 3.2)
θ_b	$\frac{10\pi}{180}$	rad	Angular separation of the closest upper joints, measured from the center of the upper joints (see Fig. 3.2)
h_0	.2	m	Distance between upper and lower planes, when the platform is at "zero" (see Fig. 3.1)
m	2.849	Kg	Mass of the top plate
J	$\begin{bmatrix} 0.0277 & 0.0 & 0.0 \\ 0.0 & 0.0277 & 0.0 \\ 0.0 & 0.0 & 0.0553 \end{bmatrix}$	Kgm^2	The moment of inertia of the platform
ω_{na}	$100\,2\pi$	rad/s	Natural frequency of the actuator
ξ_a	.3	[none]	Damping factor of the actuator
β_{an}	1	[none]	Gain factor for the input to force relation in the actuator
α_{ac}	$0.1\,2\pi$	rad/s	First pole of the accelerometer
β_{ac}	$10^4\,2\pi$	rad/s	Second (and last) pole of the accelerometer

Table 3.1. Physical Quantities Used in the Model.

Symbol	Meaning
$\mathbf{Q}$	Linear momentum
m	Mass
$\mathbf{H}$	Angular momentum
$\mathbf{v}$	Linear velocity
$\mathbf{J}$	Inertia matrix
$\mathbf{w}$	Angular velocity (vector)
$\mathbf{F}$	Force acting on the center of mass
$\mathbf{T}$	Torque acting on the top plate
ϕ	Yaw
θ	Pitch
ψ	Roll
$\mathbf{M}$	Matrix that converts $\mathbf{w}$ into the Euler angles derivatives
$\boldsymbol{\alpha}$	Euler parameters vector $\boldsymbol{\alpha} = [\phi\,\theta\,\psi]^T$
$\mathbf{a}$	Acceleration
$\mathbf{L}_i$	Force acting on joint i
F_i	Force produced by the actuator i
$\mathbf{e}$	Input force vector, generated by the actuators
$\mathbf{a}_i$	Acceleration of joint i
$\mathbf{b}_i$	Position of upper joint i
$\mathbf{B}_i$	Position of lower joint i
$\mathbf{r}_i$	Vector that connects $\mathbf{p}$ to $\mathbf{b}_i$
$\boldsymbol{\mathcal{F}}$	Form factor for force ($\mathbf{F} = \boldsymbol{\mathcal{F}}\,\mathbf{e}$)
$\boldsymbol{\mathcal{T}}$	Form factor for torque ($\mathbf{T} = \boldsymbol{\mathcal{T}}\mathbf{F}_{inp}$)
$\mathbf{a}_i$	Acceleration of joint i
$\mathbf{p}$	Position of the top plate
$\frac{F(s)}{I(s)}$	Transfer function of the actuator (force as output and current as input)
$\mathbf{v}_j$	Velocity of the joint
v_l	Velocity of the joint along the actuator axis
b_a	Viscosity coefficient
$\mathbf{r}_i$	Vector that connects $\mathbf{b}_c$ to the joint i ($\mathbf{r}_i = \mathbf{b}_i - \mathbf{b}_c = \mathbf{b}_i - \mathbf{p}$)

Table 3.2. Symbols Used in the Mathematical Model.

D. FREE-BODY MODEL

In order to make the problem more tractable, it is assumed that all forces and torques are measured with respect to an inertial references system (defined in Section C). The most basic equations for a free-body model are the equations of momentum conservation (Equations (3.1) and (3.2)). These qualities do not change if no external torque or force is applied to the body. The linear (**Q**) and angular (**H**) momentum are defined as:

$$\mathbf{Q} \triangleq m\mathbf{v} \tag{3.1}$$

$$\mathbf{H} \triangleq \mathbf{J}\mathbf{w}, \tag{3.2}$$

where m is the mass, **J** the inertia matrix, **w** the angular velocity and **v** the linear velocity (all with respect to the top plate).

The force **F** and torque **T** acting on the top plate are

$$\mathbf{F} = \dot{\mathbf{Q}} = \dot{m}\mathbf{v} + m\dot{\mathbf{v}} \tag{3.3}$$

$$\mathbf{T} = \dot{\mathbf{H}} = \dot{\mathbf{J}}\mathbf{w} + \mathbf{J}\dot{\mathbf{w}}. \tag{3.4}$$

Equations (3.3) and (3.4) can be simplified if the mass and the inertia matrix can be considered constant, as it is the case when the equipment mounted on the top plate can be considered a rigid body. With this assumption $\dot{m} = 0$ and $\dot{\mathbf{J}} = 0$ and Equations (3.3) and (3.4) can be simplified to

$$\mathbf{F} = m\dot{\mathbf{v}} \tag{3.5}$$

$$\mathbf{T} = \mathbf{J}\dot{\mathbf{w}}. \tag{3.6}$$

E. EULER ANGLES

There are two main approaches that can be used to define the angular velocity: Euler angles and Euler parameters (also known as quaternions).

The first approach is adequate for angles within bounds, since this approach has singularity problems. Furthermore, it uses transcendental functions (sin, cos and tan), making its computation expensive. Using the azimuth-elevation-roll sequence and according to [28], the derivatives of the Euler angles are

$$\dot{\boldsymbol{\alpha}} = \begin{bmatrix} \dot{\phi} \\ \dot{\theta} \\ \dot{\psi} \end{bmatrix} = \begin{bmatrix} 1 & \tan\theta\sin\phi & \tan\theta\cos\phi \\ 0 & \cos\theta & -\sin\theta \\ 0 & \frac{\sin\phi}{\cos\theta} & \frac{\cos\phi}{\cos\theta} \end{bmatrix} \mathbf{w} = \mathbf{M}(\boldsymbol{\alpha})\,\mathbf{w} \tag{3.7}$$

and the singularity is at $\theta = \pi/2$. The platform movements are small, with all angles being less than 15^o, and the singularity will never be reached. Without the singularity, the only drawback of the Euler angles approach is its computational requirements.

The other possibility is to use Euler parameters (quaternions). According to [28], they can be written as

$$\begin{bmatrix} \dot{e_1} \\ \dot{e_2} \\ \dot{e_3} \\ \dot{e_4} \end{bmatrix} = -\frac{1}{2} \begin{bmatrix} w_x e_2 + w_y e_3 + w_z e_4 \\ -w_x e_1 - w_z e_3 - w_y e_4 \\ -w_y e_1 + w_z e_2 - w_x e_4 \\ -w_z e_1 - w_y e_2 - w_x e_3 \end{bmatrix}, \tag{3.8}$$

with the constraining equation

$$e_1^2 + e_2^2 + e_3^2 + e_4^2 = 1, \tag{3.9}$$

where e_1, e_2, e_3 and e_4 are the quaternions.

This approach has two main advantages over using Euler angles: there is no singularity and the updates require only standard multiplications. The Euler angles approach was selected for this model.

Assuming that the body and inertial frames have the same origin, a vector in the inertial frame ${}^{o}\mathbf{p}$ can be transformed into the body frame using the transformation [28]

$$
\begin{aligned}
{}^{b}\mathbf{p} &= \begin{bmatrix} c\theta c\phi & c\theta s\psi & -s\theta \\ -c\phi s\psi + s\phi s\theta c\psi & c\phi c\psi + s\phi s\theta s\psi & s\phi c\theta \\ s\phi s\psi + c\phi s\theta c\psi & -s\phi c\psi + c\phi s\theta s\psi & c\phi c\theta \end{bmatrix} {}^{o}\mathbf{p} && (3.10) \\
&= {}^{b}\mathbf{R}_{o}\,{}^{o}\mathbf{p}, && (3.11)
\end{aligned}
$$

were c stands for cos and s for sin. The transformation matrix ${}^{b}\mathbf{R}_{o}$ is orthonormal and invertible for the small angles that the Precision Pointing Hexapod can produce. The inverse transformation is ${}^{o}\mathbf{R}_{b} = {}^{b}\mathbf{R}_{o}{}^{-1}$.

Using the Euler angles and the assumption of constant mass and inertia matrix, a simple model can be written as

$$
\begin{aligned}
\begin{bmatrix} \dot{\mathbf{p}} \\ \dot{\mathbf{v}} \\ \dot{\boldsymbol{\alpha}} \\ \dot{\mathbf{w}} \end{bmatrix} &= \begin{bmatrix} \mathbf{v} \\ \frac{1}{m}\mathbf{F} \\ \mathbf{M}(\boldsymbol{\alpha})\mathbf{w} \\ \mathbf{J}^{-1}\mathbf{T} \end{bmatrix} \\
&= \begin{bmatrix} \mathbf{v} \\ \frac{1}{m}\mathbf{F} \\ \begin{bmatrix} 1 & \tan\theta\sin\phi & \tan\theta\cos\phi \\ 0 & \cos\theta & -\sin\theta \\ 0 & \frac{\sin\phi}{\cos\theta} & \frac{\cos\phi}{\cos\theta} \end{bmatrix} \mathbf{w} \\ \mathbf{J}^{-1}\mathbf{T} \end{bmatrix}, && (3.12)
\end{aligned}
$$

where the force **F** and the torque **T** act on the center of mass of the top plate.

This model describes a body floating in free space and has arbitrary force and torque as inputs. Therefore, this system is controllable as is its linearized version. The main problem with this model is, however, that the force and torque are not controlled directly: they are generated by the six actuators.

F. FORCES ACTING ON THE TOP PLATE

Disregarding the gravitational effects, there are only six external forces and no external torque acting on the top plate (through the joints). A mathematical relationship must be found that can translate these forces into the resultant force and torque. It is assumed that the actuators are mass-less and the forces generated by the actuators are parallel to the actuator's axis and act only at the joints.

The force acting on the center of mass is the summation of all forces acting on the body. Defining $\mathbf{L}_i$ as the force acting on the joint i and $\mathbf{e} \triangleq [e_1 \dots e_6]^T$ as the force produced by the actuators, the resultant force is

$$\begin{aligned} \mathbf{F} &= \sum_{i=1}^{6} \mathbf{L}_i \\ &= \sum_{i=1}^{6} e_i \frac{\mathbf{b}_i - \mathbf{B}_i}{\|\mathbf{b}_i - \mathbf{B}_i\|}, \end{aligned} \tag{3.13}$$

where e_i is the force produced by the actuator i, $\mathbf{b}_i$ is the position of upper joint i and $\mathbf{B}_i$ is the position of the lower joint i.

$$\begin{aligned} \mathbf{b}_i &= \mathbf{p} + \mathbf{r}_i \\ &= \mathbf{p} + {}^b\mathbf{R}_o \mathbf{r}_{o,i}. \end{aligned} \tag{3.14}$$

Defining $\boldsymbol{\mathcal{F}}_i \triangleq \frac{\mathbf{b}_i - \mathbf{B}_i}{\|\mathbf{b}_i - \mathbf{B}_i\|}$, the force $\mathbf{F}$ can be written as

$$\begin{aligned}
\mathbf{F} &= \sum_{i=1}^{6} \boldsymbol{\mathcal{F}}_i e_i \\
&= \begin{bmatrix} | & | & | & | & | & | \\ \boldsymbol{\mathcal{F}}_1 & \boldsymbol{\mathcal{F}}_2 & \boldsymbol{\mathcal{F}}_3 & \boldsymbol{\mathcal{F}}_4 & \boldsymbol{\mathcal{F}}_5 & \boldsymbol{\mathcal{F}}_6 \\ | & | & | & | & | & | \end{bmatrix} \begin{bmatrix} e_1 \\ e_2 \\ e_3 \\ e_4 \\ e_5 \\ e_6 \end{bmatrix} \\
&= \boldsymbol{\mathcal{F}}(\mathbf{p}, \boldsymbol{\alpha})\, \mathbf{e}. \qquad (3.15)
\end{aligned}$$

The torque can be evaluated in a similar manner. Each force has a associated torque when translated to the center of mass and these torques can then be summed to produce the total torque $\mathbf{T}$. First, define a vector $\mathbf{r}_i$ as

$$\mathbf{r}_i = {}^{b}\mathbf{R}_o \mathbf{r}_{o,i}, \qquad (3.16)$$

where $\mathbf{p}$ is the position of the center of mass of the top plate and $\mathbf{b}_i$ is the position of the joint i.

Therefore, the overall torque can be written as

$$\begin{aligned}
\mathbf{T} &= \sum_{i=1}^{6} \mathbf{r}_i \times \mathbf{L}_i \\
&= \sum_{i=1}^{6} \mathbf{r}_i \times \left(e_i \frac{\mathbf{b}_i - \mathbf{B}_i}{\|\mathbf{b}_i - \mathbf{B}_i\|} \right) \\
&= \sum_{i=1}^{6} e_i \left(\mathbf{r}_i \times \frac{\mathbf{b}_i - \mathbf{B}_i}{\|\mathbf{b}_i - \mathbf{B}_i\|} \right) \\
&= \boldsymbol{\mathcal{T}}(\mathbf{p}, \boldsymbol{\alpha})\, \mathbf{e}, \qquad (3.17)
\end{aligned}$$

where $\boldsymbol{\mathcal{T}}_i \triangleq \mathbf{r}_i \times \frac{\mathbf{b}_i - \mathbf{B}_i}{\|\mathbf{b}_i - \mathbf{B}_i\|}$.

The results of Equations (3.15) and (3.17) provide a linear relationship between the input forces and the resulting force and torque. By using these results, the plant model can be rewritten as

$$\begin{bmatrix} \dot{\mathbf{p}} \\ \dot{\mathbf{v}} \\ \dot{\boldsymbol{\alpha}} \\ \dot{\mathbf{w}} \end{bmatrix} = \begin{bmatrix} \mathbf{v} \\ \frac{1}{m}\boldsymbol{\mathcal{F}}\mathbf{e} \\ \mathbf{M}(\boldsymbol{\alpha})\,\mathbf{w} \\ \mathbf{J}^{-1}\boldsymbol{\mathcal{T}}\mathbf{e} \end{bmatrix}, \tag{3.18}$$

where the parameters of $\boldsymbol{\mathcal{F}}(\mathbf{p},\boldsymbol{\alpha})$ and $\boldsymbol{\mathcal{T}}(\mathbf{p},\boldsymbol{\alpha})$ were dropped for compactness and are implicit.

G. ACTUATORS

The force of the actuators cannot be controlled directly. The controller's output is a number that is converted to a voltage/current and then sent to the actuator. The actual force produced depends on the actuator's internal dynamics.

The actuators installed on the Precision Pointing Hexapod are voice-coils, which are basically a coil in the inside and a magnet on the outside (Figure 3.3). A current flowing in the coil generates a magnetic field that interacts with the magnetic element creating the force, which is linear for small displacements. Both a spring force and a viscous force must also be taken into account. Therefore, the equation relating the force generated by the actuator to the current flowing through it and the position is

$$F(t) = K_i i(t) - K_x x(t) - b\dot{x}(t) - m_a\ddot{x}(t), \tag{3.19}$$

where K_i is the gain from current to force and b, m_a and K_x are the viscous friction, moving mass and spring constant of the actuator.

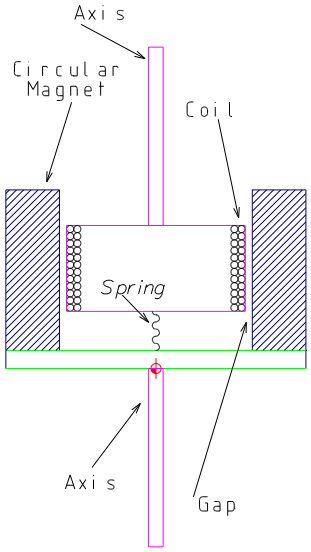

Figure 3.3. Actuator Diagram.

The force produced by the actuator must be written in terms of the inertial coordinate system. The displacement x is the distance traveled by the joint along the unity vector $\frac{\mathbf{b}_i - \mathbf{B}_i}{\|\mathbf{b}_i - \mathbf{B}_i\|} = \boldsymbol{\mathcal{F}}_i$

$$\begin{aligned} x_i &= (\mathbf{b}_i - \mathbf{b}_{0,i})^T \boldsymbol{\mathcal{F}}_i \\ &= (\mathbf{p} + \mathbf{r}_i - \mathbf{b}_{0,i})^T \boldsymbol{\mathcal{F}}_i \\ &= \left(\mathbf{p} + {}^b\mathbf{R}_o \mathbf{r}_{0,i} - \mathbf{b}_{0,i}\right)^T \boldsymbol{\mathcal{F}}_i. \end{aligned}$$

Since $\mathbf{b}_{o,i} = \mathbf{r}_{0,i}$, this becomes

$$x = \left(\mathbf{p} + {}^b\mathbf{R}_o \mathbf{b}_{0,i} - \mathbf{b}_{0,i}\right)^T \boldsymbol{\mathcal{F}}_i. \tag{3.20}$$

The velocity v_i of the joint i is the sum of the velocity of the center of mass and the velocity of the joint with respect to the center of mass. Since the latter is produced by the angular velocity of the top plate, the resulting expression is

$$\begin{aligned} v_i &= (\mathbf{v} + \mathbf{w} \times \mathbf{r}_i)^T \boldsymbol{\mathcal{F}}_i \\ &= \left(\mathbf{v} + \mathbf{w} \times {}^b\mathbf{R}_o \mathbf{r}_{o,i}\right)^T \boldsymbol{\mathcal{F}}_i. \end{aligned} \tag{3.21}$$

Similarly, the acceleration of the joint i is the acceleration of the center of mass summed to the centripetal acceleration:

$$\mathbf{a}_i = \mathbf{a} + \mathbf{w} \times (\mathbf{w} \times \mathbf{r}_i). \tag{3.22}$$

Projecting $\mathbf{a}_i$ it on the struts' axes leads to:

$$\begin{aligned} a_i &= (\mathbf{a} + \mathbf{w} \times (\mathbf{w} \times \mathbf{r}_i))^T \boldsymbol{\mathcal{F}}_i \\ a_i &= \left(\mathbf{a} + \mathbf{w} \times \left(\mathbf{w} \times {}^b\mathbf{R}_o \mathbf{r}_{o,i}\right)\right)^T \boldsymbol{\mathcal{F}}_i. \end{aligned} \tag{3.23}$$

Substituting x, $\dot{x}$ and $\ddot{x}$ into Equation (3.19), the force on joint i is

$$\begin{aligned} F_i(t) = {} & K_i i_i(t) - \left(K_x \left(\mathbf{p} + {}^b\mathbf{R}_o \mathbf{b}_{0,i} - \mathbf{b}_{0,i}\right) + b \left(\mathbf{v} + \mathbf{w} \times {}^b\mathbf{R}_o \mathbf{r}_{o,i}\right) + \right. \\ & \left. m_a \left(\mathbf{a} + \mathbf{w} \times \left(\mathbf{w} \times {}^b\mathbf{R}_o \mathbf{r}_{o,i}\right)\right)\right)^T \boldsymbol{\mathcal{F}}_i, \end{aligned} \tag{3.24}$$

assuming it is parallel to the actuator's axis. All the terms of this equation are known states except for the input $i_i(t)$.

It is important to mention that the output of the controller is not a current, but a voltage. This voltage is sent to a DC amplifier and its output goes to the actuators. The amplifier's bandwidth is $200Hz$ and the time constant of the actuator's LR circuit is $1ms$. Therefore, the model developed in this section is valid only up to $200Hz$. If higher frequencies are needed, then the electrical dynamics must also be modeled.

1. Model With Actuators

The force Equation (3.24) can be used in Equations (3.12) to generate a more complete model. To do that, Equation (3.24) must be written in a more compact form. Defining

$$\begin{aligned} h_i \triangleq {} & \left(K_x \left(\mathbf{p} + {}^b\mathbf{R}_o \mathbf{b}_{0,i} - \mathbf{b}_{0,i}\right) + b \left(\mathbf{v} + \mathbf{w} \times {}^b\mathbf{R}_o \mathbf{r}_{o,i}\right) + \right. \\ & \left. m_a \left(\mathbf{a} + \mathbf{w} \times \left(\mathbf{w} \times {}^b\mathbf{R}_o \mathbf{r}_{o,i}\right)\right)\right)^T \boldsymbol{\mathcal{F}}_i, \end{aligned} \tag{3.25}$$

$$\mathbf{h} \triangleq [h_1 \dots h_6]^T \tag{3.26}$$

and

$$\mathbf{u} \triangleq [i_1 \dots i_6]^T . \tag{3.27}$$

Equation (3.12) can be rewritten as

$$\begin{aligned}
\begin{bmatrix} \dot{\mathbf{p}} \\ \dot{\mathbf{v}} \\ \dot{\boldsymbol{\alpha}} \\ \dot{\mathbf{w}} \end{bmatrix} &= \begin{bmatrix} \mathbf{v} \\ \frac{1}{m}\boldsymbol{\mathcal{F}}\,\mathbf{e} \\ \mathbf{M}(\boldsymbol{\alpha})\,\mathbf{w} \\ \mathbf{J}^{-1}\boldsymbol{\mathcal{T}}\,\mathbf{e} \end{bmatrix} \\
&= \begin{bmatrix} \mathbf{v} \\ \frac{1}{m}\boldsymbol{\mathcal{F}} \begin{bmatrix} F_1 \dots F_6 \end{bmatrix}^T \\ \mathbf{M}(\boldsymbol{\alpha})\,\mathbf{w} \\ \mathbf{J}^{-1}\boldsymbol{\mathcal{T}} \begin{bmatrix} F_1 \dots F_6 \end{bmatrix}^T \end{bmatrix} \\
&= \begin{bmatrix} \mathbf{v} \\ \frac{1}{m}\boldsymbol{\mathcal{F}}\,(K_i\mathbf{u} - \mathbf{h}) \\ \mathbf{M}(\boldsymbol{\alpha})\,\mathbf{w} \\ \mathbf{J}^{-1}\boldsymbol{\mathcal{T}}\,(K_i\mathbf{u} - \mathbf{h}) \end{bmatrix},
\end{aligned} \tag{3.28}$$

with **h** and **u** as defined in Equations (3.25), (3.26) and (3.27).

H. ACCELEROMETERS

All hexapods used for vibration control reviewed in the literature have some kind of sensor to measure the vibration built into the strut. The Precision Pointing Hexapod is not an exception and has accelerometers built inline with the actuator's axis. Section II.C.1 (p. 15) describes the

mounting bracket and the accelerometers, while Table 3.3 shows the relevant specifications of the accelerometers.

	Value	Unit
Range	± 2	g
Sensitivity	1,000	mV/g
Resonant Freq. (nom.)	1.2	kHz
Freq. Response ($\pm 5\%$)	300	Hz
Linearity	± 1	%FS
Transverse Sensitivity (nom.)	< 1	%
Phase Shift (10Hz, nom.)	2	degree
Resolution (0.5 to 100Hz)	0.1	mg_{rms}

Table 3.3. Accelerometer Specifications.

As seen in Section G, the model is only valid up to $200Hz$ due to restrictions of the actuator's model. Since $200Hz$ is within the accelerometer's bandwidth, their dynamic can be considered just a constant. It is also important to realize that the accelerometers mounted on the struts measure DC level, and this model does not limit this behavior.

The accelerometers measure the acceleration of the joint projected on the actuator's axis. The measurement can then be written as

$$a_i = \mathbf{a}_i{}^T \frac{\mathbf{b}_i - \mathbf{B}_i}{\|\mathbf{b}_i - \mathbf{B}_i\|} = \mathbf{a}_i{}^T \boldsymbol{\mathcal{F}}_i, \tag{3.29}$$

where a_i is the measurement of accelerometer i and $\mathbf{a}_i$ is the acceleration at the joint i. This acceleration was evaluated in Equation (3.23).

Using the above result and defining $\mathbf{K}_{a,}$ as the accelerometers' constant gain, the measurement equations become

$$\mathbf{m} = \begin{bmatrix} a_1 \\ \vdots \\ a_6 \end{bmatrix} = \begin{bmatrix} \mathbf{K}_{a,} \left(\mathbf{a} + \mathbf{w} \times \left(\mathbf{w} \times {}^b\mathbf{R}_o \mathbf{r}_{o,1}\right)\right)^T \boldsymbol{\mathcal{F}}_1 \\ \vdots \\ \mathbf{K}_{a,} \left(\mathbf{a} + \mathbf{w} \times \left(\mathbf{w} \times {}^b\mathbf{R}_o \mathbf{r}_{o,6}\right)\right)^T \boldsymbol{\mathcal{F}}_6 \end{bmatrix}. \tag{3.30}$$

Therefore, the last equation is the measurement equation for the state-space model described in Equation (3.28), which can be used for vibration simulation purposes.

IV. VIBRATION SUPPRESSION

A. CHAPTER LAYOUT

This chapter contains the details of the Adaptive Disturbance Canceller. First, Section B derives the Multiple-Error LMS method.

Section C presents an overview of the Adaptive Disturbance Canceller. The mathematical details, including a convergence analysis, are presented in Section D.

Note that the Adaptive Disturbance Canceller isolates the vibrations at the assigned frequencies only. As a result, Section D.3 presents a study of the behavior of the controller in the presence of unassigned frequencies on the error signal.

Section E presents simulations results obtained with the Adaptive Disturbance Canceller. The model derived in Chapter III was used to simulate the PPH in Section E.2. The Adaptive Disturbance Canceller is a SISO controller and multiple controllers might interact with one another on a distributed controller configuration. Thus, full nonlinear model simulations are of special interest.

B. MULTIPLE-ERROR LEAST MEAN SQUARED

Advances in Digital Signal Processing techniques led to several estimation techniques and many of these are also valuable for noise cancellation. Techniques commonly applied in noise cancellation are usually based on adaptive algorithms. The general approach is shown in Figure 4.1.

Among adaptive filter implementations used to cancel the disturbance signal $d[n]$ one of the simplest and best understood is the Least Mean Square method (see [29] for a detailed description

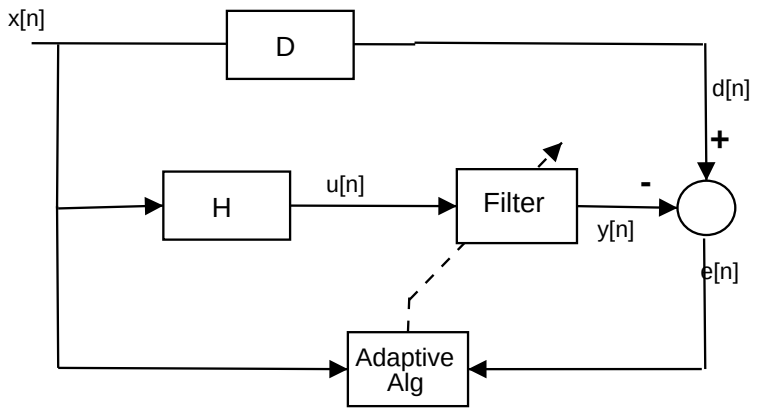

Figure 4.1. Noise Cancellation Problem.

and specific properties). This filter assumes an all-pole plant (H) and minimizes the cost function

$$J = \mathbf{E}\left\{|\mathbf{e}[n]|^2\right\}, \tag{4.1}$$

where $\mathbf{E}\{\bullet\}$ is the expectation operator. Additionally, the LMS is a first order method, which contributes to its simplicity and reduced computational effort in comparison with more sophisticated algorithms.

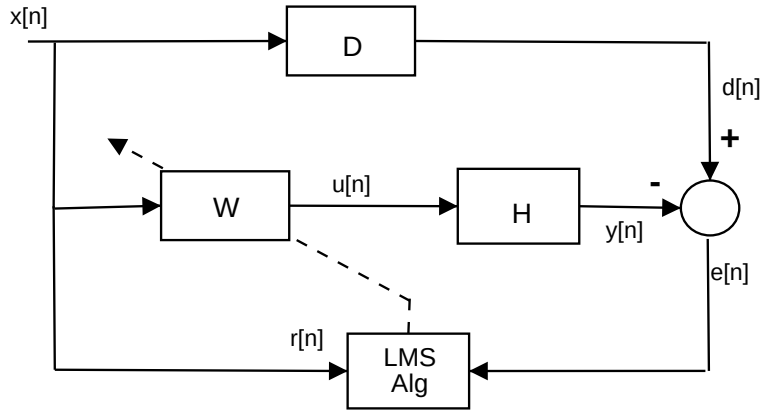

Figure 4.2. An Adaptive Vibration Controller.

The vibration problem has one additional complication when compared to the noise cancellation problem: the transfer function H is *after* the filter. In fact, the filter provides the inputs to the plant H. An updated diagram, reflecting the vibration control problem is shown in Figure 4.2.

It is important to realize that Figure 4.1 and Figure 4.2 only differ on the position of the plant and the controller: they are switched. Unfortunately, the very fact of switching the plant and the filter prevents a straight LMS from being used for control. The LMS filter has a weight update equation in the form

$$\mathbf{W}[n+1] = \mathbf{W}[n] + \mu e^*[n]\,\mathbf{u}[n], \tag{4.2}$$

and since the plant is placed after the filter, a change on $u[n]$ will not reflect on $e[n]$, but on $e[n+1]$ (the LMS assumes an all-pole plant). Therefore, $e[n]$ does *not* depend on $u[n]$ and the LMS method cannot be applied directly to the vibration control problem.

Widrow[30] and Burgess[31] solved this problem working independently in 1981. Their method used an estimated model of the plant and is called Filtered-X LMS. This algorithm inherits most of the characteristics of the simple LMS scheme. Unfortunately, the Filtered-X LMS method does not address one important issue: MIMO systems. Elliot, Stothers and Nelson generalized the original Filtered-X LMS in 1987[12], presenting the Multiple-Error LMS. The new algorithm was able to control MIMO plants, but still possesses the restriction of having a single signal correlated with all disturbances. In essence, the Multiple-Error LMS transforms the MIMO plant into a SIMO plant, with a single input ($x[n]$) and several outputs ($e_o[n]$) (see derivation in Section 1). The structure of the controller proposed in [12] can be seen in Figure 4.3.

Both the Multiple-Error LMS and the Filtered-X LMS approaches, as well as their variants, seem to be the most common active vibration control/isolation algorithms in use today. They are among the least expensive in terms of computational requirements and are comparatively simple to implement. The Multiple-Error LMS, due to its widespread acceptance, is used in this work as a benchmark and is presented next.

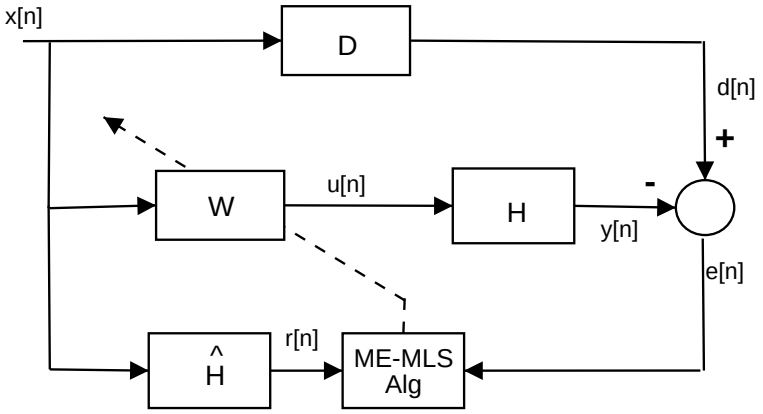

Figure 4.3. LMS for Vibration Control.

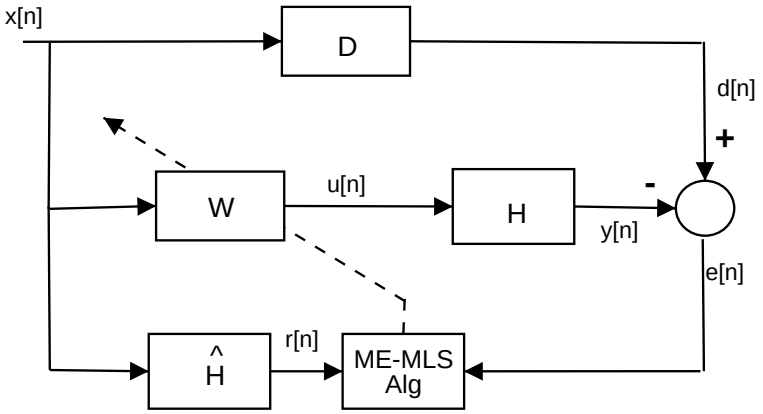

Figure 4.4. Multiple-Error LMS.

1. Derivation of the Multiple-Error LMS

The Multiple-Error LMS assumes that the MIMO plant H (Figure 4.4) can be modeled as a Finite Impulse Response (FIR) filter or order M with Q outputs and P inputs. Thus, the q^{th} output $y_{q,p}[n]$ due to the input p is given by:

$$y_{q,p}[n] = \sum_{m=0}^{M} h_{q,p}[m]\, u_p[n-m], \tag{4.3}$$

assuming that the Q disturbances $d_q[n]$ acting on the system are correlated to the signal $x[n]$, which must be measurable.

Further, assuming $\mathbf{W}$ to be a matrix of dimensions $S \times P$, the signal $u[n]$ can be generated as

$$u_p[n] = \sum_{s=0}^{S-1} w_{s,p}[n]\, x[n-s]. \tag{4.4}$$

Substituting the input value derived in Equation (4.4) into Equation (4.3), the output of the plant at time n is

$$\begin{aligned} y_q[n] &= \sum_{p=0}^{P-1} \sum_{m=0}^{M} h_{q,p}[m]\, u_p[n-m] \\ &= \sum_{p=0}^{P-1} \sum_{m=0}^{M} h_{q,p}[m] \sum_{s=0}^{S-1} w_{s,p}[n-m]\, x[n-m-s] \\ &= \sum_{p=0}^{P-1} \sum_{m=0}^{M} \sum_{s=0}^{S-1} h_{q,p}[p]\, w_{s,p}[n-m]\, x[n-m-s]. \end{aligned} \tag{4.5}$$

The error can be then computed as

$$\begin{aligned} e_q[n] &= d_q[n] - y_q[n] \\ &= d_q[n] - \sum_{p=0}^{P-1} \sum_{m=0}^{M} \sum_{s=0}^{S-1} h_{q,p}[p]\, w_{s,p}[n-m]\, x[n-m-s]. \end{aligned} \tag{4.6}$$

Following the same reasoning that is used in the derivation of the LMS method, $\mathbf{W}$ must be updated minimizing the cost function

$$J = \mathbf{E}\left\{ \sum_{q=0}^{Q-1} e_q^2[n] \right\}. \tag{4.7}$$

By using the steepest descent and μ as the learning rate, the weight can be adjusted as follows:

$$\begin{aligned} w_{s,p}[n] &= w_{s,p}[n] - \mu \frac{\partial J[n]}{\partial w_{s,p}[n]} \\ &= w_{s,p}[n] - \mu \frac{\partial \mathbf{E}\left\{\sum_{q=0}^{Q-1} e_q^2[n]\right\}}{\partial w_{s,p}[n]} \\ &= w_{s,p}[n] - \mu \sum_{q=0}^{Q-1} \frac{\partial \mathbf{E}\left\{e_q^2[n]\right\}}{\partial w_{s,p}[n]}. \end{aligned} \tag{4.8}$$

Unfortunately, computing the expectation $\mathbf{E}\left\{e_q^2[n]\right\}$ in real time is impossible, but the same approximation used in the derivation of the standard LMS algorithm can be made here:

$$\mathbf{E}\left\{e_q^2[n]\right\} \approx e_q^2[n]. \tag{4.9}$$

By using the above approximation and proceeding with the calculation of $w_{s,p}[n+1]$:

$$\begin{aligned} w_{s,p}[n+1] &\approx w_{s,p}[n] - \mu \sum_{q=0}^{Q-1} \frac{\partial \left\{e_q^2[n]\right\}}{\partial w_{s,p}[n]} \\ &\approx w_{s,p}[n] - 2\mu \sum_{q=0}^{Q-1} e_q[n] \frac{\partial e_q[n]}{\partial w_{s,p}[n]}. \end{aligned} \tag{4.10}$$

Next, substituting the error $e_q[n]$ from Equation (4.6) into Equation (4.10), $w_{s,p}[n+1]$ can be evaluated as

$$\begin{aligned} w_{s,p}[n+1] \approx\ & w_{s,p}[n] + \\ & 2\mu \sum_{q=0}^{Q-1} e_q[n] \frac{\partial \left(\sum_{p'=0}^{P-1} \sum_{m=0}^{M} \sum_{s'=0}^{S-1} h_{q,p'}[m] w_{s',p'}[n-m] x[n-m-s']\right)}{\partial w_{q,i}[n]}. \end{aligned} \tag{4.11}$$

Assuming that the weights change slowly (μ small), then, $w_{s,p}[n-m] \approx w_{s,p}[n]$ and the previous equation can be simplified to

$$\begin{aligned} w_{s,p}[n+1] &\approx w_{s,p}[n] + \\ &\quad 2\mu\sum_{q=0}^{Q-1} e_q[n] \frac{\partial\left(\sum_{p'=0}^{P-1}\sum_{m=0}^{M}\sum_{s'=0}^{S-1} h_{q,p'}[m] w_{s',p'}[n-m] x\left[n-m-s'\right]\right)}{\partial w_{s,p}[n]} \\ &\approx w_{s,p}[n] + \\ &\quad 2\mu\sum_{q=0}^{Q-1} e_q[n] \frac{\partial\left(\sum_{p'=0}^{P-1}\sum_{m=0}^{M}\sum_{s'=0}^{S-1} h_{q,p'}[m] w_{s',p'}[n] x\left[n-m-s'\right]\right)}{\partial w_{q,i}[n]} \\ &\approx w_{s,p}[n] + \\ &\quad 2\mu\sum_{q=0}^{Q-1} e_q[n] \left(\sum_{p'=0}^{P-1}\sum_{m=0}^{M}\sum_{s'=0}^{S-1} h_{q,p'}[m] \frac{\partial w_{s',p'}[n]}{\partial w_{s,p}[n]} x[n-m-s']\right). \end{aligned} \tag{4.12}$$

Note that the derivative $\frac{\partial w_{s',p'}[n]}{\partial w_{s,p}[n]}$ is different from zero only if $p = p'$ and $s = s'$. Therefore, Equation (4.12) collapses to

$$w_{s,p}[n+1] \approx w_{s,p}[n] + 2\mu \sum_{q=0}^{Q-1} e_q[n] \sum_{m=0}^{M} h_{q,p}[m]\, x[n-m-s]. \tag{4.13}$$

Now, defining $r_{q,p}[n]$ as

$$r_{q,p}[n] \triangleq \sum_{m=0}^{M} h_{q,p}[m]\, x[n-m] \tag{4.14}$$

then, Equation (4.13) becomes

$$w_{s,p}[n+1] \approx w_{s,p}[n] + 2\mu \sum_{q=0}^{Q-1} e_q[n]\, r_{q,p}[n-s]. \tag{4.15}$$

Equation (4.15) is then used to define the weight update equation for the Multiple-Error LMS:

$$w_{s,p}[n+1] \triangleq w_{s,p}[n] + 2\mu \sum_{q=0}^{Q-1} e_q[n]\, r_{q,p}[n-s]. \tag{4.16}$$

One important characteristic of the Multiple-Error LMS method is that a plant model is needed to generate $r_{q,p}[n]$. Actually, the term $\sum_{m=0}^{M} h_{q,p}[p]\, x[n-m-s]$ can be interpreted as being the q^{th} output of the plant when the p^{th} input is $x[n-s]$ and all the other inputs are zero.

C. PROPOSED METHOD

For a time-invariant or slowly varying tonal disturbance, having a full model of the plant or a controller designed to work over a frequency band is an overkill. The system is only excited at a particular frequency and thus, the transfer functions are reduced to single complex numbers. Assuming that the plant is linear and stable, it is possible to generate any arbitrary sinusoidal at the output of the system and thus cancel any sinusoidal disturbance. A controller using this approach was presented in 1998 by Bertran and Montoro [18]. The proposed controller needs, for the studied case, only a few assumptions: a stable linear SISO plant, tonal disturbances with known frequencies and the plant without zeros at the frequencies of interest. A block diagram describing the controller is shown in Figure 4.5.

The controller proposed can be summarized as follows: assuming that the plant H is linear (see Figure 4.5), then, for any sinusoidal signal $d[n]$ with frequency ω_c it is possible to find a sinusoidal input $x[n]$ such that $y[n] = -d_n$ (if $\mathcal{H}\left(e^{j\omega_c}\right) \neq 0$). Usually one would write the input as

$$x[n] = X\cos(\omega_c n + \beta_x). \tag{4.17}$$

Several algorithms which compute the optimal value of x_n by minimizing $e[n] = y[n] + d[n]$ are available, but almost all assume that $y[n]$ is a linear combination of the parameters. The input Equation (4.17) can be changed to the equivalent form

$$x[n] = a\cos(\omega_c n) + b\sin(\omega_c n). \tag{4.18}$$

Next, assuming that $\mathcal{H}\left(e^{j\omega_c}\right) = \alpha e^{j\beta}$, the steady-state output $y[n]$ can be written as

$$y[n] = a\alpha\cos(\omega_c n + \beta) + b\alpha\sin(\omega_c n + \beta). \tag{4.19}$$

Using this form, the output $y[n]$ is linear in the parameters a and b and most adaptive algorithms can be used to find a and b. Bertran and Montoro used an update similar to the one

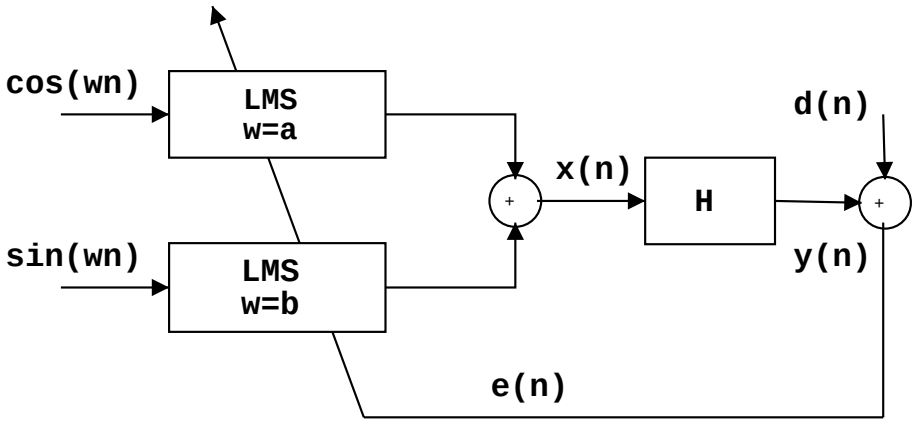

Figure 4.5. Adaptive Disturbance Canceller.

defined in the LMS method:

$$a[n+1] = a[n] + \mu e[n]\cos(\omega_c n) \tag{4.20}$$

$$b[n+1] = b[n] + \mu e[n]\sin(\omega_c n), \tag{4.21}$$

with

$$e[n] = y[n] + d[n]. \tag{4.22}$$

D. MATHEMATICAL ANALYSIS

1. Stability

Bertran and Montoro derived the stability analysis for the setup presented in this paper, but the particular plant assumed is not appropriate for the Stewart Platform problem. Therefore, a more general approach is presented in the following discussion.

The disturbance $d[n]$ can be written as

$$d[n] = \bar{A}\mathcal{H}\left(e^{j\omega_c}\right)e^{j\omega_c n}, \tag{4.23}$$

where ω_c is the frequency of the disturbance.

Assuming μ small, $A[n]$ changes slowly and the output $y[n]$ can be written as

$$y[n] \approx A[n]\,\mathcal{H}\left(e^{j\omega_c}\right)e^{j\omega_c n}. \tag{4.24}$$

Thus, since $e[n] = y[n] + d[n]$, the error is

$$\begin{aligned} e[n] &= d[n] + y[n] \\ &= \left(\bar{A} + A[n]\right)\mathcal{H}\left(e^{j\omega_c}\right)e^{j\omega_c n} \\ &= \tilde{A}[n]\,\mathcal{H}\left(e^{j\omega_c}\right)e^{j\omega_c n}. \end{aligned} \tag{4.25}$$

Using the weight update equation and the definition of $\tilde{A}[n] \triangleq \bar{A} + A[n]$, the update equation for $\tilde{A}[n]$ is given by

$$A[n+1] = A[n] + \mu e[n]\,e^{-j\omega_c n}.$$

Adding $\bar{A}$ to both sides of the previous equation leads to

$$\tilde{A}[n+1] = \tilde{A}[n] + \mu e[n]\,e^{-j\omega_c n}. \tag{4.26}$$

Also note that algorithm convergence may be proven if $\left|\tilde{A}[n+1]\right| < \left|\tilde{A}[n]\right|$, for all integer values of n. Therefore,

$$\begin{aligned} \left|\tilde{A}[n+1]\right|^2 &= \tilde{A}^*[n+1]\tilde{A}[n+1] \\ &= \left(\tilde{A}^*[n] + \mu e^*[n]\,e^{j\omega_c n}\right)\left(\tilde{A}[n] + \mu e[n]\,e^{-j\omega_c n}\right) \\ &= \left|\tilde{A}[n]\right|^2 + \tilde{A}^*[n]\,\mu e[n]\,e^{-j\omega_c n} + \tilde{A}[n]\mu^* e^*[n]\,e^{j\omega_c n} + |\mu|^2\,|e[n]|^2. \end{aligned} \tag{4.27}$$

Now, using the error value from Equation 4.25, the above expression is reduced to

$$\begin{aligned} \left|\tilde{A}[n+1]\right|^2 = {} & \left|\tilde{A}[n]\right|^2 + \tilde{A}^*[n]\,\mu\tilde{A}[n]\,\mathcal{H}\left(e^{j\omega_c}\right)e^{j\omega_c n}e^{-j\omega_c n} + \\ & \tilde{A}[n]\mu^*\tilde{A}^*[n]\,\mathcal{H}^*\left(e^{j\omega_c}\right)e^{-j\omega_c n}e^{j\omega_c n} + \\ & |\mu|^2\tilde{A}^*[n]\,\mathcal{H}^*\left(e^{j\omega_c}\right)e^{-j\omega_c n}\tilde{A}[n]\,\mathcal{H}\left(e^{j\omega_c}\right)e^{j\omega_c n}. \end{aligned}$$

Applying complex conjugate properties, the final expression for $\left|\tilde{A}[n+1]\right|^2$ is given by

$$\begin{aligned}\left|\tilde{A}[n+1]\right|^2 &= \left|\tilde{A}[n]\right|^2 + 2Re\left\{\tilde{A}[n]\mu^*\tilde{A}^*[n]\,\mathcal{H}^*\left(e^{j\omega_c}\right)\right\} + |\mu|^2\left|\tilde{A}[n]\right|^2\left|\mathcal{H}\left(e^{j\omega_c}\right)\right|^2 \\ &= \left|\tilde{A}[n]\right|^2\left(1 + 2Re\left\{\mu\mathcal{H}\left(e^{j\omega_c}\right)\right\} + |\mu|^2\left|\mathcal{H}\left(e^{j\omega_c}\right)\right|^2\right), \end{aligned} \tag{4.28}$$

and it can be concluded that $\lim_{n\to\infty}\left|\tilde{A}[n]\right|^2 = 0$ provided that

$$1 + 2Re\left\{\mu\mathcal{H}\left(e^{j\omega_c}\right)\right\} + |\mu|^2\left|\mathcal{H}\left(e^{j\omega_c}\right)\right|^2 < 1,$$

or, equivalently,

$$2Re\left\{\mu\mathcal{H}\left(e^{j\omega_c}\right)\right\} + |\mu|^2\left|\mathcal{H}\left(e^{j\omega_c}\right)\right|^2 < 0.$$

The weight $A[n]$ converges to $-\bar{A}$, as $\tilde{A}[n] = \bar{A} + A[n]$. Thus, the error converges to zero.

Assuming that $\left|\mu\mathcal{H}\left(e^{j\omega_c}\right)\right| << 1$, the stability criterion can be simplified to

$$Re\left\{\mu\mathcal{H}\left(e^{j\omega_c}\right)\right\} < 0. \tag{4.29}$$

As a guideline, μ can be selected by using

$$\mu = \frac{\mathcal{H}^*\left(e^{j\omega_c}\right)}{10\left|\mathcal{H}\left(e^{j\omega_c}\right)\right|^2}, \tag{4.30}$$

where the magnitude of the plant is not critical and the phase must be known within $\pm\pi/2$. This guideline is not strict and the model of the plant does not need to be precisely known.

2. Optimal Weights

Assuming that the controller converges, then $y[n] = -d[n]$. Assuming that the disturbance $d[n]$ is

$$d[n] = D_c e^{j(\omega_c n + \gamma_c)}, \tag{4.31}$$

then, the output $y[n]$ can be evaluated as

$$\begin{aligned} e[n] &= y[n] + d[n] \\ &= y[n] + D_c e^{j(\omega_c n + \gamma_c)}. \end{aligned}$$

The convergence of the algorithm ensures that the error converges to zero and $A[n]$ converges to a constant. Therefore,

$$\begin{aligned} e[n] &= y[n] + d[n] \\ 0 &= A\mathcal{H}\left(e^{j\omega_c}\right) e^{j\omega_c n} + D_c e^{j(\omega_c n + \gamma_c)}. \end{aligned}$$

Defining $\mathcal{H}\left(e^{j\omega_c}\right) = \alpha e^{j\beta}$, the previous expression becomes

$$\begin{aligned} 0 &= D_c e^{j(\omega_c n + \gamma_c)} + \alpha A e^{j(\omega_c n + \beta)} \\ D_c e^{j(\omega_c n + \gamma_c)} &= -\alpha A_* e^{j(\omega_c n + \beta)} \\ A_*[n] &= \frac{D_c}{\alpha} e^{j(\gamma_c - \beta + \pi)}, \end{aligned} \tag{4.32}$$

where A_* is the optimal weight.

The real coefficients a_* and b_* are obtained by rewriting Equation (4.32) in the real form

$$\begin{aligned} a_* &= -\frac{D_c}{\alpha}\cos(\gamma_c - \beta) \\ b_* &= -\frac{D_c}{\alpha}\sin(\gamma_c - \beta). \end{aligned} \tag{4.33}$$

3. Crosstalk

It is important to verify how the algorithm behaves in the presence of uncontrolled frequencies. For such an analysis the disturbance is assumed to contain two complex exponentials at frequencies ω_c and ω_{nc}. Thus

$$d[n] = D_c e^{j\omega_c n + j\gamma_c} + D_{nc} e^{j\omega_{nc} n + j\gamma_{nc}}, \tag{4.34}$$

where ω_c is the disturbance to be suppressed and ω_{nc} is not to be suppressed.

It is assumed that $\exists N \in \mathbb{N}$ (where $\mathbb{N}$ denotes the set of Natural numbers) such that $A[n] = A[n+N]$ and

$$\begin{cases} k_c \triangleq N\frac{\omega_c}{2\pi} \in \mathbb{N}, \\ k_\delta \triangleq N\frac{\delta_\omega}{2\pi} \in \mathbb{N}, \text{ and} \\ k_{nc} \triangleq N\frac{\omega_{nc}}{2\pi} \in \mathbb{N}. \end{cases}$$

The input of the plant can be written in the complex exponential form as

$$x[n] = A[n]\,\mathrm{e}^{j\omega_c n}. \tag{4.35}$$

Taking the DFT of $x[n]$ and applying the frequency shift property, $\mathcal{X}(k)$ becomes

$$\mathcal{X}(k) = \mathcal{A}(k-k_c).$$

The output $y[n]$ is

$$y[n] \quad = \quad x[n] * h[n],$$

and therefore, $\mathcal{DFT}\{y[n]\}$ is

$$\begin{aligned} \mathcal{Y}(k) &= \mathcal{X}(k)\,\mathcal{H}\left(\mathrm{e}^{j2\pi\frac{k}{N}}\right) \\ &= \mathcal{A}(k-k_c)\,\mathcal{H}\left(\mathrm{e}^{j2\pi\frac{k}{N}}\right). \end{aligned} \tag{4.36}$$

The weights $A[n]$ are updated as

$$A[n+1] = A[n] + \mu e[n]\,\mathrm{e}^{-j\omega_c n}. \tag{4.37}$$

Since $e[n] = y[n] + d[n]$, Equation (4.37) can be rewritten as

$$\begin{aligned} A[n+1] &= A[n] + \mu(y[n] + d[n])\, e^{-j\omega_c n} \\ &= A[n] + \mu e^{-j\omega_c n} y[n] + \mu e^{-j\omega_c n}\left(D_c e^{j\omega_c n + j\gamma_c} + D_c e^{j\omega_{nc} n + j\gamma_{nc}}\right) \\ &= A[n] + \mu e^{-j\omega_c n} y[n] + \mu D_c e^{j\gamma_c} e^{j\omega_c n} e^{-j\omega_c n} + \mu D_{nc} e^{j\gamma_{nc}} e^{j\omega_{nc} n} e^{-j\omega_c n} \\ &= A[n] + \mu e^{-j\omega_c n} y[n] + \mu D_c e^{j\gamma_c} + \mu D_{nc} e^{j\gamma_{nc}} e^{j\delta_\omega n}. \end{aligned} \tag{4.38}$$

Applying the DFT to Equation 4.38, leads to

$$\begin{aligned} \mathcal{DFT}\{A(n+1)\} &= \mathcal{DFT}\{A[n]\} + \mu\mathcal{DFT}\left\{e^{-j\omega_c n} y[n]\right\} + \\ &\quad \mu D_c e^{j\gamma_c}\mathcal{DFT}\{1\} + \mu D_{nc} e^{j\gamma_{nc}}\mathcal{DFT}\left\{e^{j\delta_\omega n}\right\}. \end{aligned}$$

Using DFT properties, the previous equation becomes

$$\mathcal{A}(k)\, e^{j\frac{2\pi k}{N}} = \mathcal{A}(k) + \mu\mathcal{Y}(k + k_c) + \mu D_c e^{j\gamma_c}\delta(k) + \mu D_{nc} e^{j\gamma_{nc}}\delta(k - k_\delta). \tag{4.39}$$

By substituting $\mathcal{Y}(k)$ from Equation (4.36) into Equation (4.39) leads to

$$\mathcal{A}(k)\, e^{j\frac{2\pi k}{N}} = \mathcal{A}(k) + \mu\mathcal{A}(k)\,\mathcal{H}\left(e^{j2\pi\frac{k+k_c}{N}}\right)\mu D_c e^{j\gamma_c}\delta(k) + \mu D_{nc} e^{j\gamma_{nc}}\delta(k - k_\delta). \tag{4.40}$$

The final expression can then be obtained by grouping the terms in $\mathcal{A}(k)$

$$\begin{aligned} \mathcal{A}(k)\left(e^{j\frac{2\pi k}{N}} - 1 - \mu\mathcal{H}\left(e^{j\left(\frac{2\pi k}{N} + \omega_c\right)}\right)\right) &= \mu D_c e^{j\gamma_c}\delta(k) + \\ &\quad \mu D_{nc} e^{j\gamma_{nc}}\delta(k - k_\delta). \end{aligned} \tag{4.41}$$

Equation (4.41) shows that the weights have components only at $k = 0$ and $k = k_\delta$ and thus the error only has components at ω_c and ω_{nc}. Therefore, *the controller does not create new frequencies.* Influence of the controller in the error at $\omega = \omega_{nc}$ is evaluated by replacing $k = k_\delta$ in Equation (4.41) which leads to

$$\begin{aligned} \mathcal{A}(k_\delta)\left(e^{j\frac{2\pi k_\delta}{N}} - 1 - \mu\mathcal{H}\left(e^{j\left(\frac{2\pi k_\delta}{N} + \omega_c\right)}\right)\right) &= \mu D_c e^{j\gamma_c}\delta(k_\delta) + \mu D_{nc} e^{j\gamma_{nc}}\delta(k_\delta - k_\delta) \\ &= \mu D_{nc} e^{j\gamma_{nc}}. \end{aligned} \tag{4.42}$$

Thus,

$$\mathcal{A}(k_\delta) = \frac{\mu D_{nc} e^{j\gamma_{nc}}}{e^{j\frac{2\pi k_\delta}{N}} - 1 - \mu\mathcal{H}\left(e^{j\omega_{nc}}\right)}. \tag{4.43}$$

Similar results may be obtained by evaluating Equation (4.41) at $k = 0$

$$\begin{aligned}\mathcal{A}(0)\left(e^{j\frac{2\pi 0}{N}} - 1 - \mu\mathcal{H}\left(e^{j\left(\frac{2\pi 0}{N}+\omega_c\right)}\right)\right) &= \mu D_c e^{j\gamma_c}\delta(0) + \mu D_{nc} e^{j\gamma_{nc}}\delta(0-k_\delta) \\ &= \mu D_c e^{j\gamma_c}. \end{aligned}\tag{4.44}$$

Thus,

$$\mathcal{A}(0) = \frac{D_c e^{j\gamma_c}}{\mathcal{H}\left(e^{j\omega_c}\right)}. \tag{4.45}$$

Using the fact that $\mathcal{Y}(k) = \mathcal{A}(k-k_c)\,\mathcal{H}\left(e^{j2\pi\frac{k}{N}}\right)$, $\mathcal{E}(k) = \mathcal{Y}(k) + \mathcal{D}(k)$ can be evaluated as

$$\begin{aligned}\mathcal{E}(k) &= \mathcal{Y}(k) + D_{nc} e^{j\gamma_{nc}}\delta(k-k_\delta) + D_c e^{j\gamma_c}\delta(k) \\ &= \mathcal{A}(k-k_c)\,\mathcal{H}\left(e^{j2\pi\frac{k}{N}}\right) + D_{nc} e^{j\gamma_{nc}}\delta(k-k_{nc}) + D_c e^{j\gamma_c}\delta(k-k_c) \\ &= \left(\frac{D_c e^{j\gamma_c}}{\mathcal{H}\left(e^{j\omega_c}\right)}\delta(k-k_c) + \frac{\mu D_{nc} e^{j\gamma_{nc}}}{e^{j\frac{2\pi k_\delta}{N}} - 1 - \mu\mathcal{H}\left(e^{j\omega_{nc}}\right)}\delta(k-k_{nc})\right)\mathcal{H}\left(e^{j2\pi\frac{k}{N}}\right) + \\ &\quad D_{nc} e^{j\gamma_{nc}}\delta(k-k_{nc}) + D_c e^{j\gamma_c}\delta(k-k_c). \end{aligned}\tag{4.46}$$

At this point, Equation (4.46) shows that the error has components at ω_c and ω_{nc} only. Furthermore, the disturbance at ω_{nc} does not affect the error at ω_c. Accordingly, the disturbance at ω_c does not affect the error at the frequency ω_{nc}. Thus, the controller does not generate new frequencies.

Evaluating Equation (4.46) at $k = k_{nc}$ the error due to the noncontrolled disturbance is

$$\mathcal{E}(k_{nc}) = \frac{\mu D_{nc} e^{j\gamma_{nc}}}{e^{j\frac{2\pi k_\delta}{N}} - 1 - \mu\mathcal{H}\left(e^{j\omega_{nc}}\right)}\mathcal{H}\left(e^{j\omega_{nc}}\right) + D_{nc} e^{j\gamma_{nc}}. \tag{4.47}$$

Assuming that δ_ω is small ($k_\delta << N$), then $e^{\frac{2\pi k_\delta}{N}} \approx 1$ and Equation (4.47) can be simplified to

$$\begin{aligned}
\mathcal{E}(k_{nc}) &= \frac{\mu D_{nc} e^{j\gamma_{nc}}}{e^{j\frac{2\pi k_\delta}{N}} - 1 - \mu\mathcal{H}\left(e^{j\omega_{nc}}\right)} \mathcal{H}\left(e^{j\omega_{nc}}\right) + D_{nc} e^{j\gamma_{nc}} \\
&\approx \frac{\mu D_{nc} e^{j\gamma_{nc}}}{-\mu\mathcal{H}\left(e^{j\omega_{nc}}\right)} \mathcal{H}\left(e^{j\omega_{nc}}\right) + D_{nc} e^{j\gamma_{nc}} \\
&\approx D_{nc} e^{j\gamma_{nc}} \left(1 - \frac{1}{\mathcal{H}\left(e^{j\omega_{nc}}\right)} \mathcal{H}\left(e^{j\omega_{nc}}\right)\right) \\
&\approx 0. \qquad (4.48)
\end{aligned}$$

Equation (4.48) shows that the error tends to zero when the assigned frequency tends to the exact disturbance frequency (δ_ω tends to zero). This important result shows that there is not discontinuity in the solution in the vicinity of the true solution, provided ω_{nc} is not a zero or pole of the plant.

However, assuming δ_ω is sufficiently large and $|\mu\mathcal{H}\left(e^{j\omega_{nc}}\right)| << 1$, leads to

$$\begin{aligned}
\mathcal{E}(k_{nc}) &= \frac{\mu D_{nc} e^{j\gamma_{nc}}}{e^{j\frac{2\pi k_\delta}{N}} - 1 - \mu\mathcal{H}\left(e^{j\omega_{nc}}\right)} \mathcal{H}\left(e^{j\omega_{nc}}\right) + D_{nc} e^{j\gamma_{nc}} \\
&\approx \frac{\mu D_{nc} e^{j\gamma_{nc}}}{e^{j\frac{2\pi k_\delta}{N}} - 1} \mathcal{H}\left(e^{j\omega_{nc}}\right) + D_{nc} e^{j\gamma_{nc}} \\
&\approx D_{nc} e^{j\gamma_{nc}} \left(1 + \frac{\mu}{e^{j\frac{2\pi k_\delta}{N}} - 1} \mathcal{H}\left(e^{j\omega_{nc}}\right)\right). \qquad (4.49)
\end{aligned}$$

So, using $|\mu\mathcal{H}\left(e^{j\omega_{nc}}\right)| << 1$ and assuming that $\|e^{j\delta_\omega} - 1\| \approx 1$, Equation (4.49) may be approximated by

$$\begin{aligned}
\mathcal{E}(k_{nc}) &\approx D_{nc} e^{j\gamma_{nc}} \left(1 + \frac{\mu}{e^{j\frac{2\pi k_\delta}{N}} - 1} \mathcal{H}\left(e^{j\omega_{nc}}\right)\right) \\
&\approx D_{nc} e^{j\gamma_{nc}}. \qquad (4.50)
\end{aligned}$$

The above result shows that the controller has very little impact on the component at ω_{nc} when this frequency is far from ω_c and μ is small.

E. SIMULATIONS

Simulations are conducted to verify the mathematical development and to verify whether the assumptions made are reasonable. Recall that stability conditions were derived assuming a single frequency on the error signal, and thus it is important to verify the behavior of the controller if other frequencies are present in $e[n]$. Additionally, the Adaptive Disturbance Canceller is a SISO controller; therefore, it is necessary to verify if it can control a hexapod, as it is a strongly coupled MIMO plant.

1. Single-Input/Single-Output System

The first simulation is intended to evaluate the algorithm convergence when the disturbance consisted of a single tone. The method was implemented in Simulink as described by Equations (4.20) and (4.21). The plant used was a second order system with a natural frequency of $100Hz$ and damping of 3% and its output was sampled $1,000$ times per second. The controller also ran at a $1KHz$ sampling rate. White noise was added to the error signal, with $SNR = 20dB$. The results are shown in Fig. 4.6.

Results show that the controller works as expected, even for such a high noise level. In addition, note that the controller does not affect the system at uncontrolled frequencies.

The next simulation studies the controller behavior when two tones are present in the disturbance signal ($f_c = 33Hz$ and $f_{nc} = 47Hz$), where $33Hz$ is the disturbance to be suppressed. Figure 4.7 shows that the controller cancels the assigned frequency and does not change the unassigned one ($47Hz$). The weights exhibits components at $f = 0Hz$ (from f_c), $f = 14Hz$ and $f = 80Hz$. The latter two values are predicted by theoretical results, since $|f_d - f_c| = 14Hz$ and $f_c + f_d = 80Hz$. Figure 4.8 shows the performance of the algorithm when noise is added to the sensors ($e[n]$).

Theoretical results predicted that this controller cannot be applied directly when the phase

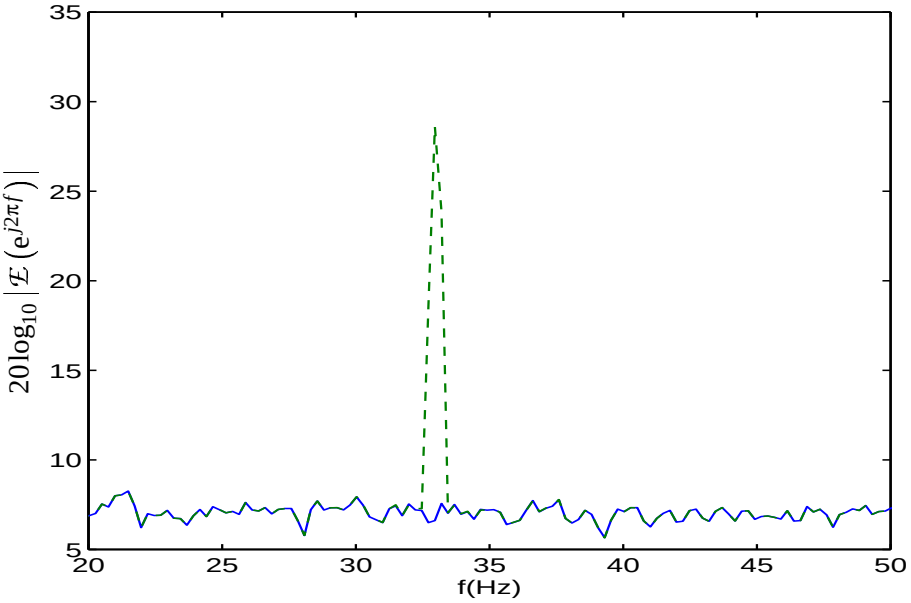

Figure 4.6. Single Noisy Tone.

of the plant is $\frac{\pi}{2}+2k\pi$ because $|1+\mu\alpha e^{j\beta}| = |1+j\mu\alpha\sin(\beta)| > 1$. In order to verify how sensitive to this parameter the method is, the plant was changed so that its phase at f_c is almost 90^o. Figures 4.9 and 4.10 show the resulting performance of the controller. As expected, the maximum $|\mu|$ is very small and thus the convergence rate is very slow.

The last SISO simulation tests the performance of the algorithm when several controlled and some uncontrolled frequencies are present. Figure 4.11 demonstrates the results for four controlled (10, 14, 34, and 36Hz) and three uncontrolled (13, 35 and 40Hz) tones. Noise was added to the error signal. It is relevant to mention that among the controlled frequencies there were 34, 35 and 36Hz, where only 34 and 36Hz are to be suppressed. The goal was to verify how selective the algorithm is. Results show the tone at 35Hz is left untouched while the tones at 34 and 36Hz are attenuated.

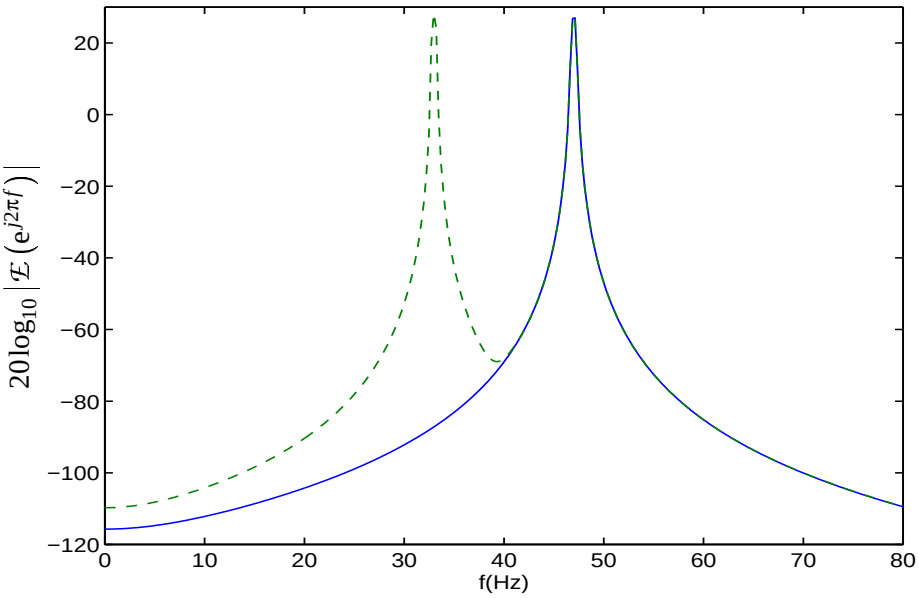

(a) Error

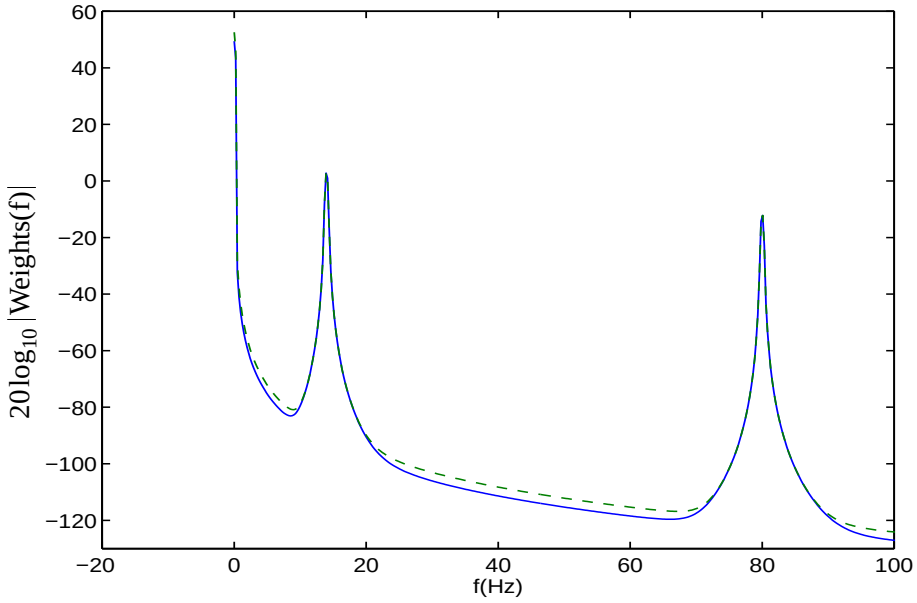

(b) Weights

Figure 4.7. Case B, No Noise.

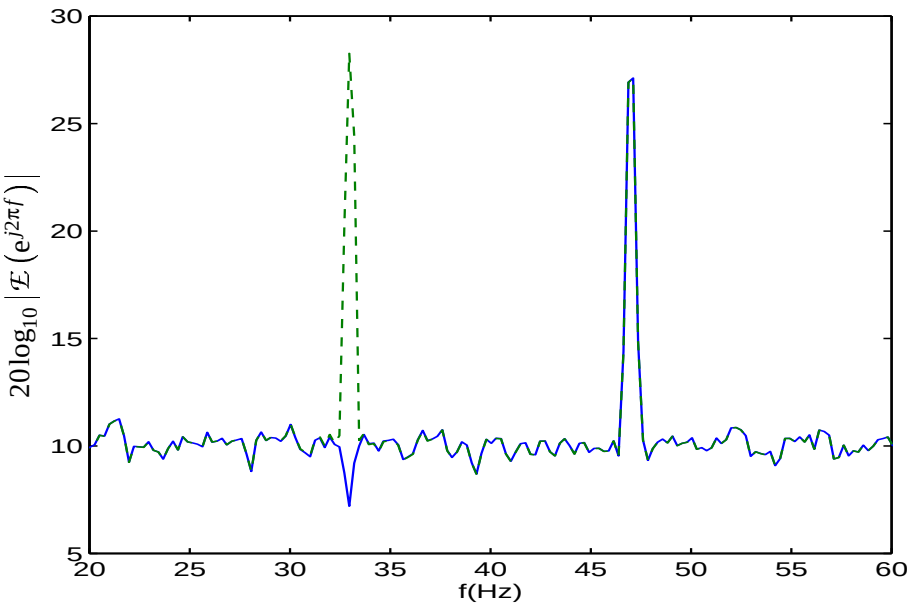

— controller on - - - controller off

(a) Error

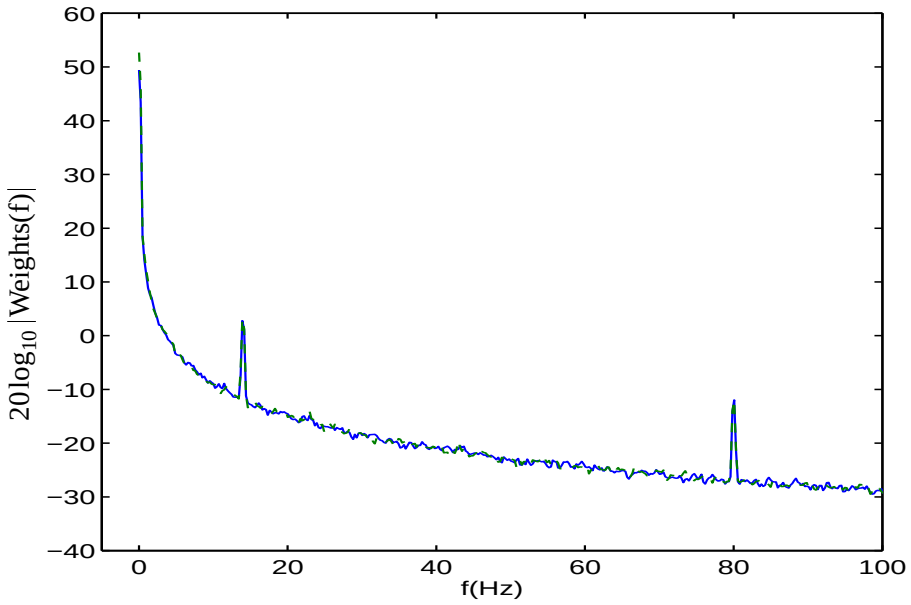

(b) Weights

Figure 4.8. Case B, Noisy.

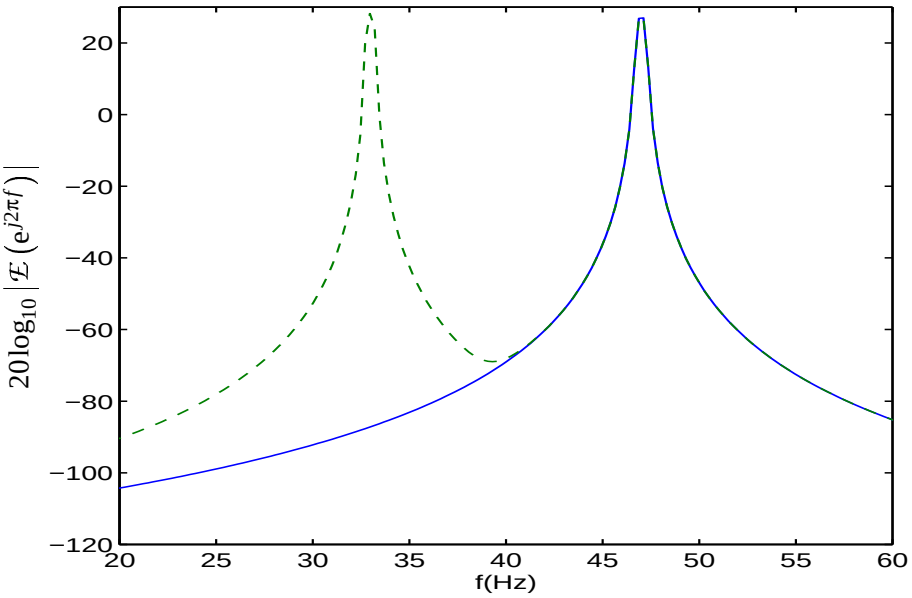

— controller on - - - controller off

(a) Error

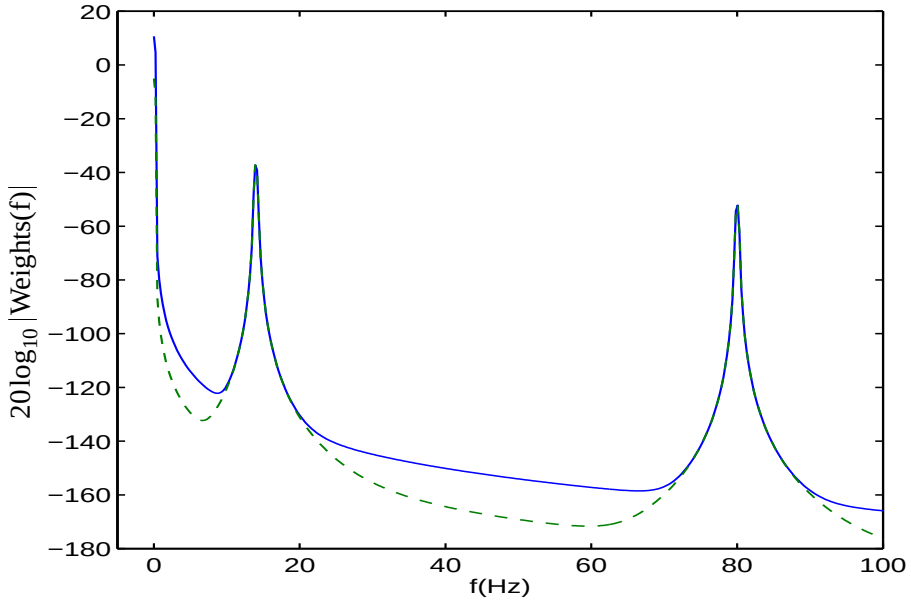

(b) Weights

Figure 4.9. Case C, No Noise.

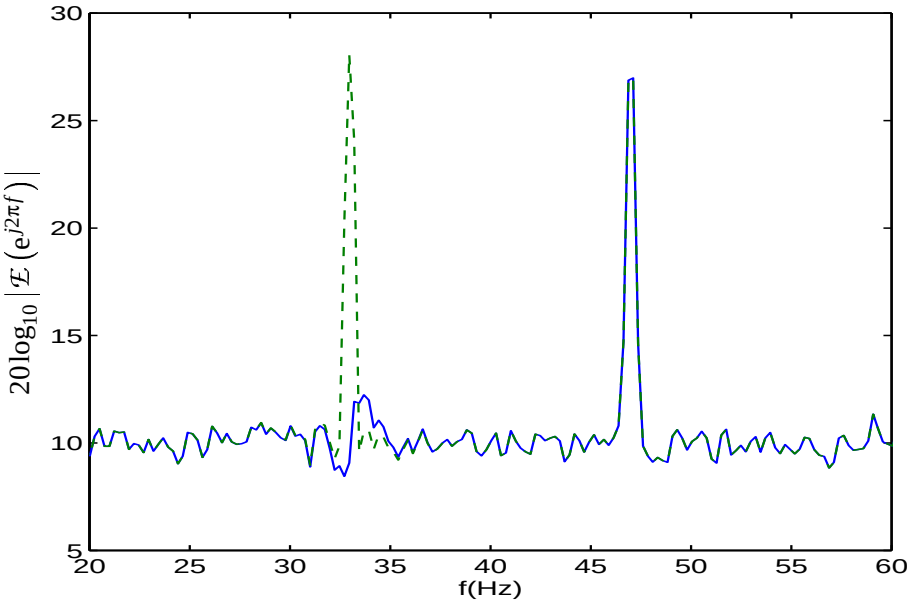

— controller on - - - controller off

(a) Error

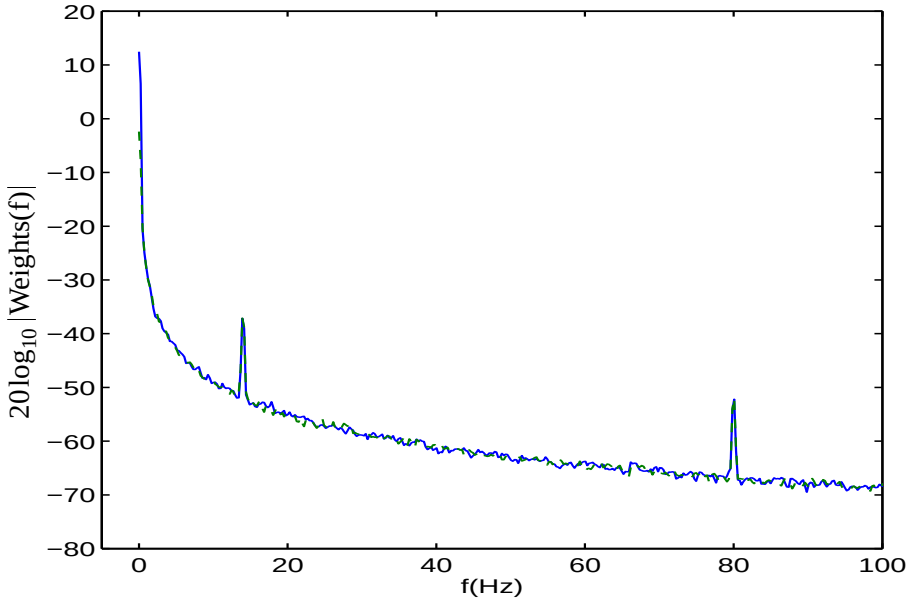

(b) Weights

Figure 4.10. Case C, Noisy.

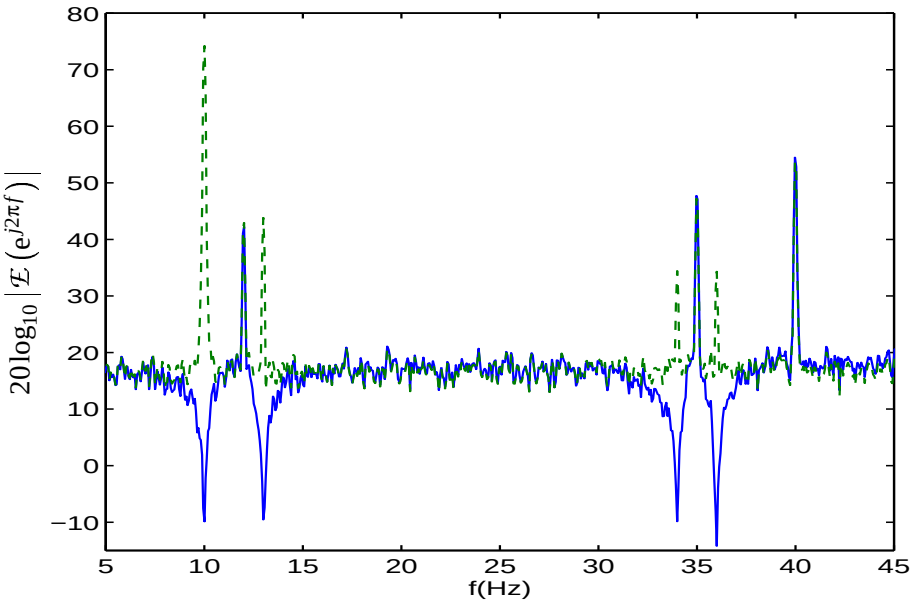

— controller on - - - controller off

Figure 4.11. Case D: Four Controlled and Three Uncontrolled Tones.

2. Multiple-Input/Multiple-Output System: The PPH

The Precision Pointing Hexapod is a highly coupled system as it is impossible to move any node separately from the others. The Adaptive Disturbance Canceller was developed as a SISO controller and either the controller, must be generalized to a MIMO approach, or a multiple-SISO approach must be taken (also called decentralized control). Previous attempts in using decentralized control had mixed success. Beavers [11] did not obtain a good performance for higher frequencies and the performance for lower frequencies was poorer than the one obtained by using the MIMO methods (Multiple-Error LMS, *Repetitive Control* and *Clear Box* [4, 14, 13]). Good results using distributed control (six independent SISO controllers) were obtained with some controllers [27, 32]. Since previous work exhibited mixed results, the mathematical model developed in Chapter III (p. 23) is followed to verify if the coupling is a limiting factor for the use of the Adaptive Disturbance Canceller on hexapods.

The simulation setup was exactly the same as that used in Section E (p. 55), but a multiple-SISO implementation was used and the plant was changed to an *S-Function* implementing the model of the hexapod according to Equations (3.28) and (3.30), on pg. 36. Simulations were made to excite the piston (bouncing), tilt/tip, twist and shear modes (see Figure 4.12).

The first case simulated shows the performance of the controller for the vibration axis coinciding with the z-axis and no rotational component (piston mode), with a frequency of $40Hz$. The results are shown in Figures 4.13 and 4.14. As one can see, the decentralized controller performed reasonably well and no competition among the controllers was seen in steady-state. The nonlinearities in the plant model are responsible for the harmonics seen in the error signal observed in Figure 4.13(a).

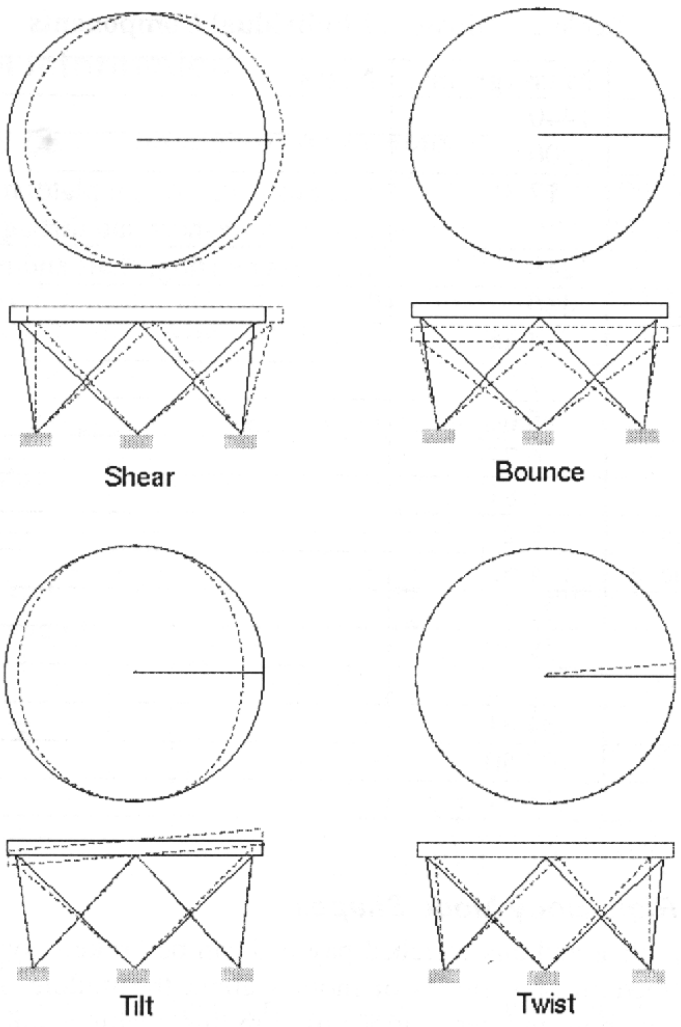

Figure 4.12. Hexapod modes [5].

The second case simulated was the twist mode in which the actuators needed to move symmetrically in order to cancel the vibration. As Figures 4.15 and 4.16 show, the performance was as expected and was the same as that obtained in the piston mode.

In the next case, a more general vibration disturbance was simulated by making each component of the signal d_n have a different amplitude (namely 1, 3, 2, -4, 3 and $-2m/s^2$). Figures 4.17 and 4.18 show the controller performed as well as in the previous two cases.

The last simulation added a second tonal ($50Hz$) disturbance to the previous case (amplitudes 2,1,6,-12,1 and $-5m/s^2$). This disturbance was not assigned to the controller and therefore, was not being controlled. The amplitudes were the same as those for Case 3. It can be seen in Figure 4.20 that the controller performed as expected.

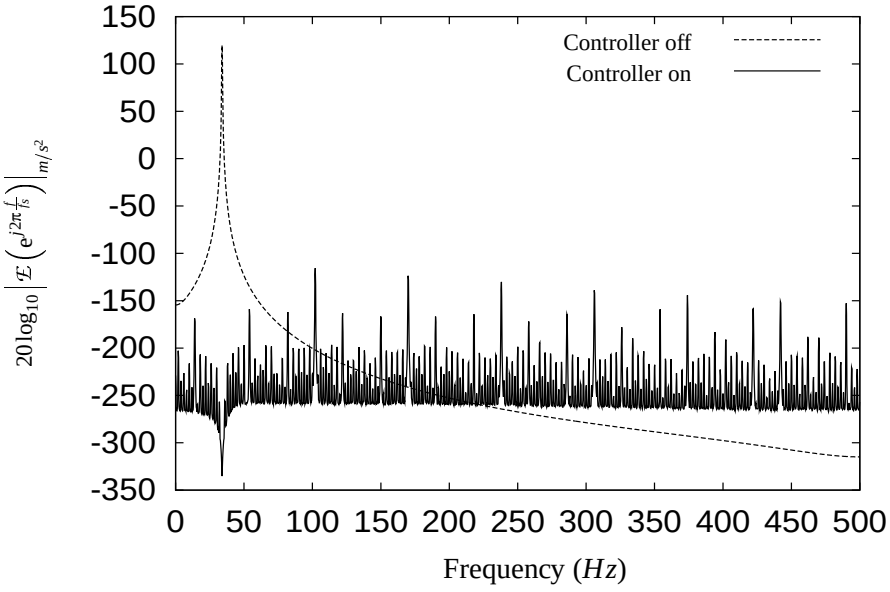

(a) Error

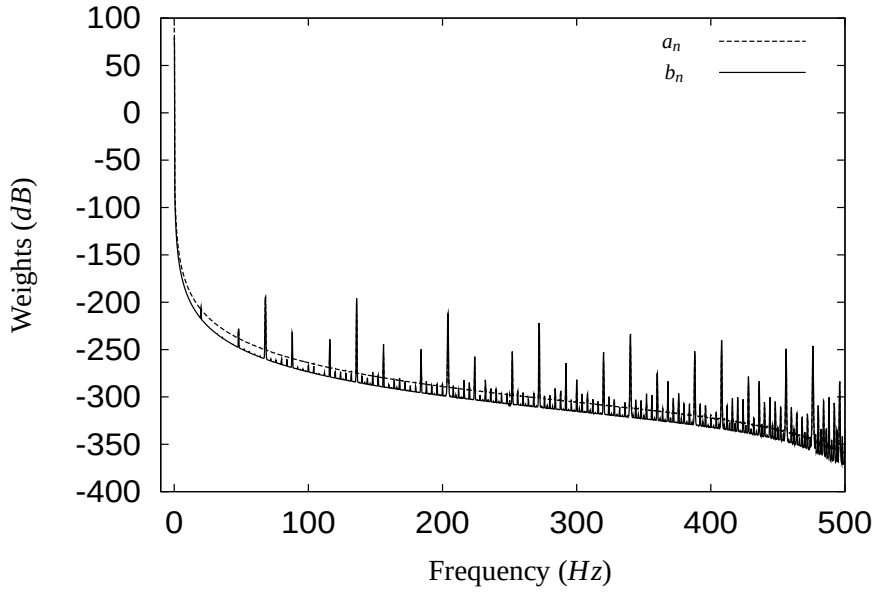

(b) Weights

Figure 4.13. PPH Simulation, Case 1, No Noise (Accelerometer #1).

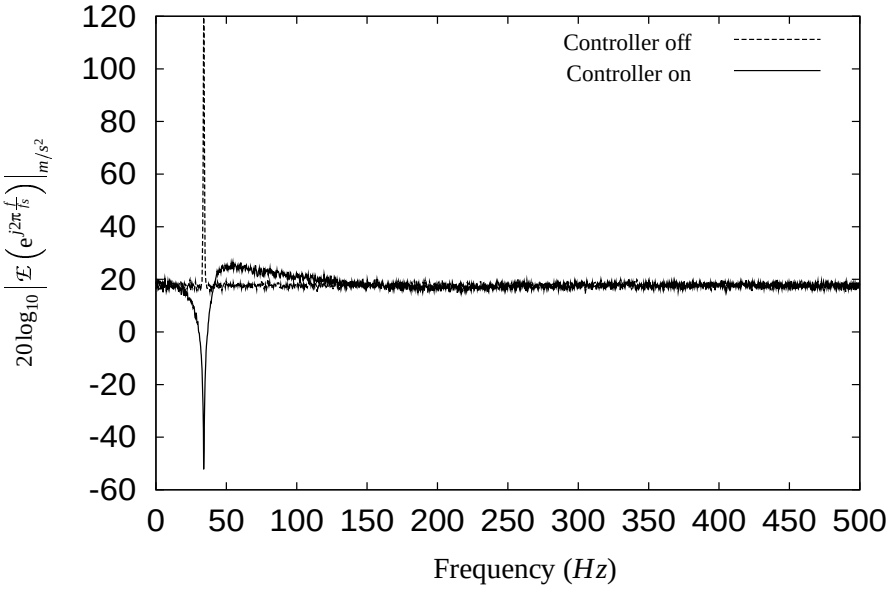

(a) Error

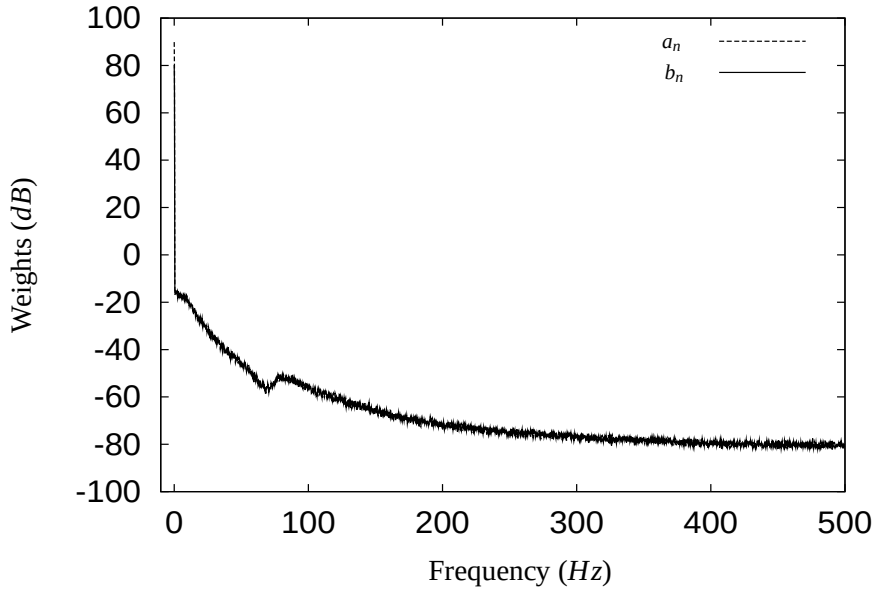

(b) Weights

Figure 4.14. PPH Simulation, Case 1, Noisy ($SNR_d = 50dB$) (Accelerometer #1).

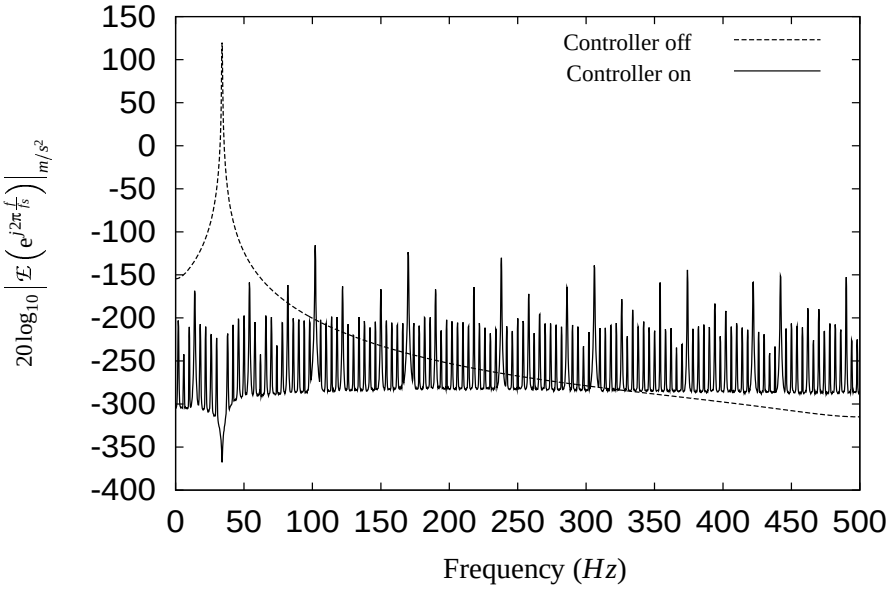

(a) Error

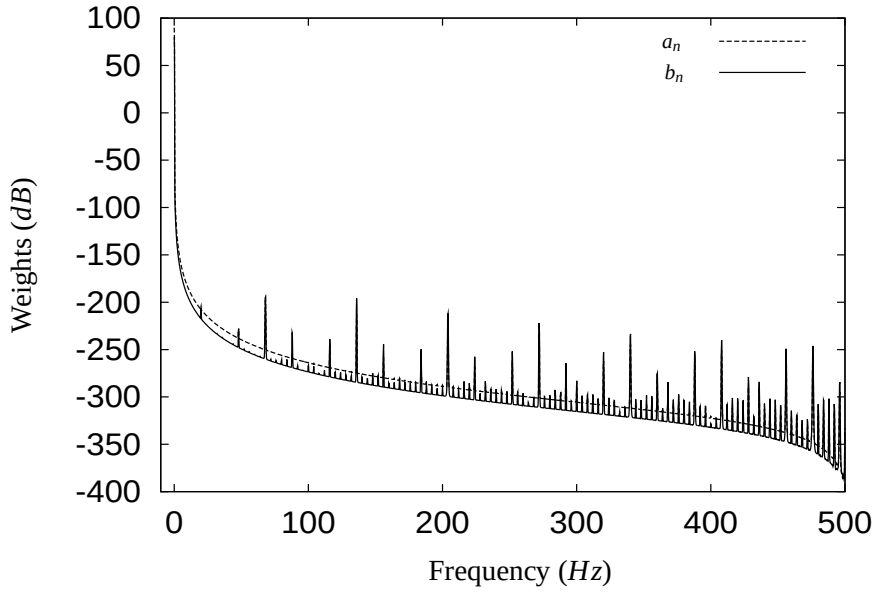

(b) Weights

Figure 4.15. PPH Simulation, Case 2, No Noise (Accelerometer #1).

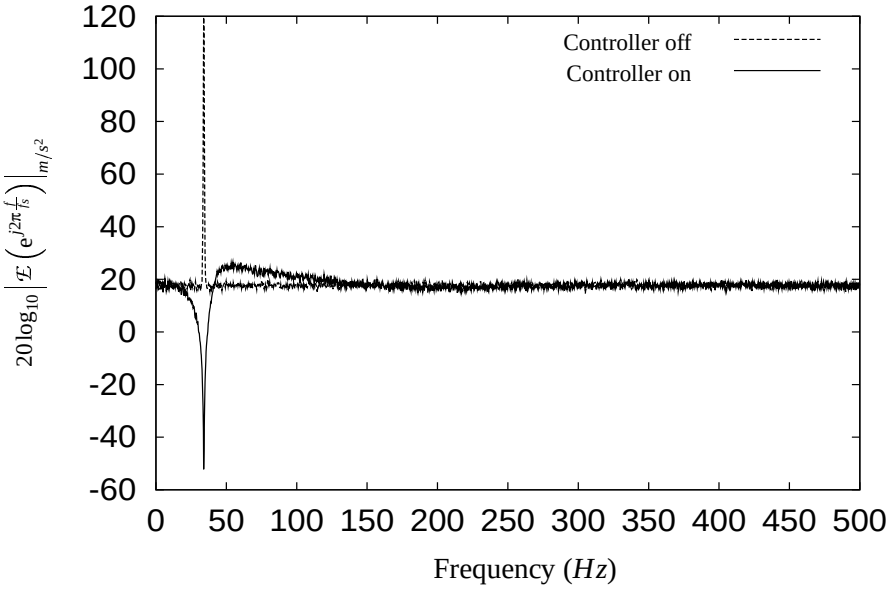

(a) Error

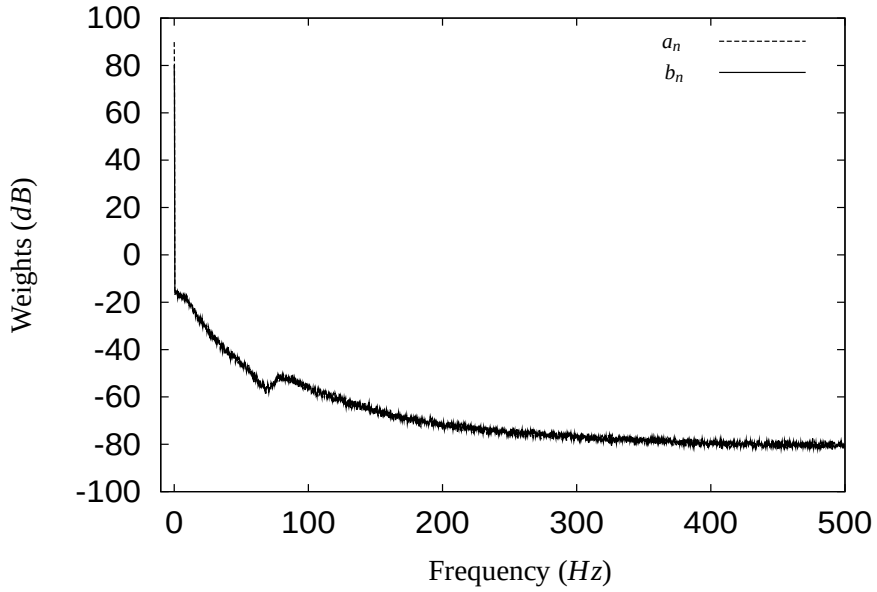

(b) Weights

Figure 4.16. PPH Simulation, Case 2, Noisy ($SNR_d = 50dB$) (Accelerometer #1).

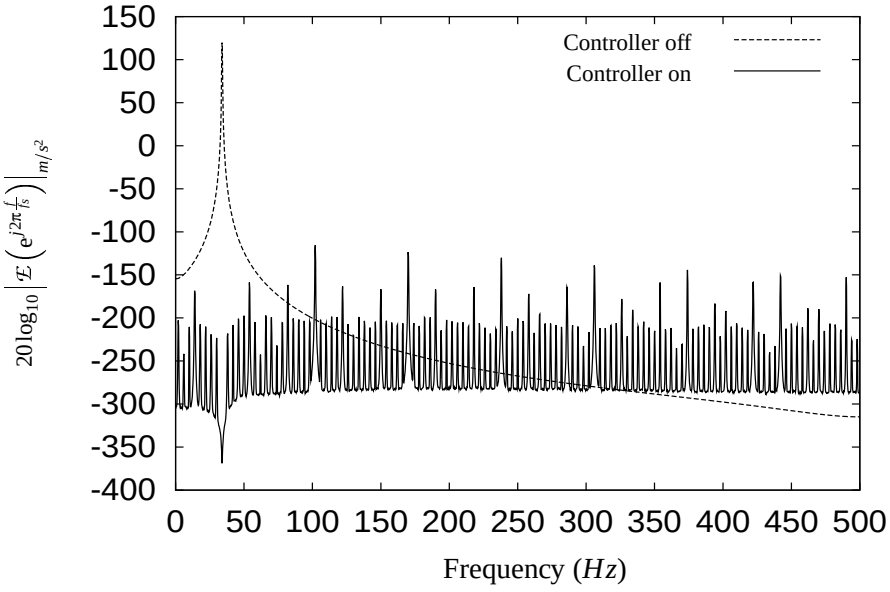

(a) Error

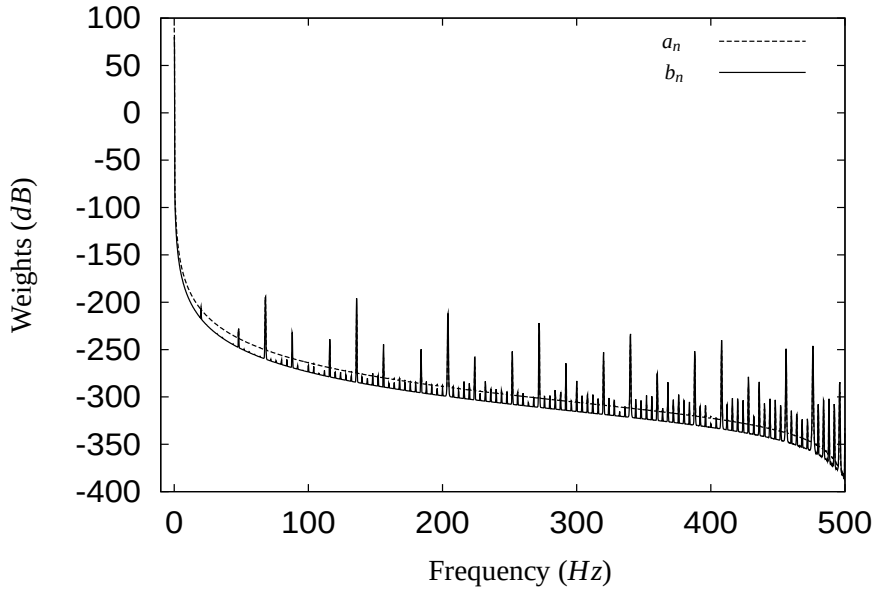

(b) Weights

Figure 4.17. PPH Simulation, Case 3, No Noise (Accelerometer #1).

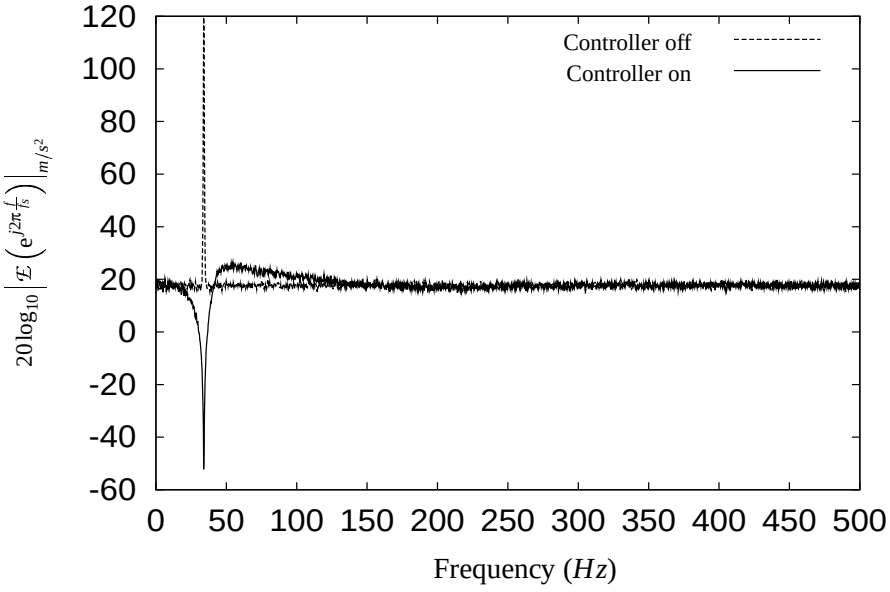

(a) Error

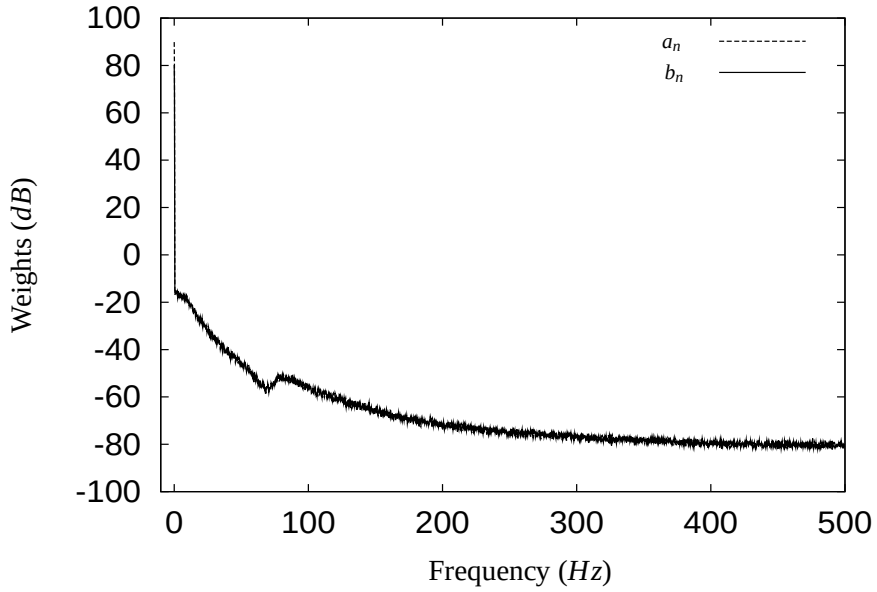

(b) Weights

Figure 4.18. PPH Simulation, Case 3, Noisy ($SNR_d = 50dB$) (Accelerometer #1).

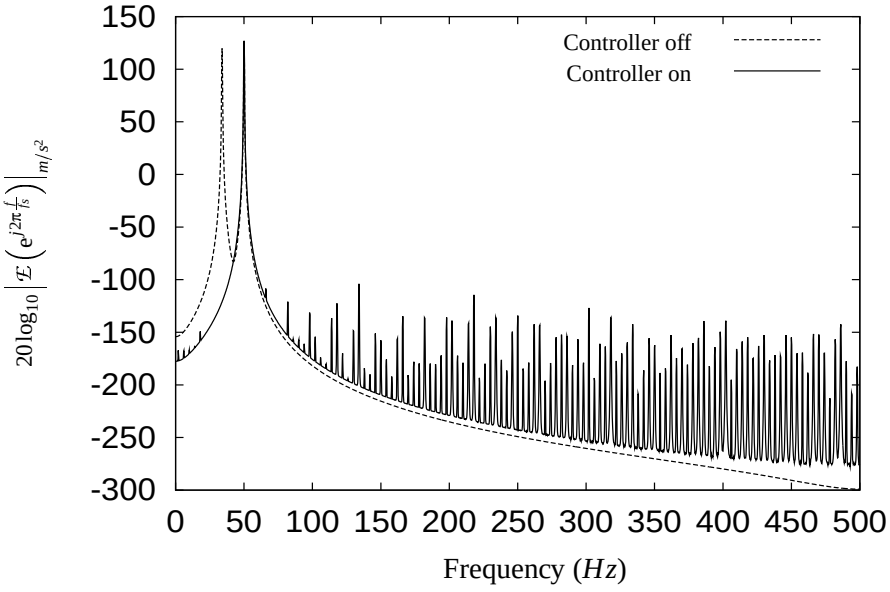

(a) Error

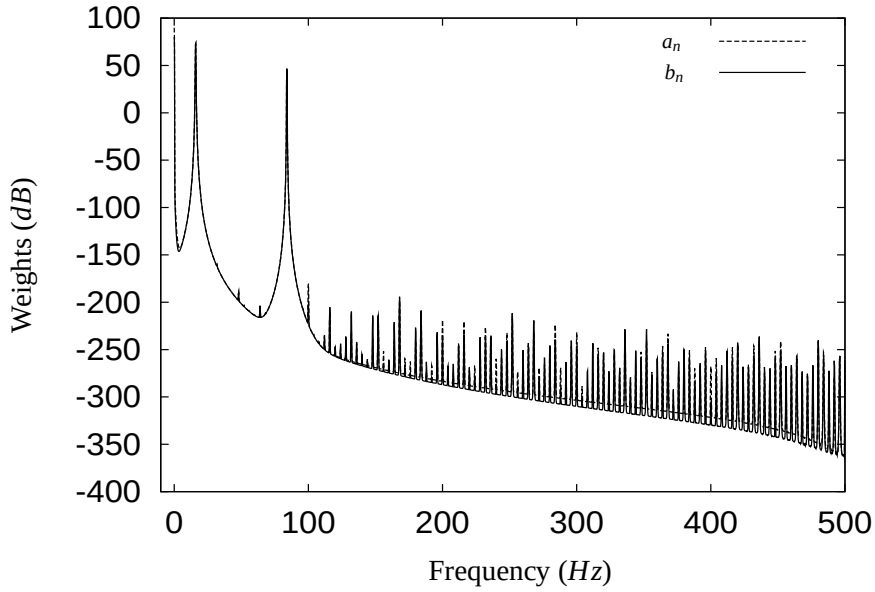

(b) Weights

Figure 4.19. PPH Simulation, Case 4, No Noise (Accelerometer #1).

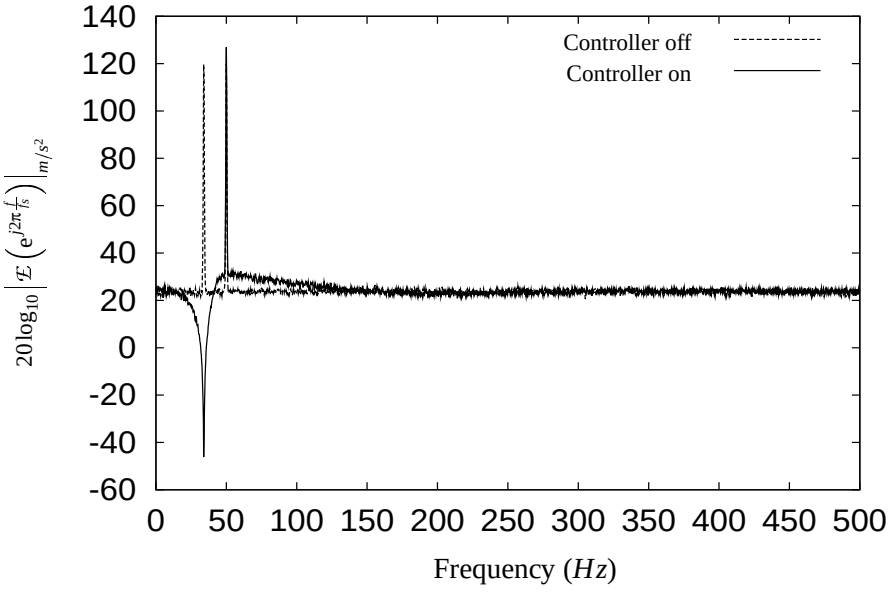

(a) Error

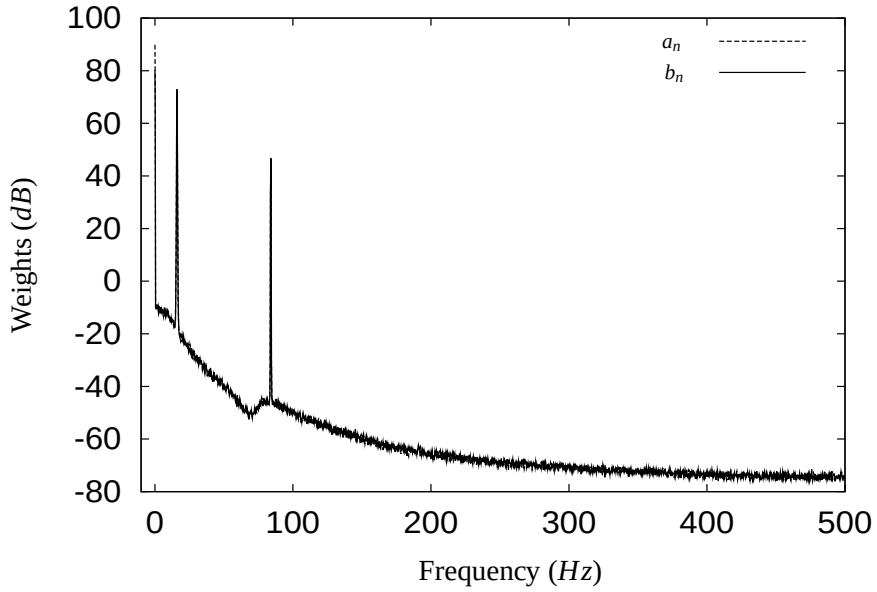

(b) Weights

Figure 4.20. PPH Simulation, Case 4, Noisy ($SNR_d = 50dB$) (Accelerometer #1).

F. COMMENTS

The simulations verified the theoretical results and the Adaptive Disturbance Canceller exhibited good performance even when used in a distributed configuration and in the presence of strong nonlinearities. It is also important to mention that the vibration suppression was not degraded by the presence of noise in the measurements. This result was consistent for both the SISO and the MIMO simulations.

The simulations also confirmed the theoretical results about the unassigned frequencies: the controller does not affect the error at frequencies different from the assigned ones, indicating that this controller is very selective.

It is important to recognize that the properties mentioned in the last two paragraphs are interrelated: one exists because of the other and vice-versa. Since the controller uses a synthetic signal as input, it is very insensitive to noise. But a synthetic reference signal assigned to an incorrect frequency will prevent the controller from canceling the disturbance.

As expected, the controller did not generate any new frequency in the SISO simulations, which used a linear plant. The Precision Pointing Hexapod model used in the MIMO simulations considers the geometric nonlinearities of the hexapod. These nonlinearities generated harmonics that appear over the entire range of frequencies, although the harmonics are very small because the displacement of the top plate is small and thus the angles are small. Nonetheless, this effect is expected to be amplified if other nonlinearities sources are present, such as static friction and backslash.

Note that one important limitation of this method is the requirement for the precise frequency of the disturbance or the performance will suffer considerably. This effect was already observed by Tsuei et al. in [33], which presented a modified version of the Filtered-X LMS with synthetic input.

THIS PAGE INTENTIONALLY LEFT BLANK

V. COMPUTATIONAL COST ESTIMATION

A. OVERVIEW

This chapter compares the computational cost required to implement the Adaptive Disturbance Canceller and the Multiple-Error LMS method. Both computational complexity and memory requirements are compared.

Section B defines the methodology followed to estimate the computational cost. Section C and Section D present the computational cost for the Multiple-Error LMS and the Adaptive Disturbance Canceller respectively.

Section E compares the computational cost and memory requirements for both controllers. One example is presented in which a hexapod is used to suppress three tones with one harmonic each.

B. BASIC CONCEPTS

Vibration control requires large amounts of computational power. The frequencies involved are usually higher than the traditional control methods; therefore, the sampling rates are also higher. One of the main purposes of this research is to study a vibration method that requires minimal computational resources. The controller, after being implemented, should consume the least amount of electrical power possible. Additionally, the computer system should require as little space as possible, since electrical power, weight and space are very expensive in space applications. Ideally, a single low-power microcontroller, with no external memory and no external A/D converters should be used.

Floating point operations *used to be* the most expensive operations; consequently, the complexity of an algorithm is traditionally measured by counting floating-point operations. It was not uncommon for a simple floating-point multiplication to be emulated in software or to need a dedicated external chip to be executed. The advances in microelectronics changed the picture: CPUs have evolved. The new DSP CPUs can perform one floating-point multiplication as fast as they can perform one floating-point summation or even integer math. Table 5.1 shows the specifications of an embeddable microcontroller/DSP (Hitachi's SH7410, a CPU for embedded devices). This microcontroller CPU has a DSP unit embedded, interrupt controllers, memory, A/D converters, timers, etc. The power consumption is very small (0.5W versus about 60W for an Intel's Pentium III or an AMD's Athlon). Therefore, if a vibration control solution can fit in a few dozen kilobytes of ROM and does not need more than a few kilobytes of RAM, the savings in space, weight and power are *very* significant. As an even simpler alternative, the controller could be converted to use integer arithmetic or floating-point emulation and use a CPU that does not support floating-point. These are more easily available and come with a wider array of features (some featuring eight 12bits A/D conversors and eight D/A conversors), making it possible to implement the controller with very few components and little power consumption.

Voltage	$3.3V$
Operating current	110 to $210mA$
Operating power consumption	0.36 to $0.69W$
Standby current	$5\mu A$
Standby power	$20\mu W$
Time per operation (fetch, multiply and divide)	$33ns/operation$
ROM	$48Kb$
RAM	$8Kb$
Cycle/instruction basic instructions	1 cycle
Cycles needed for DSP multiplication	1 cycle
Cycles needed for integer multiplication	1 to 4 cycles
Interrupt controller embedded	
Other Features	Timers, A/D converters, serial communication

Table 5.1. Main Characteristics of the SH7410 (SH-DSP, SH2 Family).

In the light of the realities of the new CPUs, evaluating an algorithm purely by its floating-point complexity is clearly not enough anymore. Using a single measure is no longer possible, since the performance of an algorithm will depend heavily on the implementation and on the architecture of the hardware.

The goal of the computational cost evaluation in this research is more ambitious than just comparing different methods. It is intended to be used as a guideline to evaluate if a particular CPU can be used to implement the algorithm in real time. As such, the evaluation of complexity estimate will not measure only floating-point operations. The following items will be counted:

- *Floating-Point Multiplication/Division ($\mathbb{M}_f$)* . These are some of the most important operations as their cost can be much higher than most other operations when the computer does not have floating-point operations implemented in hardware.
- *Floating-Point Sum/Subtraction ($\mathbb{S}_f$).* Important for the same reasons as presented above.
- *Integer Multiplication ($\mathbb{M}_i$).* Integer operations can be very fast in complex CPUs. But the low-cost and low-power ones can usually be slower for multiplication, taking several cycles.
- *Integer Division ($\mathbb{D}_i$).* Integer divisions are a complex case. Some low-end CPUs may not implement a full set of division operations. Thus some sort of software emulation may be needed.
- *Integer Sum/Subtraction ($\mathbb{S}_i$).* These operations are among the fastest ones, but also among the most frequent. For fast CPUs, they are as fast as multiplications and divisions. But for low-end CPUs, summations/subtractions are much faster.
- *Matrix Element Access ($\mathbb{M}_{atr}$).* Almost every operation in a computer occurs in the CPU, and most involve registers themselves or register and memory. Fetching data from memory to registers takes time, which is very important for matrix manipulations. Even taking into account

that matrix operations frequently use the same base address, they still involve mathematical operations on the index prior to fetching the actual value.

- *Transcendental Functions ($\mathbb{T}_{ranc}$).* The actual implementation of these functions varies depending on the algorithm used. Some dedicated hardware are can of performing some of these operations, but usually they require several CPU cycles. While this may not be perceptible in fast parallelizing CPUs, the cost can be quite high for simpler ones. Operations not provided by the CPU must be emulated in software and, again, the computation time is very dependent on the algorithm, implementation and desired precision.

C. MULTIPLE-ERROR LMS

A reference must be established in order to evaluate the numerical complexity of the proposed vibration suppression method. The most natural one is the Multiple-Error LMS due to its widespread acceptance.

The ultimate objective of any vibration control algorithm is to generate inputs for the plant H, which in the Multiple-Error LMS is done by using the Equation (4.4), reproduced below:

$$u_i[n] = \sum_{q=0}^{Q-1} w_{q,i}[n]\, x[n-q], \tag{5.1}$$

where $x[n]$ is the reference signal, $w_{q,i}[n]$ is the weight matrix and Q is the order of the filter and u_i is the i^{th} input of the plant ($0 < i < N_i + 1$).

The number of operations necessary is

$$\begin{aligned}
\mathbb{N}\{u_i[n]\} &= \mathbb{N}\left\{ \sum_{q=0}^{Q-1} w_{q,i}[n]\, x[n-q] \right\} \\
&= (Q-1)\,\mathbb{S}_f + Q\mathbb{N}\left\{ w_{q,i}[n]\, x[n-q] \right\} \\
&= (Q-1)\,\mathbb{S}_f + Q\,(1\mathbb{M}_f + 1\mathbb{S}_i + 2\mathbb{M}_{atr}) \\
&= (Q-1)\,\mathbb{S}_f + Q\mathbb{M}_f + Q\mathbb{S}_i + 2Q\mathbb{M}_{atr},
\end{aligned} \tag{5.2}$$

where $\mathbb{N}\{\bullet\}$ means *number of operations required to evaluate* $\bullet$.

Therefore, the number of operations required to calculate the whole vector $\mathbf{u}[n]$ is

$$\mathbb{N}\{\mathbf{u}[n]\} = N_i(Q-1)\mathbb{S}_f + N_iQ\mathbb{M}_f + N_iQ\mathbb{S}_i + 2N_iQ\mathbb{M}_{atr}. \tag{5.3}$$

The next step is to calculate the weights at time $n+1$. To do that, one of the intermediate steps is to evaluate $r_{o,i}$ for all q's:

$$\begin{aligned}
\mathbb{N}\{r_{o,i}[n]\} &= \mathbb{N}\left\{\sum_{p=0}^{P} h_{o,i}[p]\,x[n-p]\right\} \\
&= P\mathbb{S}_f + (P+1)\,\mathbb{N}\{h_{o,i}[p]\,x[n-p]\} \\
&= P\mathbb{S}_f + (P+1)\,(1\mathbb{M}_f + 1\mathbb{S}_i + 2\mathbb{M}_{atr}) \\
&= P\mathbb{S}_f + (P+1)\,\mathbb{M}_f + (P+1)\,\mathbb{S}_i + 2\,(P+1)\,\mathbb{M}_{atr},
\end{aligned} \tag{5.4}$$

where P is the order of the estimate of the plant and $h_{o,i}[n]$ is the estimate of the o^{th} output of the plant, due to the i^{th} input.

Therefore, the weight update operations count is

$$\begin{aligned}
\mathbb{N}\{w_{q,i}[n+1]\} &= \mathbb{N}\left\{w_{q,i}[n] + 2\mu\sum_{o=0}^{N_o-1} e_o[n]\,r_{o,i}[n-q]\right\} \\
&= 1\mathbb{M}_{atr} + 1\mathbb{S}_f + \mathbb{N}\left\{2\mu\sum_{o=0}^{N_o-1} e_o[n]\,r_{o,i}[n-q]\right\} \\
&= 1\mathbb{M}_{atr} + 1\mathbb{S}_f + 1\mathbb{M}_f + \mathbb{N}\left\{\sum_{o=0}^{N_o-1} e_o[n]\,r_{o,i}[n-q]\right\} \\
&= 1\mathbb{M}_{atr} + 1\mathbb{S}_f + 1\mathbb{M}_f + (N_o-1)\,\mathbb{S}_f + N_o\mathbb{N}\{e_o[n]\,r_{o,i}[n-q]\} \\
&= 1\mathbb{M}_{atr} + 1\mathbb{S}_f + 1\mathbb{M}_f + (N_o-1)\,\mathbb{S}_f + \\
&\quad N_o\,(1\mathbb{M}_f + 1\mathbb{S}_i + 1\mathbb{M}_{atr} + \mathbb{N}\{r_{o,i}[n-q]\}).
\end{aligned} \tag{5.5}$$

The computational effort to evaluate $r_{o,i}[n]$ is given by Equation (5.4) and is $P\mathbb{S}_f + (P+1)\,\mathbb{M}_f + (P+1)\,\mathbb{S}_i + 2\,(P+1)\,\mathbb{M}_{atr}$. Since Equation (5.5) needs time to be shifted to $n-q$,

one integer sum must be added to the result

$$\begin{aligned}
\mathbb{N}\left\{w_{q,i}[n+1]\right\} &= 1\mathbb{M}_{atr}+1\mathbb{S}_f+1\mathbb{M}_f+(N_o-1)\,\mathbb{S}_f+ \\
&\quad N_o\mathbb{M}_f+N_o\mathbb{S}_i+N_o\mathbb{M}_{atr}+ \\
&\quad N_o\left(P\mathbb{S}_f+(P+1)\,\mathbb{M}_f+(P+1)\,\mathbb{S}_i+2\,(P+1)\,\mathbb{M}_{atr}+\mathbb{S}_i\right) \\
&= \left(N_o+1+2N_o\,(P+1)\right)\mathbb{M}_{atr}+\left(1+(No-1)+N_oP\right)\mathbb{S}_f+ \\
&\quad \left(1+N_o+N_o\,(P+1)\right)\mathbb{M}_f+\left(N_o+N_o\,(P+1)+N_o\right)\mathbb{S}_i \\
&= \left(1+N_o\,(1+2\,(P+1))\right)\mathbb{M}_{atr}+N_o\,(P+1)\,\mathbb{S}_f+ \\
&\quad \left(1+N_o\,(P+2)\right)\mathbb{M}_f+N_o\,(P+2)\,\mathbb{S}_i. \qquad (5.6)
\end{aligned}$$

Therefore, it is possible to evaluate the computational effort to evaluate the matrix **W** (of dimensions QxN_i) by using Equation (5.6)

$$\begin{aligned}
\mathbb{N}\{\mathbf{W}[n+1]\} &= N_iQ\left(1+N_o\,(1+2\,(P+1))\right)\mathbb{M}_{atr}+N_iQN_o\,(P+1)\,\mathbb{S}_f+ \\
&\quad N_iQ\left(1+N_o\,(P+2)\right)\mathbb{M}_f+N_iQN_o\,(P+2)\,\mathbb{S}_i. \qquad (5.7)
\end{aligned}$$

Therefore, the total computational effort required to implement the Multiple-Error LMS algorithm is the sum of the effort to compute $\mathbf{u}[n]$ and $\mathbf{W}[n+1]$

$$\begin{aligned}
\mathbb{N}\{\mathbf{W}[n+1]\}+\mathbb{N}\{\mathbf{u}[n]\} &= N_iQ\left(1+N_o\,(1+2\,(P+1))\right)\mathbb{M}_{atr}+N_iQN_o\,(P+1)\,\mathbb{S}_f+ \\
&\quad N_iQ\left(1+N_o\,(P+2)\right)\mathbb{M}_f+N_iQN_o\,(P+3)\,\mathbb{S}_i+ \\
&\quad N_i\,(Q-1)\,\mathbb{S}_f+N_iQ\mathbb{M}_f+N_iQ\mathbb{S}_i+2N_iQ\mathbb{M}_{atr} \\
&= N_iQ\left(3+N_o\,(1+2\,(P+1))\right)\mathbb{M}_{atr}+ \\
&\quad N_i\left(Q\left(1+N_o\,(P+1)\right)-1\right)\mathbb{S}_f+ \\
&\quad N_iQ\left(2+N_o\,(P+2)\right)\mathbb{M}_f+ \\
&\quad N_iQ\left(1+N_o\,(P+2)\right)\mathbb{S}_i. \qquad (5.8)
\end{aligned}$$

Note that it is safe to assume that $P >> 1$ and $Q >> 1$ for complex plants. Applying these assumptions, an approximate estimate of the computational effort is

$$\begin{aligned}
\mathbb{N}\{ME-LMS\} &\approx N_i Q\left(3+N_o\left(1+2\left(P+1\right)\right)\right)\mathbb{M}_{atr}+ \\
&\quad N_i\left(Q\left(1+N_o\left(P+1\right)\right)-1\right)\mathbb{S}_f+ \\
&\quad N_i Q\left(2+N_o\left(P+2\right)\right)\mathbb{M}_f+ \\
&\quad N_i Q\left(1+N_o\left(P+2\right)\right)\mathbb{S}_i \\
&= 2N_i N_o PQ\mathbb{M}_{atr}+N_i N_o PQ\mathbb{S}_f+ \\
&\quad N_i N_o PQ\mathbb{M}_f+N_i N_o PQ\mathbb{S}_i \\
&= N_i N_o PQ\left(2\mathbb{M}_{atr}+\mathbb{S}_f+\mathbb{M}_f+\mathbb{S}_i\right). \qquad (5.9)
\end{aligned}$$

The implementation of the Multiple-Error LMS used for the experiments described in Section VI.D uses a plant model of order 30 and a filter order of 10. Therefore, an estimate of the number of operations would be

$$\begin{aligned}
\mathbb{N}\{ME-LMS\} &\approx N_i N_o PQ\left(2\mathbb{M}_{atr}+\mathbb{S}_f+\mathbb{M}_f+\mathbb{S}_i\right) \\
&\approx 10,800\left(2\mathbb{M}_{atr}+\mathbb{S}_f+\mathbb{M}_f+\mathbb{S}_i\right). \qquad (5.10)
\end{aligned}$$

Not desiring to enter into the details of the CPU used in the experiment, it is assumed that the CPU takes only one cycle to perform each of the computed measures. Therefore, the total number of CPU cycles needed by the algorithm for each iteration is

$$\mathbb{N}\{ME-LMS\} \approx N_i N_o Q^2\left(2+1+1+1\right)=54,000. \qquad (5.11)$$

Since the sampling rate used by the algorithms in the Ultra-Quiet Platform are is $1KHz$, that means that the CPU would need to execute more than 5410^6 instructions per second, which gives an estimate of the clock needed. The actual speed needed will also depend on the compiler

optimization, on the code implementation and on other activities that the processor may be executing in parallel (I/O, D/A conversions, A/D conversions, filtering, context switching, etc).

The microcontroller described in the previous section can execute each instruction in $33ns$, or about $3\,10^7$ instructions per second. Therefore, this microcontroller cannot be used to implement the Multiple-Error LMS on a hexapod if $P \geq 30$ and $Q \geq 10$.

1. Memory Requirements

An estimate of the algorithm memory requirements is very important to decide wether a particular hardware setup can be used for implementation or not. For microcontrollers, this estimate indicates if the controller will fit in the on-chip memory or not. For more complex CPUs, this quantity is important to verify if the application can fit in the cache memory (much faster than conventional memory).

From previous developments it is clear that the Multiple-Error LMS cannot be implemented in a low-power CPU. Since a full-fledged processor is needed, one with a large on-chip cache could be selected and ideally all the code and data would run from the cache and the speed would be improved by a large factor.

The biggest portions of RAM memory required by the Multiple-Error LMS method are used to hold the plant transfer function estimate **H** and the weight **W**. Thus, the number of values to be stored is

$$\text{mem}_h = (P+1)\, N_i N_o, \tag{5.12}$$

as the plant has order P and dimensions $N_i \times N_o$.

Similarly, the weight matrix **W** demands

$$\text{mem}_W = Q N_i. \tag{5.13}$$

The total memory required for a Multiple-Error LMS controller is approximately the sum of the memory needed for the estimate of the plant and weights

$$\text{mem}_{MELMS} \approx N_i(Q + (P+1)N_o). \tag{5.14}$$

The number of elements to be stored for the hexapod example is approximately

$$\text{mem} \approx 6 \times (10 + (30+1) \times 6) = 1,476. \tag{5.15}$$

The total memory is about 6Kbytes (4 bytes/float). This is not a very large amount and might possibly fit in the cache of the CPU (if one is present). If the code size can be kept to a small reasonable amount (a few kilobytes), then the whole code and data could run off the cache and the speed gains would be substantial.

D. ADAPTIVE DISTURBANCE CANCELLER

Cost estimation for the Adaptive Disturbance Canceller is much easier than that of the Multiple-Error LMS approach. As in the previous section, the computation starts by evaluating the input to the plant using

$$\begin{aligned}
\mathbb{N}\{u[n]\} &= \mathbb{N}\{a[n]\cos(\omega_c n) + b[n]\sin(\omega_c n)\} \\
&= \mathbb{N}\{a[n]\cos(\omega_c n)\} + \mathbb{N}\{b[n]\sin(\omega_c n)\} + 1\mathbb{S}_f - 2\mathbb{M}_{atr} - 1\mathbb{M}_f \\
&= 2(2\mathbb{M}_f + \mathbb{T}_{ranc} + 3\mathbb{M}_{atr}) + 1\mathbb{S}_f - 2\mathbb{M}_{atr} - 1\mathbb{M}_f \\
&= 3\mathbb{M}_f + 2\mathbb{T}_{ranc} + 4\mathbb{M}_{atr} + 1\mathbb{S}_f,
\end{aligned} \tag{5.16}$$

where $a[n]$ and $b[n]$ are the weights of the controller.

Please note that the time needed to fetch the variables to the memory was added as a matrix operation, which is logical for multiple-frequency and distributed implementations.

The weight update equation cost can be computed as

$$\begin{aligned}
\mathbb{N}\{a[n+1]\}+\mathbb{N}\{b[n+1]\} &= \mathbb{N}\{a[n]+\mu e[n]\cos(\omega_d n)\}+ \\
&\quad \mathbb{N}\{b[n]+\mu e[n]\sin(\omega_d n)\}-(\text{common part}) \\
&= 2\mathbb{N}\{a[n]+\mu e[n]\cos(\omega_d n)\}-4\mathbb{M}_{atr}-2\mathbb{M}_f \\
&= -2\mathbb{M}_f-2\mathbb{M}_{atr}+2\mathbb{S}_f+2\mathbb{N}\{\mu e[n]\cos(\omega_d n)\} \\
&= -2\mathbb{M}_f-2\mathbb{M}_{atr}+2\mathbb{S}_f+2\left(3\mathbb{M}_f+1\mathbb{T}_{ranc}+4\mathbb{M}_{atr}\right) \\
&= 4\mathbb{M}_f+2\mathbb{T}_{ranc}+6\mathbb{M}_{atr}+2\mathbb{S}_f. \qquad (5.17)
\end{aligned}$$

By summing values from Equation (5.16) and Equation (5.17), the cost is

$$\begin{aligned}
\mathbb{N}\{ADC\} &= \mathbb{M}_f+2\mathbb{T}_{ranc}+6\mathbb{M}_{atr}+2\mathbb{S}_f+3\mathbb{M}_f+2\mathbb{T}_{ranc}+4\mathbb{M}_{atr}+1\mathbb{S}_f \\
&= 4\mathbb{M}_f+4\mathbb{T}_{ranc}+10\mathbb{M}_{atr}+3\mathbb{S}_f. \qquad (5.18)
\end{aligned}$$

Transcendental functions are very costly, and it is reasonable to compute and store them for use in both parts of the algorithm. Ideally, these values may be stored in registers. However, the worst case, in which the values are stored in conventional memory, was assumed. Thus,

$$\mathbb{N}\{ADC\} = 4\mathbb{M}_f+2\mathbb{T}_{ranc}+14\mathbb{M}_{atr}+3\mathbb{S}_f. \qquad (5.19)$$

Note that $\mathbb{N}\{ADC\}$ may be halved when the processor used to implement the algorithm has a large number of registers or temporary variables are carefully arranged.

Now, the number of computations required, assuming N_c controllers running in parallel and N_f frequencies to be controlled, is

$$\mathbb{N}\{ADC\}_{N_c,N_f} = N_c N_f\left(4\mathbb{M}_f+2\mathbb{T}_{ranc}+14\mathbb{M}_{atr}+3\mathbb{S}_f\right). \qquad (5.20)$$

It is important to realize that the above estimate did not assume the code to be optimized, and the actual cost estimate can be improved by saving temporary results.

The actual count obtained for a hexapod case controlling controlling six frequencies (three fundamentals and three harmonics) is:

$$\mathbb{N}\{ADC\}_{6,6} = 36\left(4\mathbb{M}_f + 2\mathbb{T}_{ranc} + 14\mathbb{M}_{atr} + 3\mathbb{S}_f\right). \tag{5.21}$$

Sine/cosine functions can be evaluated by using a series expansion or a table look-up if the CPU does not have them implemented in hardware. The series expansion would take around 300 cycles ($\approx$ 20 terms) if each operation could be performed in one cycle. Since the implementation only needs 12 such expansions per cycle, the number of operations would be

$$\begin{aligned} \mathbb{N}\{ADC\}_{6,6} &\approx 36 \times (4 + 14 + 3) + 300 \times 12 \\ &\approx 4,356. \end{aligned} \tag{5.22}$$

Thus, the total time would be approximately $144\mu s$ when the CPU mentioned in Table 5.1 (p. 76) is used. Note that the calculation of the transcendental function evaluation is responsible for most of this time (82%). A table look-up would easily reduce time to a much more reasonable value (less than $100\mu s$) at the cost of added memory.

1. Memory Requirements

The Adaptive Disturbance Canceller controller requires *very* little memory, as only six variables need to be stored and some of these can be shared among different controllers. The total number of variables needed is

$$\text{mem}_{N_i,N_f} = 4N_iN_f + N_f + 1. \tag{5.23}$$

Therefore, the previous example would need 151 floating-point values, or about 604 bytes. Almost any microcontroller that is fast enough to implement the Adaptive Disturbance Canceller will have that amount of RAM embedded in the chip.

E. COMPARISON AND COMMENTS

In some ways, comparing the computational and memory requirements of both algorithms is not reasonable, since both start from different hypotheses. The Multiple-Error LMS approach requires both a reference signal and a complete model of the plant transfer function whereas the Adaptive Disturbance Canceller requires the knowledge of the disturbance frequency, no reference signal and an approximate model of the transfer function only at the frequencies of interest. Although there is some overlap, each method has different strengths. In addition, note that the Multiple-Error LMS method most certainly needs a full computing system to be implemented in real time, which means adding memory chips, interrupt controllers, A/D and D/A converters, timers, considerable space and much electrical power. Furthermore, the cost increases linearly with the plant model and the order of the filter, and, as a result, complex systems require much more computations than simpler ones.

On the other extreme is the Adaptive Disturbance Canceller, for which, in the studied example, only 4,500 operations per iteration (726 operations per assigned frequency) and 151 variables are needed for the six actuators controlling six frequencies each with emulated *sin*/*cos* calculations. The Adaptive Disturbance Canceller is also very scalable: the complexity increases linearly with the number of frequencies to be controlled, but remains constant with the plant order.

It is worth mentioning here that a full Adaptive Disturbance Canceller solution could be implemented for a hexapod with only a few chips: a microcontroller (which would include timers, A/D converters, D/A converters, watchdog, interrupt manager, serial communication, etc) and analog anti-aliasing filters. Power consumption would be quite low: most likely below $1W$. Finally, the whole controller would be small enough to be mounted in the empty space between the actuators.

Quantity	Expression
Comp. Cost	
ADC	$N_c N_f \left(4\mathbb{M}_f + 2\mathbb{T}_{ranc} + 14\mathbb{M}_{atr} + 3\mathbb{S}_f\right)$
ME-LMS	$N_i N_o PQ \left(2\mathbb{M}_{atr} + \mathbb{S}_f + \mathbb{M}_f + \mathbb{S}_i\right)$
Mem. Req.	
ADC	$4N_i N_f + N_f + 1$
ME-LMS	$N_i(Q + (P+1)N_o)$

Table 5.2. Computational Cost and Memory Requirement Estimates.

Quantity	Adaptive Disturbance Canceller	Multiple-Error LMS
Cost/iteration	$4,356$	$54,000$
Memory estimate	$\approx$ 604 bytes	$> 6,000$ bytes

Number of Frequencies: three, one harmonic each
Number of Inputs: six
Number of Outputs: six
One operation / cycle
Floating-points implemented as floats

Table 5.3. Adaptive Disturbance Canceller $\times$ Multiple-Error LMS.

THIS PAGE INTENTIONALLY LEFT BLANK

VI. EXPERIMENTAL RESULTS

A. OVERVIEW

This chapter describes the implementation of the Adaptive Disturbance Canceller on the two hexapods described in Chapter II (p. 9).

Section B gives an overview of some of the challenges faced when solving the vibration isolation problem using the Precision Pointing Hexapod. These challenges ranged from inappropriate design to hardware failure.

Section C described the results on the Precision Pointing Hexapod, which exhibits strong nonlinearities. Experiments show that the Adaptive Disturbance Canceller algorithm and the hexapod configuration are not sensitive to the vibration axis. This indicates that the hexapod and the Adaptive Disturbance Canceller are adequate for a generic, off-the-shelf vibration isolation mount.

The Ultra-Quiet Platform was specifically designed for vibration isolation and thus has better linearity properties than the Precision Pointing Hexapod, making it a better test bed for comparison with the Multiple-Error LMS. Section D (p. 104) presents the results of this comparison.

B. EXPERIMENTAL CHALLENGES

This research was to be developed entirely on the Precision Pointing Hexapod, which had not yet been delivered when the research started. Once delivered, several tests were conducted to verify its behavior and also to validate the mathematical model that had been developed prior to the availability of the hardware.

The very first experiment consisted in exciting the bounce mode, in which all the actuators were excited with the same sine wave. The output of each accelerometer was then sent to an oscilloscope and to a spectrum analyzer. The first and most important conclusion was that the system exhibited severe nonlinearity. Harmonics up to $2.4KHz$ were observed when the input signal contained only a $50Hz$ sinusoidal sampled at $1KHz$. The experiment was repeated with a $5Hz$ sinuwave and the results were not as severe. The first experiment was relevant from the vibration-isolation perspective and the second experiment was important for position control (pointing). The next experiments tested the shaker. The supplied shaker was a $25W$ ceramic shaker with frequency response peak at $42Hz$. The useful range was between 10 and $100Hz$.

Realizing potential problems with aliasing, the first experiments were made using lower frequencies ($10Hz$) in order to have all harmonics below $500Hz$. Larger travel of the actuators was needed at these lower frequencies in order to obtain an acceleration large enough to obtain a good SNR. As a result, the shaker required more power and operated very closely to its 25W specification at the lower and of the frequency range ($10Hz$). Exciting the shaker at such power levels increased its own nonlinearity effects.

The design of the hexapod, as delivered, had the accelerometer as a structural part of the strut, as shown in Figure 6.1. In this design, the full force acting on the strut passed through the case of the accelerometer.

While running the first experiments (low frequency due to aliasing problems), the algorithm sometimes became unstable and the actuators hit their limit ($40N$ each actuator). Turning off the controller manually was not an option because it was implemented in software and thus it failed when the software entered an unresponsive state. Disabling the power supply of the actuators manually was not easy because the switch is located behind the power amplifier. Even if the access were

Figure 6.1. Old Accelerometer Adapter.

easier, it still depends on a fast response by the operator. Due to the original design, the force of the impact was transmitted through the case of the accelerometers and two of them ended up being damaged.

Since two accelerometers were already damaged, all experiments were halted until the design flaw was corrected. This was done by redesigning the adapters so that the accelerometers were inline with the strut axis but no force was transmitted though its case. The new adapter, after being assembled, is shown in Figure 2.7.

Although damaging the accelerometers was no longer a concern, preventing damage to other components if the controller became unstable was still a concern. The range of the accelerometers was $\pm 2g$ or 0.5 to $4.5V$, assuming nominal sensitivity. It was then assumed that if the voltage fell outside the range of the accelerometer, then an unsafe condition occurred and preventive action had to be taken. The action selected was to curtail power from both the actuators and the shaker. In order to do that, a circuit was designed to monitor the output of one of the accelerometers. A window tested the voltage and cut the power supply of the actuators and the shaker if the voltage

was beyond safe limits. The power could only be restored by pressing the *reset* switch. A manual *panic* button was also included and had the same effect as if the accelerometer's output were beyond acceptable limits.

Although this circuitry prevented damage to the experimental hardware, it still did not solve the aliasing problems. Additional hardware filters were needed. Among the several options, switched capacitor filters were selected. These filters require only two capacitors and one integrated circuit. The cutoff frequency could be selected by an external oscillator. Switched-capacitors anti-aliasing filters were implemented for all accelerometers.

Once the safety device and anti-aliasing filters were implemented, several experiments were conducted. In order to generate acceleration levels high enough for a good SNR, the shaker had to be driven very closely to its power dissipation limits. To solve this problem, either the accelerometers or the shaker had to be changed. Therefore, the shaker was replaced by a larger model $50W$. This reduced both the overheating and the shaker nonlinearities.

The next important consideration was the ball joint clearance. The manufacturer stated that the clearance was around $2-4\mu m$ for each joint. From the simulations and experimental results it was determined that the amplitude of the vibration was in the order of $20-50\mu m$. Therefore, the joint clearance was found to be the next problem to be addressed. The best solution was to replace the ball joints by flextures. Another option was to preload the joints.

Since preloading the joints was faster and less expensive, it was the approach first tested. All joints were preloaded and the experiments repeated. Several experiments for which convergence was not achieved previously did converge after preloading the joints. This was the final setup for the experiments conducted in this research.

C. PRECISION POINTING HEXAPOD

The hardware setup is that detailed in Section II.C (p. 15). The only modification was the preloading of the joints with springs, in order to reduce the backlash present in the joints (around $3\mu m$ per joint, according to CSA). A sinusoidal signal of $50Hz$ was sent in phase and with the same amplitude to all actuators to evaluate the effect of this backlash. The power spectrum density of the accelerometers showed lines at $50Hz$ intervals until around $2.4KHz$. The solution was to preload the joints with springs. Unfortunately, this introduced axial forces on the actuators axis which, according to Moltran, created more static friction.

The controller box was implemented exactly as defined in the equations given in Section IV.C (p. 46). The parameter μ was coarsely tuned for each frequency being controlled. Adaptive Disturbance Canceller controllers were implemented in parallel and the outputs summed in order to control more than one frequency.

Several different modes of vibration were tested in order to evaluate the algorithm sensitivity. The definition of the modes is shown in Figure 4.12 (pg. 63).

1. Along Z-Axis

In this experiment the shaker was mounted directly under the bottom plate, at the center. The vibration axis was coincident with the z-axis.

The first case studied was the single tonal, at $40Hz$. Harmonics due to nonlinearities were present on the error signal. The results obtained before and after the controller are shown in Figure 6.2. As can be seen, the controller did suppress the controlled frequency ($40Hz$), but the vibration at the harmonics (80 and $120Hz$) were increased. The floor noise remained unaltered, as expected.

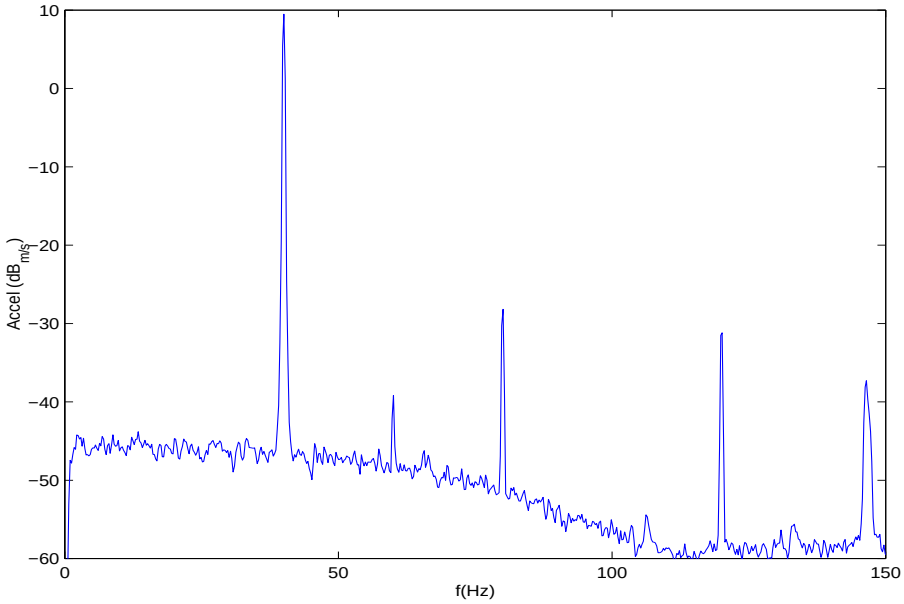

(a) Before

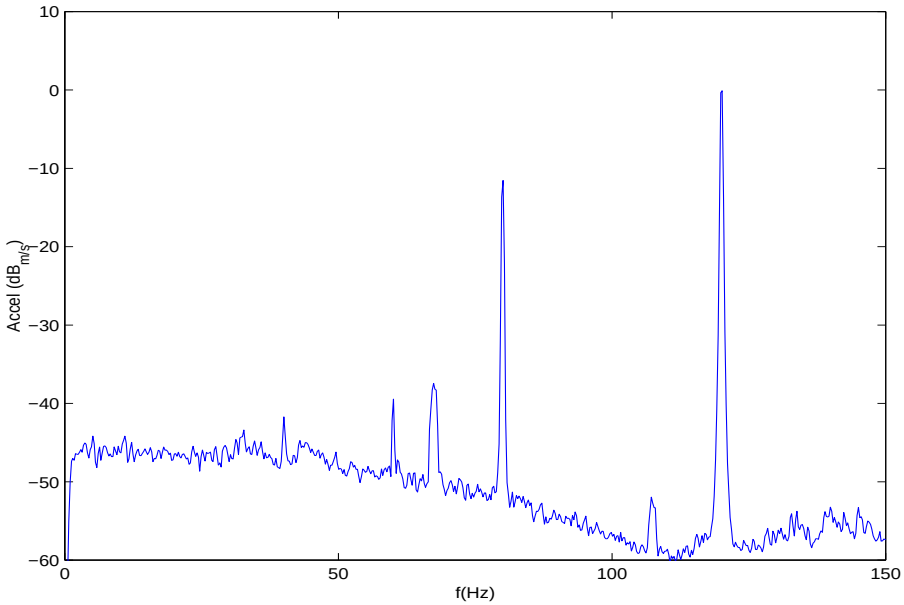

(b) After

Figure 6.2. Z-Axis, One Tone.

Figure 6.3 shows the results when 40 and 80Hz frequencies were controlled. As expected, the components of the error signal at both frequencies were reduced to the noise floor. Note that the second harmonic (120Hz) increased up to about 30dB, as it was not controlled. This effect was specifically due to the nonlinearities of the hexapod.

2. Tilt-Tip

Another interesting configuration was the tilt-tip as it was simple to understand the movement and the displacement of the actuators. The shaker was mounted with the vibration axis parallel with the z-axis, with its center located on the *x-y* plane. This configuration did not involve translational movement.

Figure 6.4 shows results for a single tone in which the selected frequency (40Hz) was suppressed. Note that the static friction is believed to be responsible for the increase on the harmonics. As expected, there was no significant change in the noise floor.

Next, the system was setup to control disturbances at 39Hz and 40Hz. As expected, the controller needed a longer time to converge. Another important finding was that the strong static friction exhibited by the actuators generated several harmonics multiple of 1Hz, which was the difference between the two frequencies. The two assigned frequencies were actually suppressed, but the energy levels on the uncontrolled harmonics were increased (Figure 6.5).

3. Twist and Shear

In this experiment the shaker was mounted with its center on the *x-y* plane, with the vibration axis perpendicular to it. This mainly excited the twist mode. The results, presented in Figures 6.6 and 6.7, were as expected.

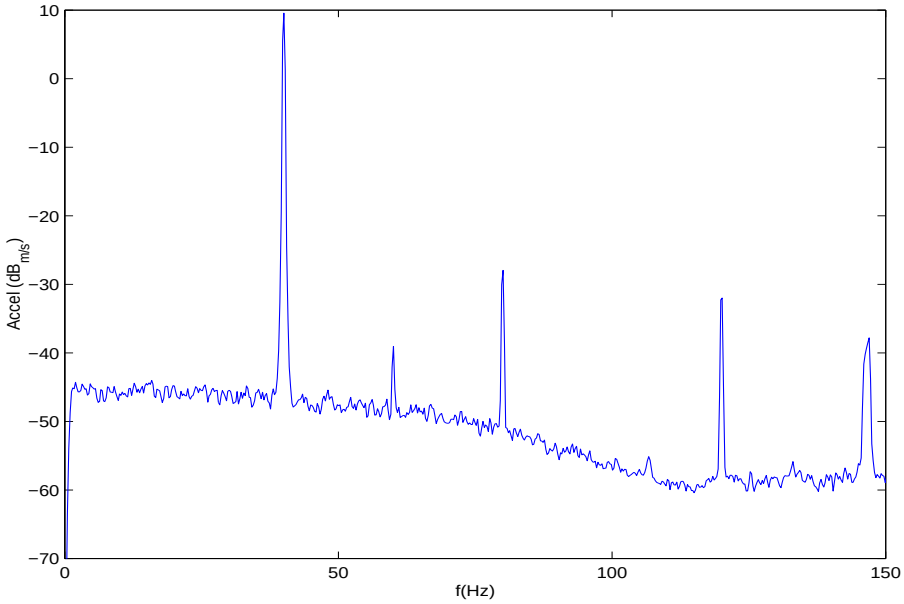

(a) Before

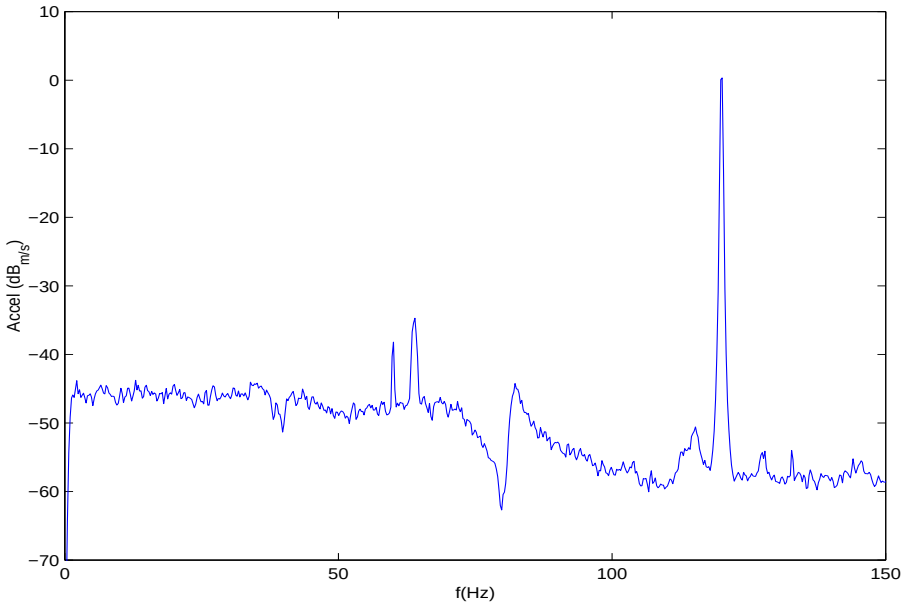

(b) After

Figure 6.3. Z-Axis, Two Tones.

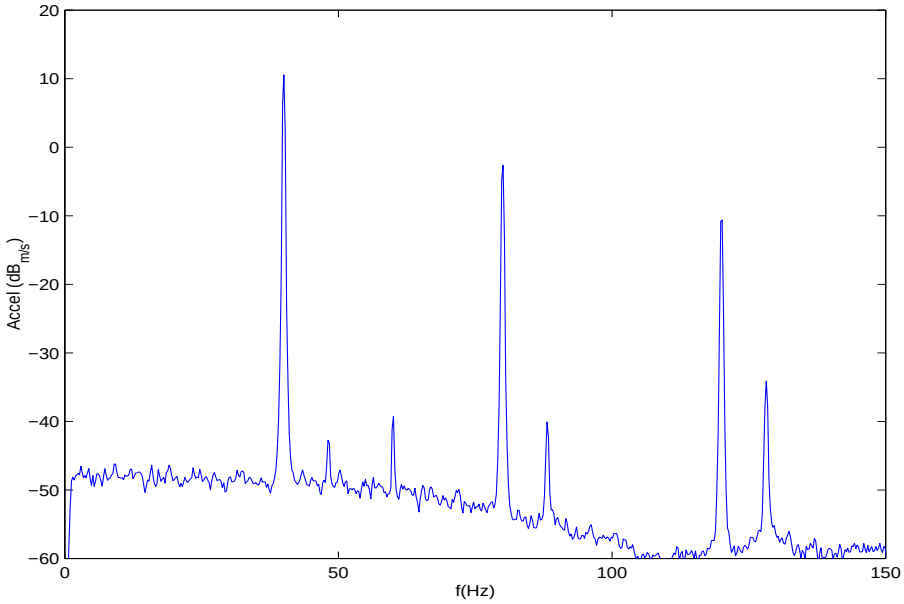

(a) Before

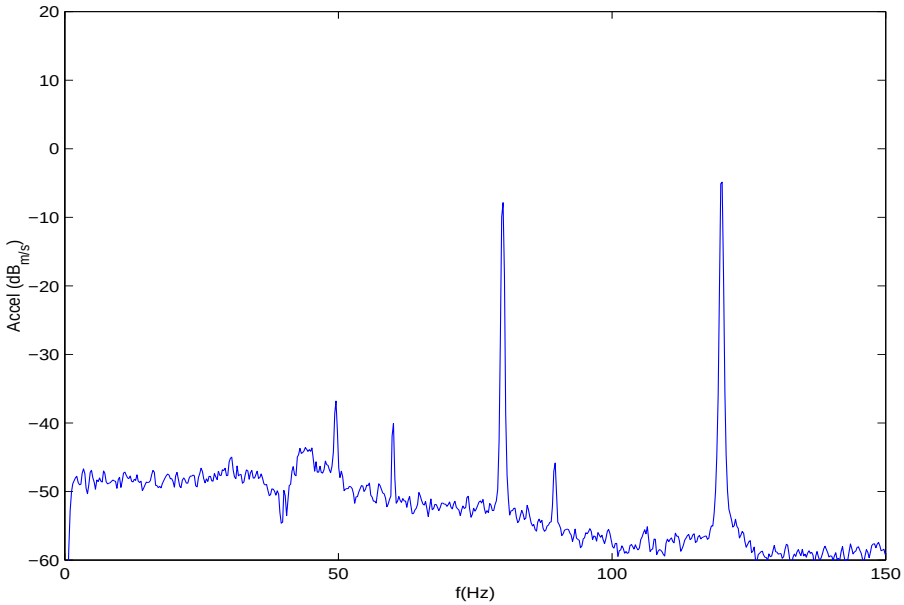

(b) After

Figure 6.4. Tilt/Tip, One Tone.

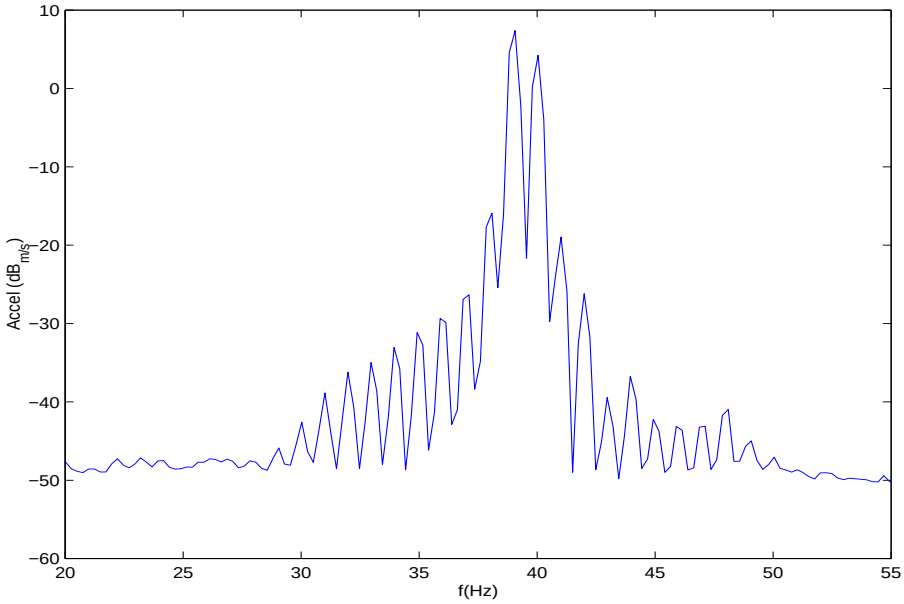

(a) Before

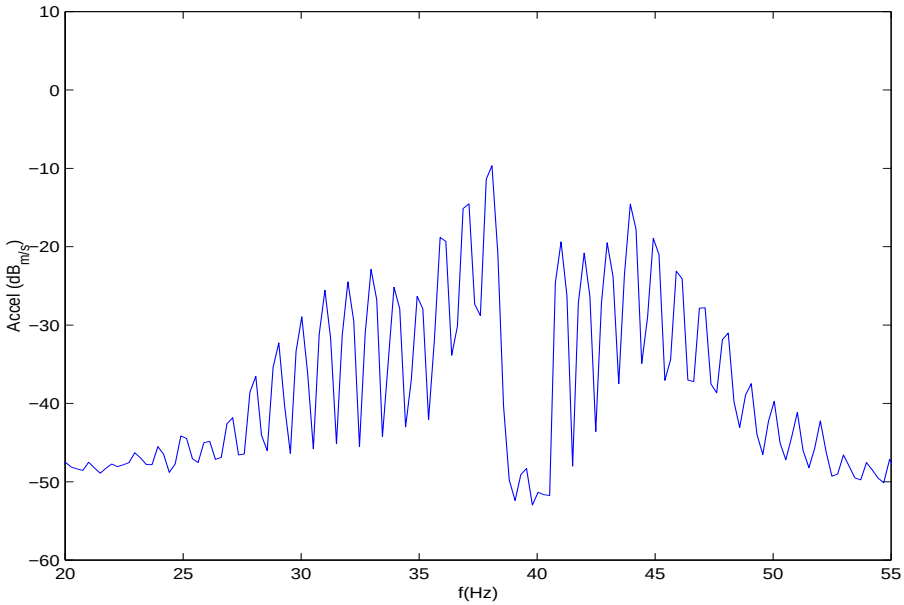

(b) After

Figure 6.5. Tilt/Tip, Two Close Tones.

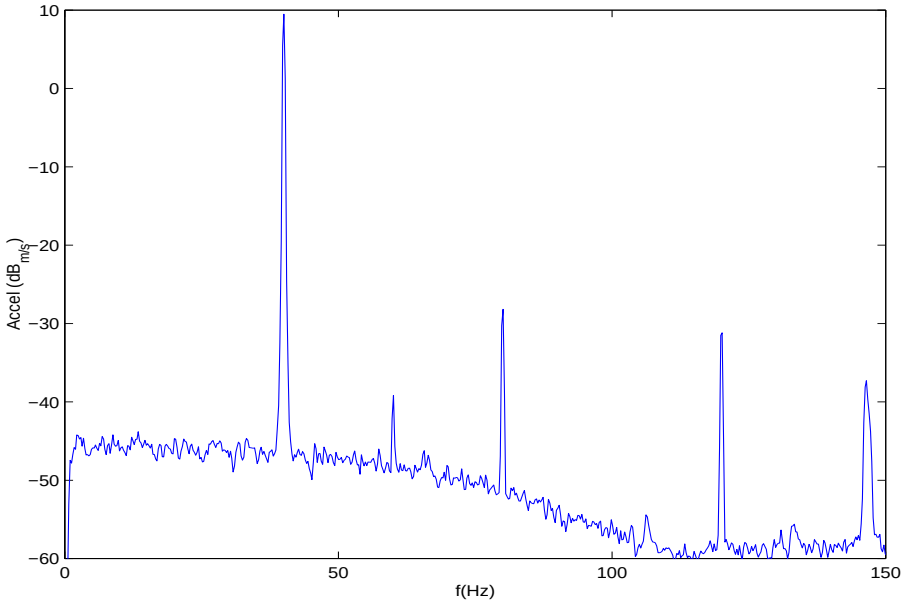

(a) Before

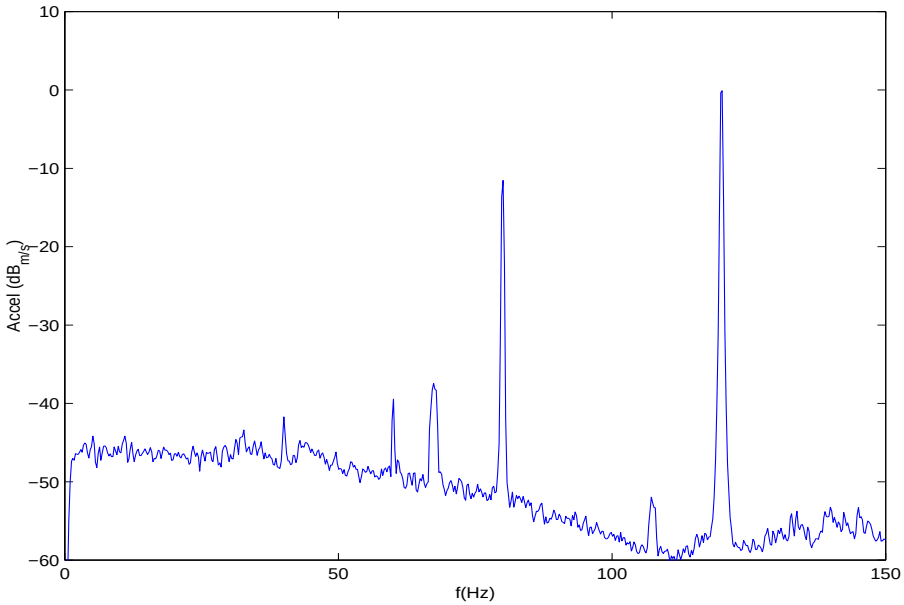

(b) After

Figure 6.6. Twist, One Tone.

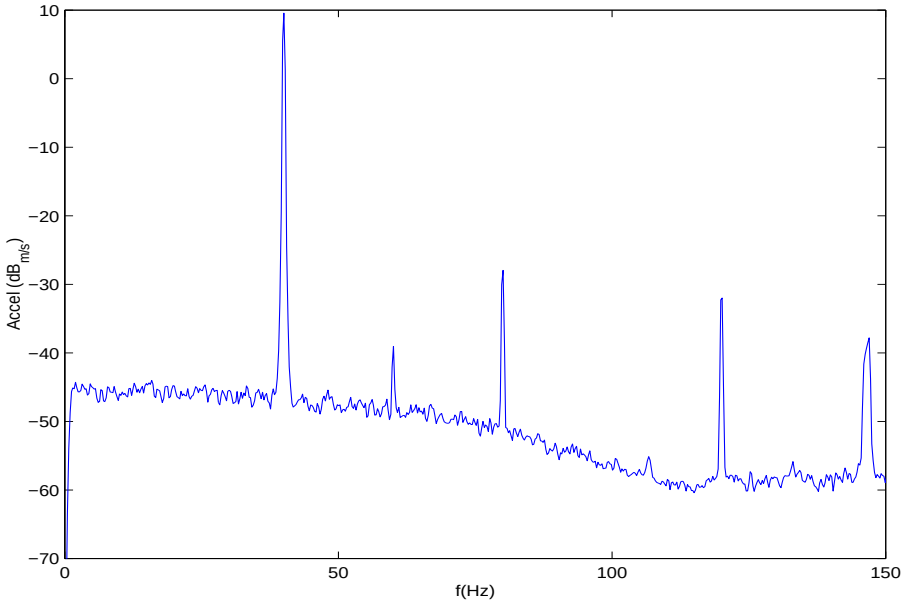

(a) Before

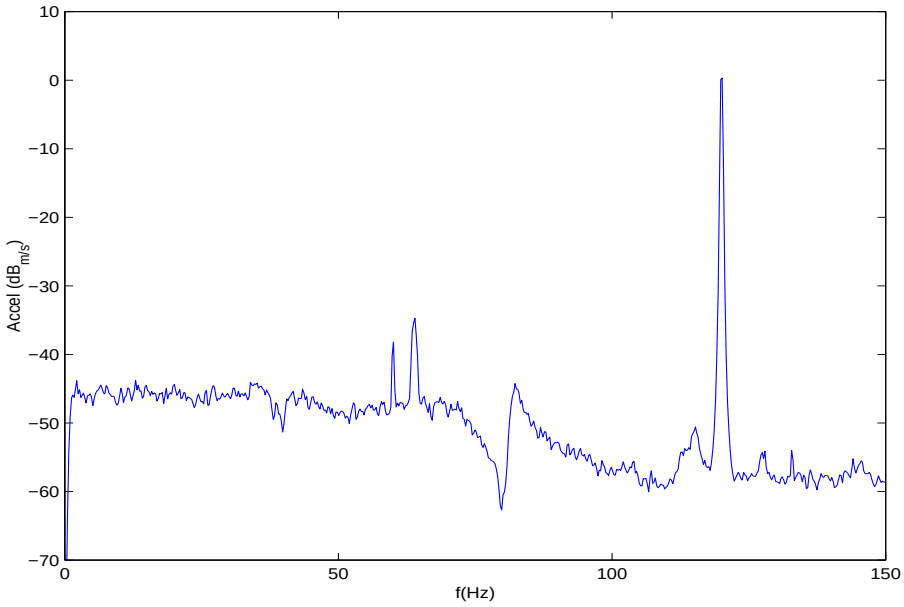

(b) After

Figure 6.7. Twist, Two Tones.

For the last experiment, shear mode, the shaker was mounted on the *x*-*y* plane, with the vibration axis along the vector $\hat{x} + \hat{y}$, where $\hat{x}$ and $\hat{y}$ are defined according to Figure 2.1. This induces a translational movement to the hexapod (much more complex than a translation along the z-axis). The results shown in Figures 6.8 and 6.9 were again as expected.

4. Comments

It is very important that the algorithm performs reasonably well in most cases, in spite of all nonlinearities exhibited by the Precision Pointing Hexapod. It is also important to mention that the sensors used in this hexapod had a very wide range $\pm 2g$, and thus the disturbance level had to be quite large in order to excite the accelerometers.

Another very interesting conclusion is that the hexapod was quite insensitive to the vibration type (linear/angular) and direction. The experiments subjected the hexapod to disturbances from several directions. The performance of the controller in all cases showed that the Stewart Platform is indeed a good configuration for a generic vibration-isolation mount.

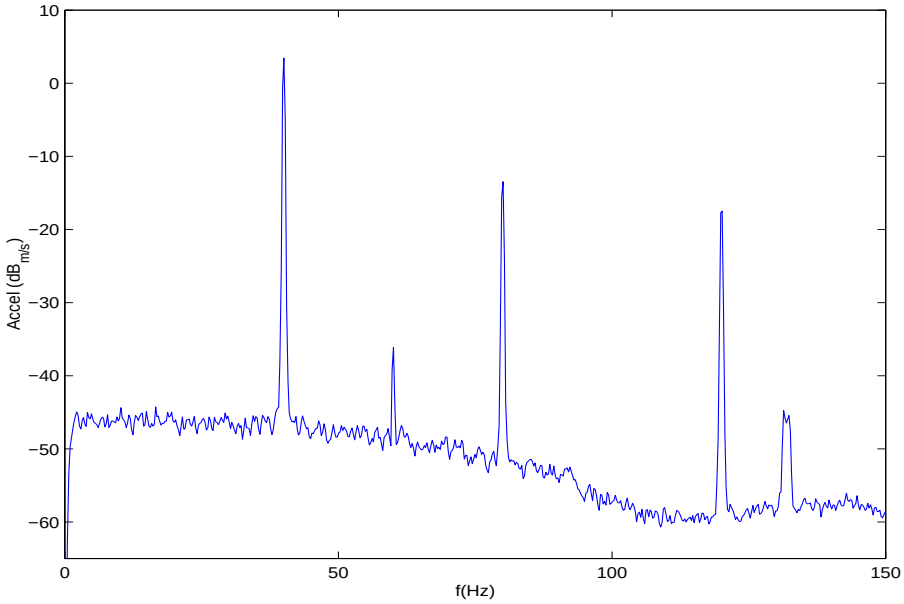

(a) Before

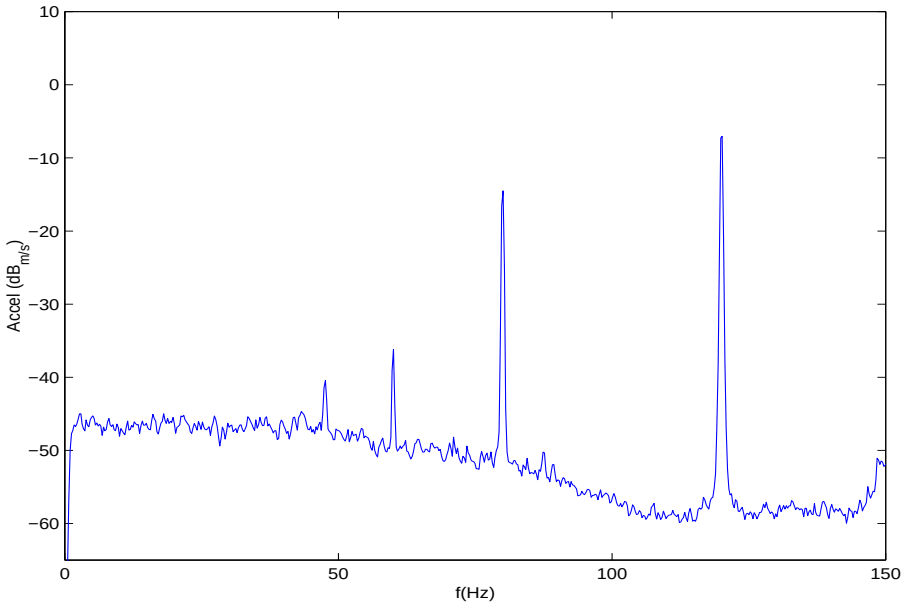

(b) After

Figure 6.8. Horizontal Shear, One Tone.

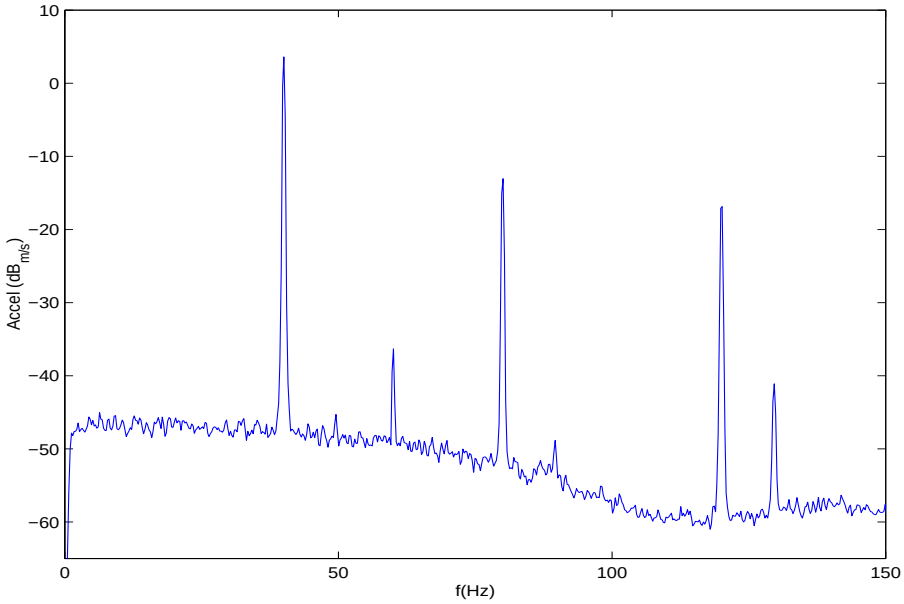

(a) Before

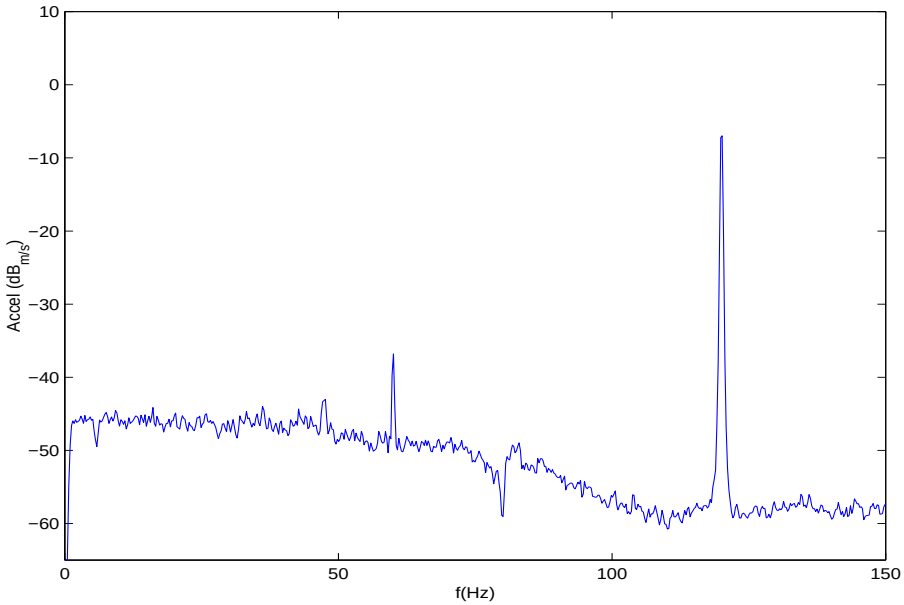

(b) After

Figure 6.9. Horizontal Shear, Two Tones.

D. COMPARING THE PRECISION POINTING HEXAPOD TO THE MULTIPLE-ERROR LMS

It is very important to compare the results obtained with the Adaptive Disturbance Canceller to those obtained with the Multiple-Error LMS algorithm, and the same hardware must be used in order to perform a fair comparison. The Ultra-Quiet Platform, described in Section II.B (p. 10), was selected because it exhibits better linearity properties than the Precision Pointing Hexapod.

1. Results

First, an experiment was se tup with a single tone at $95Hz$ in order to verify the Ultra-Quiet Platform characteristics and how well the Adaptive Disturbance Canceller performed. The results of this experiment are shown in Figure 6.10. As can be seen, the harmonics were amplified, but the desired frequency was effectively suppressed. Figure 6.10(b) shows that the controller did not affect other frequencies other than the assigned one.

Next, a second experiment was conducted in which five disturbances (65, 95, 125, 130 and $195Hz$) were to be controlled to verify the behavior of the controller under a more complex situation. LMS-based filters do not perform well under these conditions [15]. As can be seen in Figure 6.11, the Adaptive Disturbance Canceller was able to suppress all the assigned disturbances successfully. It can also be seen that the error signal for the uncontrolled case shows frequency contents other than the five tones. These are believed to be a consequence of the cross-coupling among the different frequencies due to nonlinearities. This effect was not observed in the linear simulations and was observed in the simulations using the Precision Pointing Hexapod model.

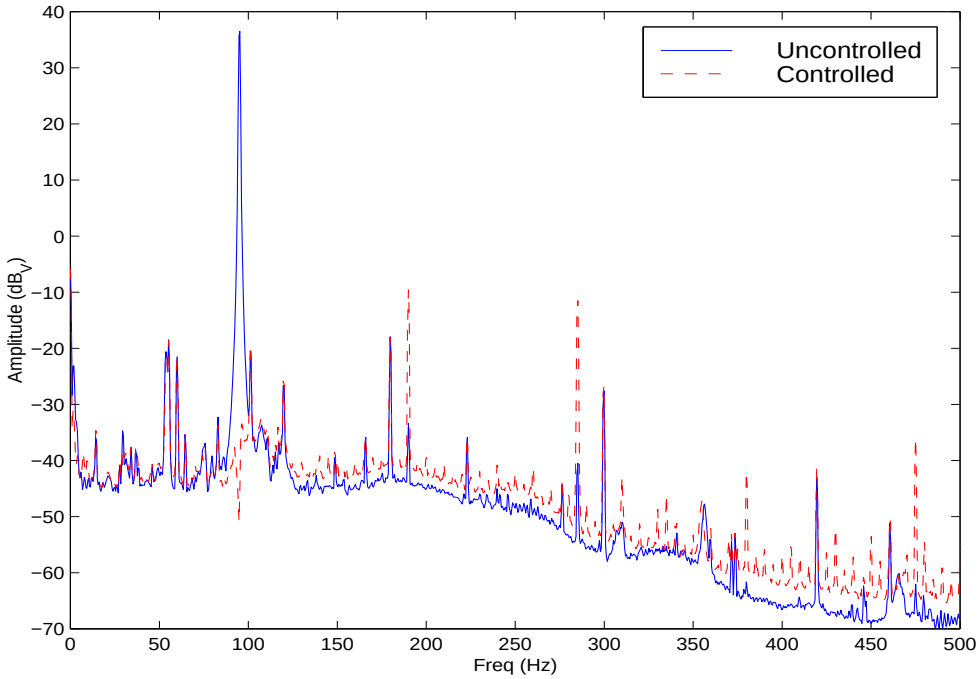

(a) Range $0 - 500Hz$

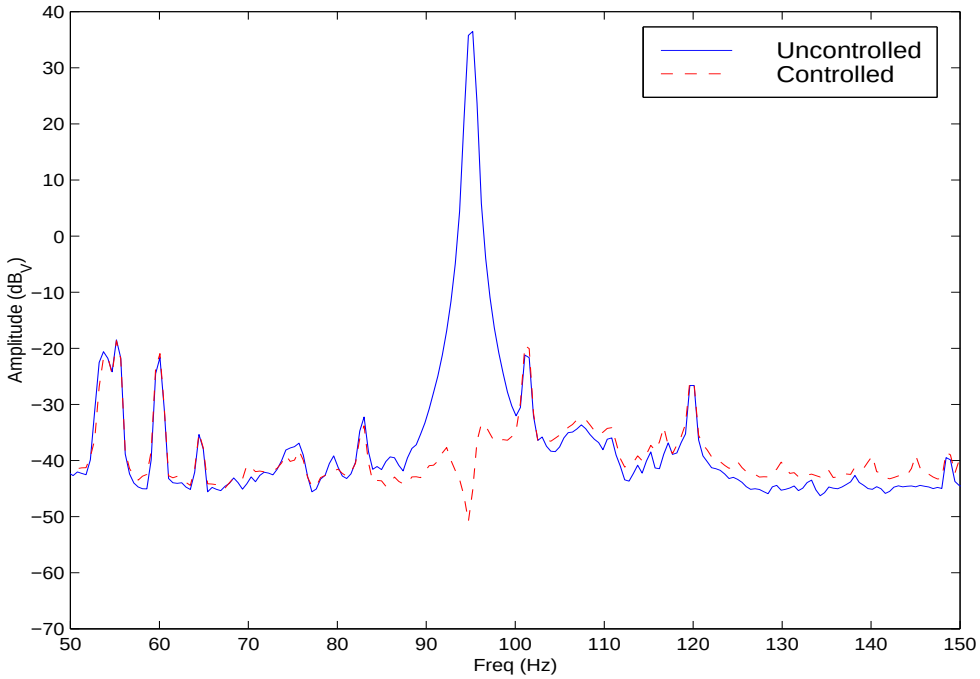

(b) Range $50 - 150Hz$

Figure 6.10. Adaptive Disturbance Canceller on UQP with One Tone.

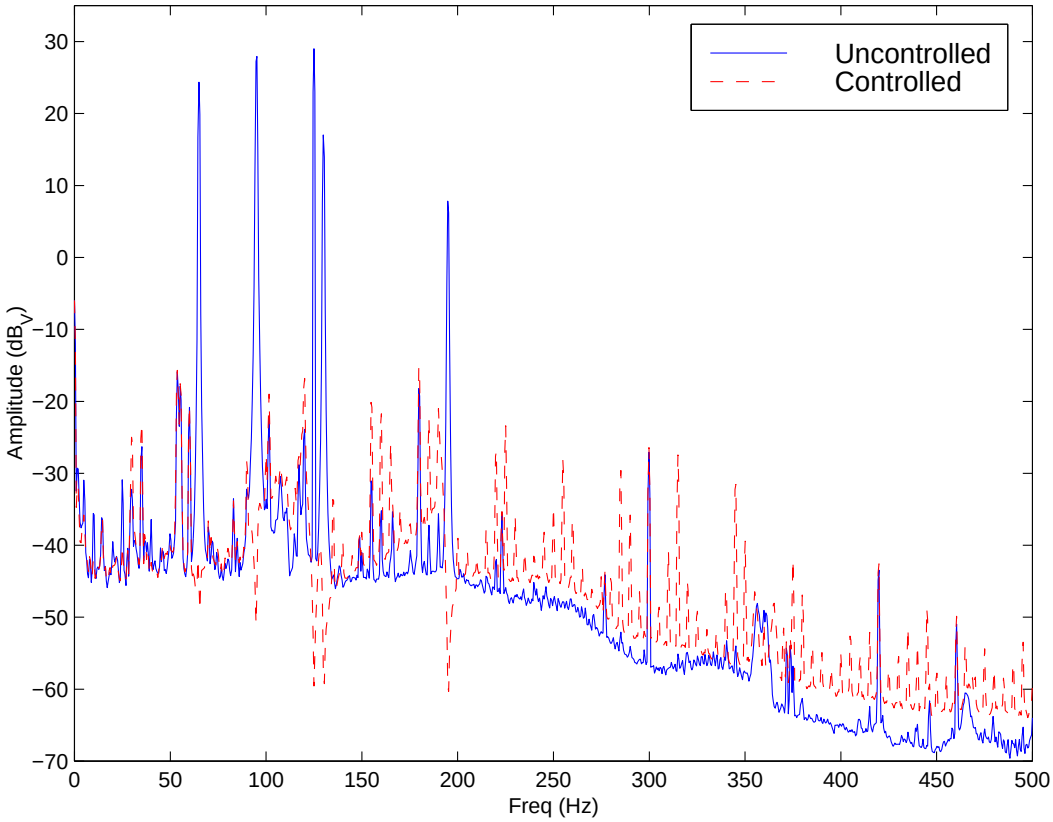

Figure 6.11. Adaptive Disturbance Canceller on UQP with Five Tones.

Having verified that the performance of the Adaptive Disturbance Canceller on the Ultra-Quiet Platform was within the expected parameters, a series of experiments were conducted in order to compare the Adaptive Disturbance Canceller method with the Multiple-Error LMS.

One important characteristic of the Multiple-Error LMS is the requirement of a reference signal. This signal is used both to generate the estimate of the signal $r[n]$ and to generate the input to the plant through the filter $\mathbf{W}$. It is expected, therefore, that a noisy reference will degrade significantly the performance of LMS-based methods. With this information in mind the ME-LMS experiments were performed with both noisy and noiseless reference signals (SNR between 21 and $25dB$).

The first set of experiments had a disturbance with a single tone at $95Hz$. As seen in Figure 6.12, both the Adaptive Disturbance Canceller and the noiseless Multiple-Error LMS had

almost the same performance over the entire spectrum. It was expected that the noisy Multiple-Error LMS would not perform as well, and this was confirmed in the experiment. The noise floor was significantly raised at higher frequencies, signaling that the Multiple-Error LMS does require a clean reference signal in order to perform well.

The second experiment considered the sum of two close sinusoidals (95 and $96Hz$). Adequately isolating closely-spaced tones is very important for large structures. The beating frequency is very small and structural nonlinearities will demodulate this low-frequency. Since most structural modes are at low frequencies, this can compromise the goal of the vibration isolation. As seen in Figure 6.13, neither of the methods was able to suppress both disturbances completely, and the Adaptive Disturbance Canceller had the worst performance. One of the explanations for the poorer performance of the Adaptive Disturbance Canceller was the tuning of the learning coefficient μ. The coefficient was coarsely tuned and was not optimized for any particular disturbance configuration.

Another important fact that the experiment uncovered was that the floor noise of the Multiple-Error LMS with noisy reference was about $20-35dB$ above the noise floor of the Adaptive Disturbance Canceller and the Multiple-Error LMS with noiseless reference.

The last experiment set compared both the Adaptive Disturbance Canceller and the noisy Multiple-Error LMS when controlling three frequencies. As seen before, the Adaptive Disturbance Canceller introduced several peaks in the power spectrum of the error due to cross-coupling introduced by nonlinearities. Figure 6.14 shows that the Adaptive Disturbance Canceller did introduce several terms due to cross-coupling, some about $10-20dB$ above the noise floor. The noise floor was also raised by $5-10dB$ compared to the uncontrolled error. Although both methods were able to suppress the disturbances, the wide-band noise introduced by the Multiple-Error LMS with noisy reference ranged from 20 to $40dB$.

2. Comments

As seen from the plots, the Adaptive Disturbance Canceller performance is very similar to the performance of the Multiple-Error LMS with noiseless reference. When noise was injected in the disturbance-correlated signal, the Multiple-Error LMS performance suffered significantly: although the actual disturbances were suppressed, the noise floor was raised considerably. The Adaptive Disturbance Canceller was not affected by this behavior because the information about the disturbance (frequency) is assumed to be known *a priori* and thus the reference can be synthetized without noise interference.

Another very important fact was cross-coupling due to nonlinearities among the several frequencies verified in the experiment when several frequencies were involved. Although this effect was first noticed using the Adaptive Disturbance Canceller, it also occurred in the noiseless Multiple-Error LMS. The most important consequence is the inability of the studied methods to deal with several simultaneous frequencies (seen in the experiment shown in Figure 6.15). This means that the most effective vibration-isolation approach is to isolate the vibration at its source, where fewer frequencies are present and thus active vibration isolation is more effective.

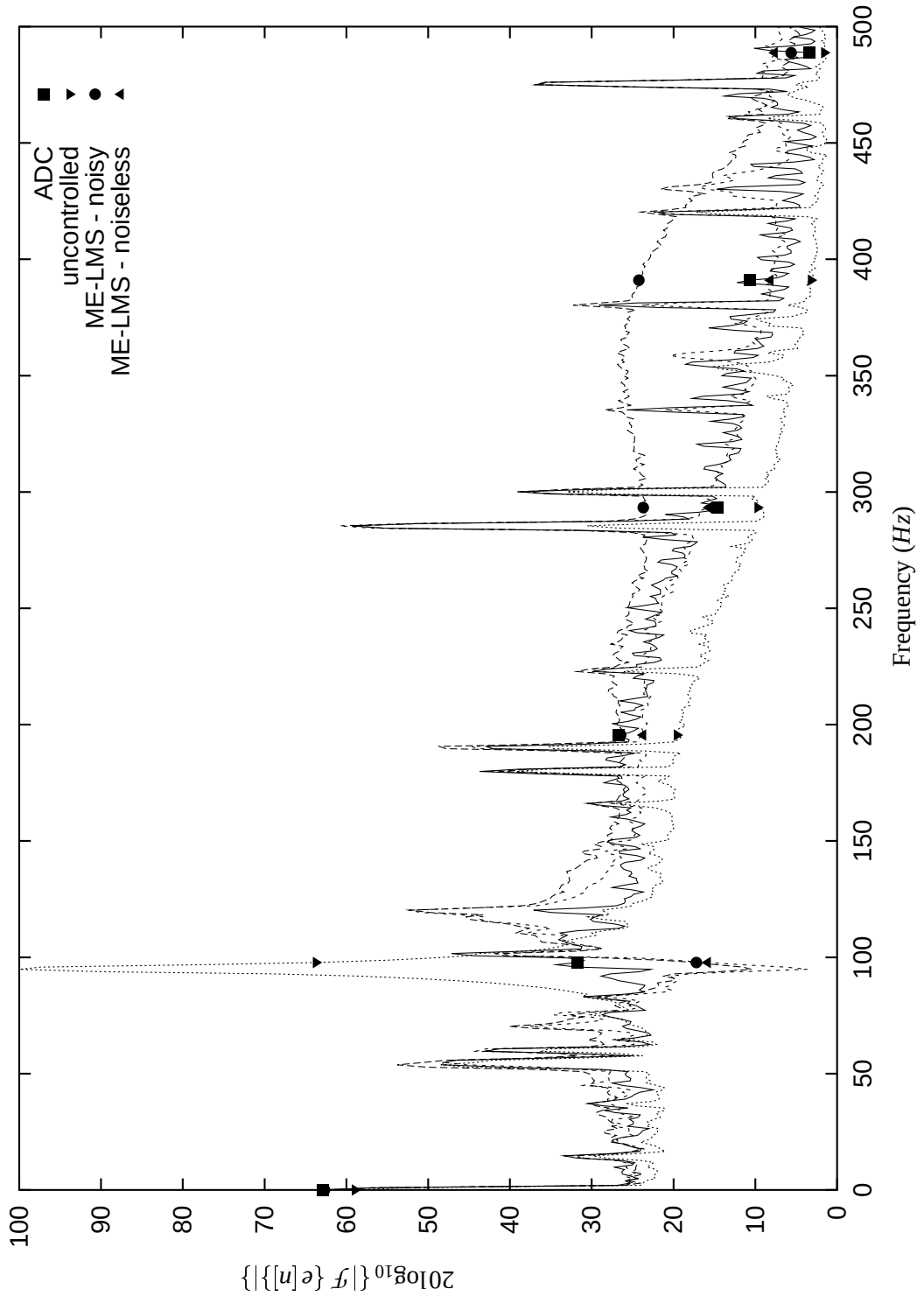

Figure 6.12. Comparison with ME-LMS — Single Tone.

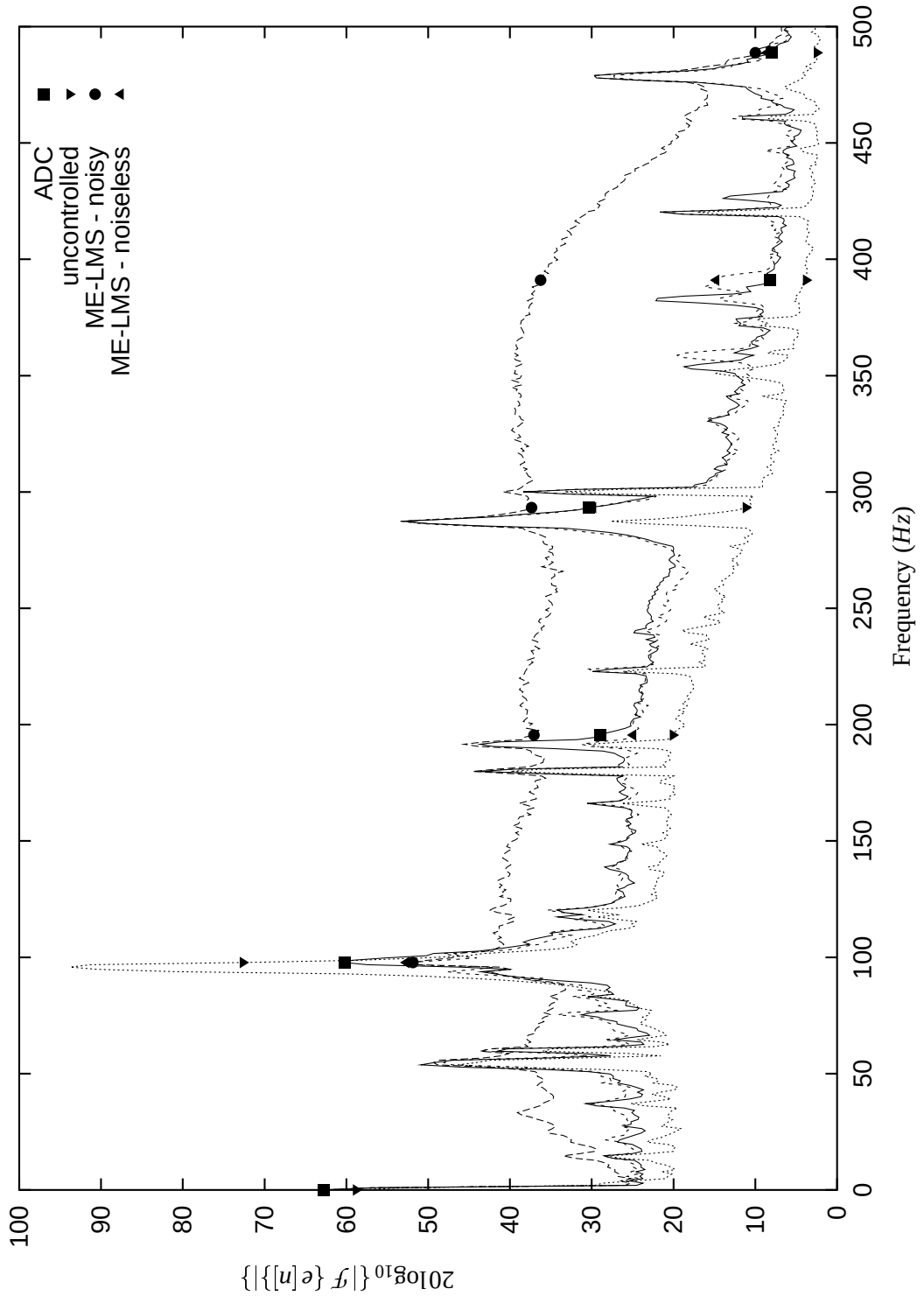

Figure 6.13. Comparison with ME-LMS — Two Tones.

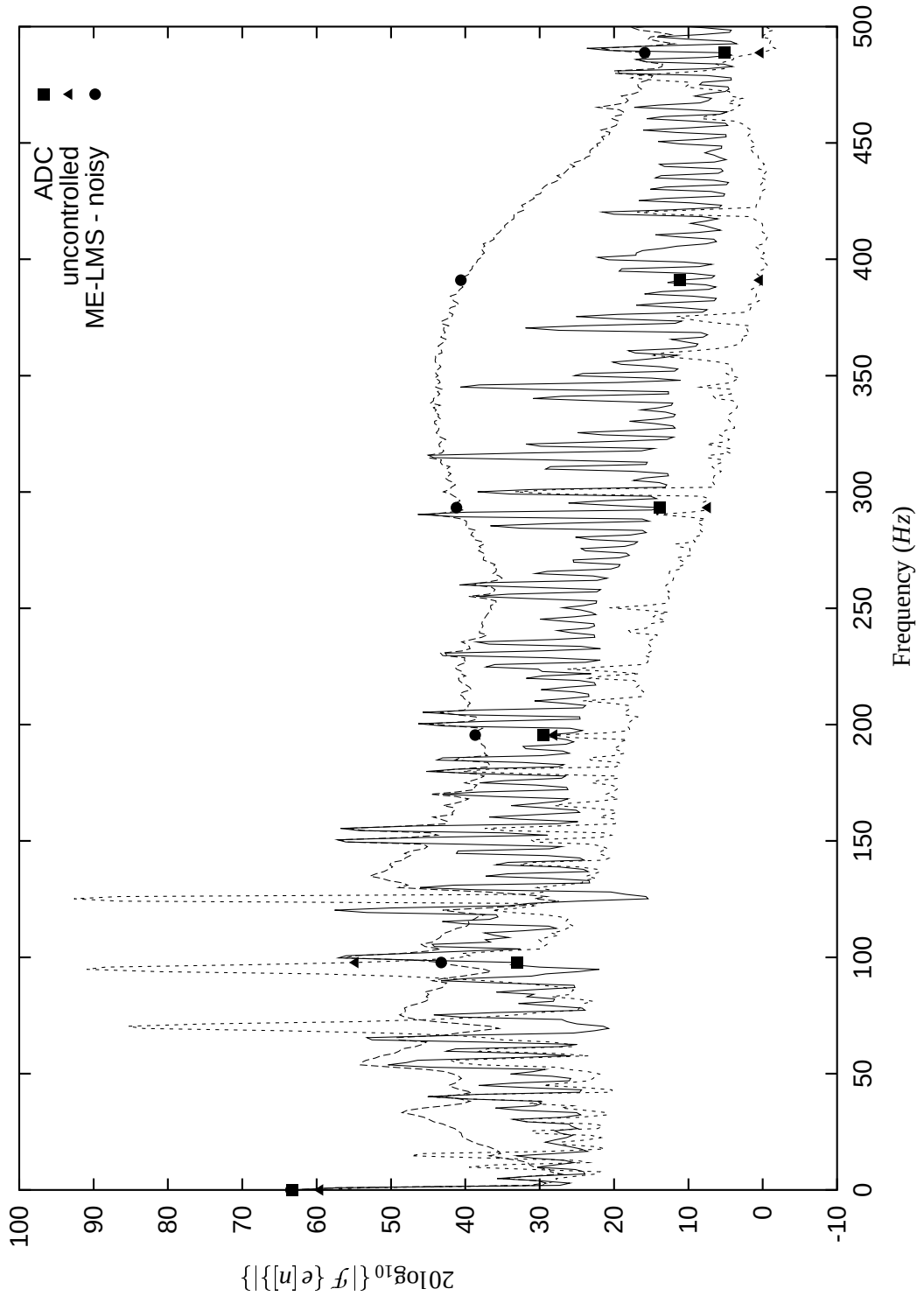

Figure 6.14. Comparison with ME-LMS — Three Tones.

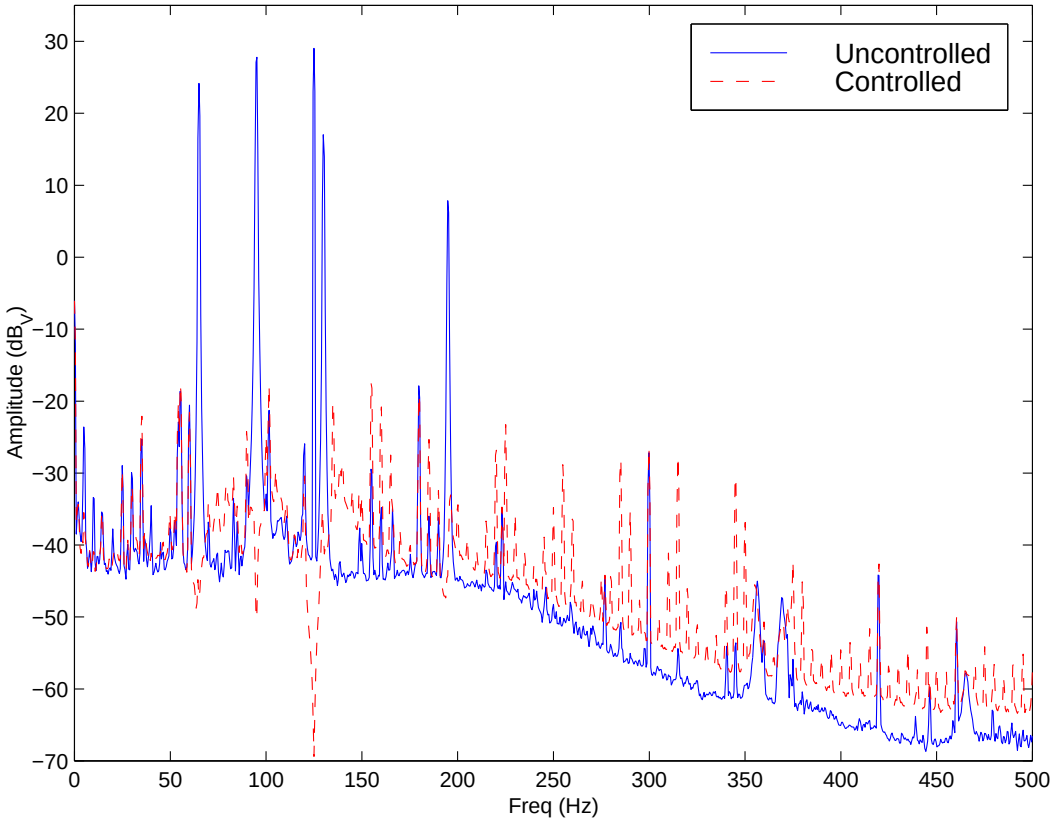

Figure 6.15. Nonlinearity Effect on the ME-LMS — Five Tones.

VII. SUMMARY AND CONCLUSIONS

The new generation of optical payloads imposes stricter requirements on the vibration levels, challenging the designers. These higher standards make it very difficult to meet the requirements using only passive isolation and thus active solutions have been pursued. The Stewart Platform is identified in the literature as the most promising system for local vibration isolation, as it can generate forces and torques in any direction. As added bonuses, hexapods exhibit very good stiffness and high force-to-weight ratio. Finally, hexapods can also be used to provide fine pointing capability to the payload if the actuators are capable of long strokes.

Several techniques for vibration isolation have been developed since 1981 when Widrow and Burgess presented the original Filtered-X LMS, but the research of vibration isolation using hexapods increased appreciably only after the first half of the 1990's when faster DSP chips became available. Unfortunately, the conditions in space are not as forgiving as on the ground: weight, space and electrical power are strictly limited. Therefore, although several vibration isolation techniques are available, the computational resources required limit their employment on current spacecraft designs.

In 1998 Bertran and Montoro presented a very simple algorithm capable of performing vibration isolation on SISO systems. Taking advantage of the fact that the hexapods used in vibration isolation use smart struts, each strut can be viewed as a SISO system, and therefore this simple method can be employed on hexapods. The algorithm is inexpensive enough to be implemented with only a small fraction of the computational requirements of the *de facto* standard Multiple-Error LMS. A deeper review of the literature revealed a lack of a stability analysis for this simpler method

that takes into account a generic plant. An analysis of the influence of non-controlled frequencies on the performance of the algorithm was also missing.

It was not known initially if the algorithm would work properly on a hexapod due to the strong coupling among the struts. Therefore, it was important to simulate the hexapod in order to evaluate the Adaptive Disturbance Canceller in a controlled environment. Due to the unique characteristics of the Precision Pointing Hexapod, an appropriate model could not be found in the research and therefore a suitable model was derived. The model takes into account all geometric nonlinearities so that it can also be used for pointing.

The Multiple-Error LMS is used a as reference throughout the work due to its acceptance and good performance. The Multiple-Error LMS algorithm was re-derived and the resulting equations used for the computational requirements estimation. So that the Adaptive Disturbance Canceller could be applied in spacecraft, a rigorous analysis of stability was provided and a guideline for the *learning coefficient* μ selection was also included.

Results show the method to be very selective and not to affect the error at frequencies unassigned to the controller. As a result, the actuators do not need to be *oversized* to prevent saturation, as is the case with the Multiple-Error LMS and other methods that use a reference signal.

Simulations on a SISO plant were conducted to validate mathematical results and confirm the algorithm high selectivity. Simulations were also conducted on the Precision Pointing Hexapod model to verify the influence of the coupling. Results show that the coupling did not compromise the performance of the controller significantly.

A full set of experiments was conducted on both hexapods. The Precision Pointing Hexapod, due to its ball joints, exhibited large nonlinearities. Despite the severe nonlinearities, the method did cancel the assigned frequencies, although the amplitude of the unassigned harmonics increased.

Experiments on the Ultra-Quiet Platform were required to compare the results against the Multiple-Error LMS algorithm. The proposed method has approximately the same performance of the Multiple-Error LMS algorithm when no noise is present on the reference signal. However, Multiple-Error LMS performance was significantly degraded, generating wide-band noise on the error signal when noise is present on the reference signal. The Adaptive Disturbance Canceller does not suffer from this problem because no reference signal is used.

The Ultra-Quiet Platform was built for vibration isolation and close attention was paid to linearity. Even so, multiple-frequency experiments showed that both methods suffered from the nonlinear effects, generating several harmonics. The effect is more dramatic in the Multiple-Error LMS implementation when noise is present in the reference signal, increasing the noise floor of the error signal at higher frequencies Both methods were able to cancel the disturbances even in the presence of nonlinearities.

Finally, computational costs for the Multiple-Error LMS and the Adaptive Disturbance Canceller methods were computed and compared. Traditional cost analysis uses floating-point operations count, but recent advances in microelectronics decreased the cost of these operations and other operations must also be counted. Additionally, memory requirements for both methods were evaluated, providing the designer with some valuable information when selecting the hardware to be used for implementation. The computational cost required by the Adaptive Disturbance Canceller can be smaller than *one tenth* of the Multiple-Error LMS requirements and similar results are obtained for the memory requirements.

A. CONTRIBUTIONS

One of the main contributions of this work is the approach from the computational efficiency perspective. Although much research has been done on vibration isolation, no work that focused on computational efficiency was available previously.

Research showed that the method selected lacked a stability analysis for a generic plant, and a stability analysis was derived. In addition, a guideline for the adaptation rate μ selection was presented.

In addition, this work provides an analysis of crosstalk interference, predicting the influence of uncontrolled frequencies, which has not been addressed by the research community until now.

A fully nonlinear state-space model suitable for vibration and position simulation of large and small angles was developed for the Precision Pointing Hexapod. This model shares the large angles characteristics found in the robotics literature, without the restriction of small accelerations and is suited for the geometry of the Precision Pointing Hexapod. The models of the actuators accelerometers were included in the model, allowing it to be used as a tool for simulation and control.

Even though simulations were used in order to better understand the method, all the theoretical results were validated experimentally. The experiments on the Precision Pointing Hexapod revealed the robustness of the method to nonlinearities. These experiments also reinforced the fact that the method is robust to sensor noise, consistently achieving suppression level below the noise floor.

A performance comparison with the Multiple-Error LMS algorithm was conducted, including cases with noisy reference, which substantially degraded the behavior. It was experimentally

shown that the Adaptive Disturbance Canceller delivers performance comparable to the Multiple-Error LMS in the optimal case of noiseless reference signal. If the Multiple-Error LMS uses a noisy reference signal, its performance is degraded and the Adaptive Disturbance Canceller offers better results.

Finally, the computational requirements analysis of both the Multiple-Error LMS and the Adaptive Disturbance Canceller methods were included. This analysis revealed that the simpler Adaptive Disturbance Canceller can deliver at least the same performance of reference method using $1/10$ or less of the computational resources when the frequency information is available.

B. SUGGESTIONS FOR FUTURE RESEARCH

Improving on the Adaptive Disturbance Canceller is not as easy as it might seem, since performance improvement must be carefully balanced against simplicity. The main research objective was to have the simplest vibration suppressor possible, and improvements might easily add complexity that will defeat the main goal.

The Adaptive Disturbance Canceller has two main weaknesses: the need for precise knowledge of the frequency and a frequency-dependent learning rate (μ). The first issue can or cannot be relevant in practical situations. Several subsystems provide as outputs their frequency or operate at a fixed, known, frequency; others do not. If the frequency is not readily available, the next best solution would be to measure the frequency directly, but this is not always possible. Again. two alternatives can be used when the frequency information is not available and cannot be measured directly: 1) estimate the frequency or 2) adapt the algorithm to track the disturbance. The first option requires significant computational resources to be implemented with good precision and introduces delay, which impairs the response of the controller to changing disturbances. For this class

of problems, using an algorithm that can track the frequency by itself is highly important. This is one of the major areas for improvement in this method, and although much time for this research was dedicated to solving this particular problem, no acceptable solution was achieved.

The other main problem is the selection of the learning rate. The algorithm, as presented in this research, uses a different learning rate for each frequency. Although the actual value of μ is not critical, it is more interesting to use a single value of μ for all frequencies. In order to do that, the transfer function of the plant at the assigned frequency must be either known or estimated online. This information could be used in several ways to improve the method's characteristics. Assuming that the plant's characteristics change slowly, this estimation does not need to use much computing power requirements, although the memory requirements will certainly increase appreciably.

Finally, the mathematical model could also be improved. The use of quaternions would make its computation faster and improve its usability. Static friction should also be included in the model of the accelerometers, which would provide more realistic simulations at lower frequencies.

LIST OF REFERENCES

[1] Kutrieb, J. and Ross, J., “Dynamics and Control of Smart Structures,” AA-4816 Final Project, Naval Postgraduate School, June 2001.

[2] Lebret, G., Liu, K., and Lewis, F. L., “Dynamic Analysis and Control of a Stewart Platform Manipulator,” *Journal of Robotic Systems,* Vol. 10, No. 5, 1993, pp. 629–655.

[3] Rahman, Z. H., Spanos, J. T., and Laskin, R. A., “Multi-Axis Vibration Isolation, Suppression and Steering System for Space Observational Applications,” *SPIE’s International Symposium on Astronomical Telescopes and Instrumentation,* Hawaii, March 1998.

[4] Edwards, S. G., *Active Narrowband Disturbance Rejection on an Ultra Quiet Platform,* Ph.D. Dissertation, Naval Postgraduate School, September 1999.

[5] Flint, E. M., *PHEX-1 (Type 1 Pointing Hexapod),* CSA Engineering, Inc., Mountain View, CA, 2000.

[6] STScI, prepared for NASA under Contract NAS5-26555, URL: http://hubble.stsci.edu/, last accessed July 2001.

[7] Stewart, D., “A Platform with Six Degrees of Freedom,” *The Institution of Mechanical Engineers*, Vol. 180, 1965-66, pp. 371–386.

[8] Wada, B. K., Rahman, Z., Kedikian, R., and Kuo, C.-P., “Vibration Isolation, Suppression and Steering (VISS),” *Journal of Intelligent Material, Systems and Structures*, Vol. 7, March 1996, pp. 241–245.

[9] Cobb, R. G. and Sullivan, J. M., "Vibration isolation and suppression system for precision payloads in space," *Smart Mater. Struct.*, Vol. 8, No. 6, 1999, pp. 798–812.

[10] Anderson, E. H. and et al., M. E. E., "Satellite Ultraquiet Isolation Technology Experiment (SUITE): Electromechanical Systems," *SPIE Conference on Industrial and Commercial Applications of Smart Structures Technologies*, Vol. 3674, Newport Beach, California, March 1999, pp. 308–328.

[11] Beavers, G. D., *System Identification of an Ultra-Quiet Vibration Isolation Platform*, Master's Thesis, Naval Postgraduate School, Monterey, CA, 1997.

[12] Ellliot, S. J., Stothers, I., and Nelson, P., "A Multiple Error LMS Algorithm and Its Application to the Active Control of Sound and Vibration," *IEEE Transactions on Acoustics, Speech, and Signal Processing*, No. 10, October 1987, pp. 1432–1434.

[13] Edwards, S. G., Agrawal, B. N., Phan, M. Q., and Longman, R. W., "Disturbance Identification and Rejection Experiments on an Ultra Quiet Platform," *Advances in the Astronautical Sciences*, Vol. 13, 2000.

[14] Chen, H.-J., Longnam, R. W., Agrawal, B. N., and Phan, M. P., "FFT-Based Clear-Box Disturbance Rejection on an Ultra Quiet Platform," *Proceedings of the* 10^{th} *AAS/AIAA Space Flight Mechanics Meeting*, Clearwater, Florida, January 2000.

[15] Chen, H.-J., *Multiple Periodic Disturbance Rejection Techniques for Vibration Isolation*, Ph.D. Dissertation, Columbia University, 2001.

[16] Flint, E., Flannery, P., Evert, M., and Anderson, E., "Cryocooler Disturbance Reduction with Single and Multiple Axis Active/Passive Vibration Control Systems," CSA, Inc. Personal communication. 2000.

[17] Kuo, S. M. and Morgan, D. R., “Review of DSP Algorithms for Acive Noise Control,” *Proceedings of the 2000 IEEE International Converence on Control Applications*, September 2000, pp. 243–248.

[18] Bertran, E. and Montoro, G., “Adaptive Suppression of Narrow-Band Vibrations,” 5^{th} *International Workshop on Advanced Motion Control*, June-July 1998, pp. 288–292.

[19] Kuo, S. M. and Ji, M. J., “Development and Analysis of an Adaptive Noise Equalizer,” *IEEE Transactions on Speech and Audio Processing*, Vol. 3, No. 3, May 1995, pp. 217–222.

[20] Li, D. and Salcudean, S. E., “Modeling, Simulation and Control of a Hidraulic Stewart Platform,” *Proceedings of the 1997 IEEE International Conference on Robotics and Automation*, April 1997, pp. 3360–3366.

[21] Fujimoto, K., Kinoshita, Y., and et al., K. M., “Derivation and Analysis of Equations for a 6-DOF Direct-Drive Wrist Joint,” *RSJ International Workshop on Inteligent Robots and Systems*, Osaka, Japan, Nov. 1991, pp. 779–784.

[22] Nguyen, C. C., Antrazi, S. S., and Zhou, Z.-L., “Adaptive Control of a Stewart Platform-Based Manipulator,” *Journal of Robotic Systems*, Vol. 10, No. 5, 1993, pp. 657–687.

[23] Fichter, E. F., “A Stewart Platform Based Manipulator: General Theory and Practical Construction,” *The International Journal of Robotics Research*, Vol. 5, No. 2, 1986, pp. 157–182.

[24] Liu, K., Fitzgerald, J., and Lewis, F. L., “Kinematic Analisys of a Stewart Platform Manipulator,” *IEEE Transactions on Industrial Electronics*, Vol. 40, No. 2, April 1993, pp. 282–293.

[25] Kosuge, K. and et al., M. O., “Input/Output Force Analysis of Stewart Platform Type of Manipulators,” *Proceedings of the 1993 IEEE/RSJ International Conference on Inteligent Robots and Systems*, July 1993, pp. 1666–1673.

[26] Stoughton, R. and Arai, T., “Optimal Sensor Placement for Forward Kinematics Evaluation of a 6-DOF Parallel Link Manipulator,” *IEEE/RSJ International Workshop on Intelligent Robots and Systems IROS’91,* November 1991, pp. 785–790.

[27] Geng, Z. J. and Haynes, L. S., “Six Degree-of-Freedom Active Vibration Control Using the Stewart Platforms,” *IEEE Transactions on Control Systems Technology*, Vol. 2, No. 1, March 1994, pp. 45–53.

[28] Leonard, B. S., “Spacecraft Attitude Determination & Control Notes (AA3818),” Course Notes. Naval Postgraduate School, Fall 1999.

[29] Haykin, S., *Adapter Filter Theory*, Prentice-Hall, Inc., 3^{rd} ed., 1996.

[30] Widrow, B., Shur, D., and Shaffer, S., “On Adaptive Inverse Control,” *Proc. 15^{th} Asilomar Conference*, 1981.

[31] Burguess, J. C., “Active Adaptive Sound Control in a Duct: A computer Simulation,” *J. Acoust. Soc. Am.*, September 1981, pp. 715–726.

[32] Rahman, Z., Spanos, J., and Laskin, R., “A Six Axis Vibration Isolation, Supression and Steering System for Space Applications,” *AIAA* 35^{th} *Aerospace Sciences Meeting & Exibit*, January 1997.

[33] Tsuei, T. G., Srinivasa, A., and Kuo, S. M., “An Adapive Feedback Active Noise System,” *Proceedings of the 2000 IEEE International Conference on Control Applications*, Septermber 2000, pp. 249–254.

[34] Huang, T. and Agrawal, B. N., “Neural Network Attitude Control of Flexible Spacecraft,” 49^{th} *International Astronautical Congress - Melbourne, Australia*, edited by I. A. Federation, Sept 28-Oct 2 1998.

[35] Hahn, W., *Stability of Motion,* Springer-Verlag, 1967.

[36] Isidori, A., *Nonlinear Control Systems,* Springer-Verlang, New York, 3^{rd} ed., 1995.

[37] Khalil, H. K., *Nonlinear Systems,* Prentice-Hall, 2nd ed., 1996.

[38] Narendra, K. S. and Taylor—, J., *Frequency Domain Methods for Absolute Stability,* Academic Press, 1973.

[39] Slotline, J.-J. E. and Li, W., *Applied Nonlinear Control*, Prentice Hall, 1991.

[40] Geng, Z. and Haynes, L. S., "Six-Degree-of-Freedom Active Vibration Isolation Using a Stewart Platform Mechanism," *Journal of Robotic Systems,* Vol. 10, No. 5, 1993, pp. 725–744.

[41] Bessala, J., Bidaud, P., and Ouezdou, F. B., "Analytical Study of Stewart Platforms Workspaces," *Proceedings of the 1996 IEEE International Conference on Robotics and Automation,* April 1996, pp. 3179–3184.

[42] Kank, J.-Y., Kim, D. H., and Lee, K.-I., "Robust Tracking Control of Stewart Platform," *IEEE Proceedings of the 35^{th} Conference on Decision and Control*, December 1996, pp. 3014–3019.

[43] Dutré, S., Bruyninkx, H., and Schutter, J. D., "The Analytical Jacobian and Its Derivative for a Parallel Manipulator," *Proceedings of the 1997 IEEE International Conference on Robotics and Automation,* April 1997, pp. 2961–2966.

[44] Widrow, B. and Stearns, S. D., *Adaptive Signal Processing,* Prentice-Hall, 1985.

[45] Kuo, B. C., *Automatic Control Systems,* Prentice Hall, 7th ed., 1995.

[46] Agrawal, B. N. and Chen, H.-J., "Active Isolation on Spacecraft Using Smart Struts," 51^{th} *International Astronautical Congress,* AIAA, Rio de Janeiro, Brazil, October 2000.

[47] Sullivan, J., Rahman, Z., Cobb, R., and Spanos, J., “Closed-loop Performance of a Vibration Isolation and Suppression System,” *Proceedings of the American Control Conference*, June 1997, pp. 3974–3978.

[48] McInroy, J. E., Neat, G. W., and O’Brien, J. F., “A Robotic Approach to Fault-Tolerant, Precision Pointing,” *IEEE Robotics & Automation Magazine*, December 1999, pp. 24–37.

[49] Wertz, J. R., editor, *Spacecraft Attitude Determination and Control*, Kluwer Academic Publishers, 1978.

[50] Lee, J. D. and Geng, Z., “Modelling and Control of Flexible Stewart Platform,” *Proceedings of the 12th International Federation on Automatic Control (IFAC) World Congress*, July 1993, pp. 145–148.

[51] Liu, K., Lebret, G., Lowe, J. A., and Lewis, F. L., “Control of a Stewart-Platform Based Robotic Milling Cell,” *Advanced Control Issues for Robot Manipulators*, Vol. 39, 1992, pp. 23–30.

[52] Oppenheim, A. V. and Schafer, R. W., *Discrete-Time Signal Processing*, Prentice Hall, 1999.

[53] Anderson, B. D. O. and Moore, J. B., *Optimal Control—Linear Quadratic Methods*, Prentice Hall Information and Science Series, Prentice Hall, 1990.

[54] Lewis, F. L., *Optimal Control*, John Wiley & Sons, 1986.

[55] Bertsekas, D. P., *Stochastic Optimal Control: The Discrete Time Case*, Academic Press, Inc., 1978.

[56] Miller, K. B., *Design of Robust Suboptimal Controllers for a Generalized Quadratic Criterion*, Master’s Thesis, Naval Postgraduate School, Monterey, CA, June 1992.

[57] CSA Engineering, Inc., URL: http://www.csaengineering.com. Last accessed August, 2000.

[58] Kienholz, D. A., "Active Alignment and Vibration Control System for a Large Airborne Optical System," CSA, Inc. 2000.

[59] Goodzeit, N. E., Raman, K. V., Paluszwek, M. A., and Waller, E. V., "Spacecraft Roll-Yaw Compensator with Orbit and Harmonic and Bandpass Filters," U.S. Patent 5,343,398, 1994.

[60] Gupta, N. K., "Frequency-Shaped Cost Functionals: Extensions of Linear Quadratic Gaussian Methods," *Journal of Guidance, Control and Dynamics*, Vol. 3, No. 6, 1980, pp. 529–535.

[61] Ljung, L. and Sordetron, T., *Theory and Practice of System Identification*, The MIT Press, 1983.

[62] Astrom, K. J. and Eykhoff, P., "System Identification — A Survey," *Automatica*, Vol. 7, 1971, pp. 127–162.

[63] Tsypkins, Y. Z., Mason, J. D., and Warkick, K., "Identification of Linear Systems in the Presence of Piecewise Polynomial Distrubances," *IEEE Proceedings: Control Theory and Applications*, Vol. 143, July 1996, pp. 305–308.

[64] Jonhson, C. D., "A Discrete-Time, Disturbance Accomodating Control Theory for Digital Control of Dyamical Systems," *Control and Dynamic Systems: Advances in Theory and Applications*, Vol. 18, 1982, pp. 223–315.

THIS PAGE INTENTIONALLY LEFT BLANK

INITIAL DISTRIBUTION LIST

1. Defense Technical Information Center

   Fort Belvoir, Virginia

2. Dudley Knox Library

   Naval Postgraduate School

   Monterey, California

3. CTA/IAE/ASB

   Sao Jose dos Campos - SP

   Brazil

   silvino@iae.cta.br

4. CTA/ITA - Biblioteca

   São José dos Campos - SP

   Brazil

   iab@bibl.ita.cta.br

5. Professor Brij N. Agrawal

   Mail Code: AA/Ag

   Dept. of Aeronautics and Astronautics

   Naval Postgraduate School

   Monterey, CA 93943

   agrawal@aa.nps.navy.mil

6. Associate Professor Roberto Cristi

Mail Code: EC/Cx

Dept. of Electrical and Computer Engineering

Naval Postgraduate School

Monterey, CA 93943

cristi@nps.navy.mil

7. Associate Professor Monique P. Fargues

   Mail Code: EC/Fa

   Dept. of Electrical & Computer Engineering

   Naval Postgraduate School

   Monterey, CA 93943

   fargues@nps.navy.mil

8. Associate Professor Man-Tak Shing

   Mail Code: CS/Sh

   Dept. of Computer Science

   Naval Postgraduate School

   Monterey, CA 93943

   shing@cs.nps.navy.mil

9. Professor Xiaoping Yun

   Mail Code: EC/Yx

   Dept. of Electrical & Computer Engineering

   Naval Postgraduate School

   Monterey, CA 93943

   yun@nps.navy.mil

10. Jeffrey B. Knorr

Professor and Chairman

Department of Electrical and Computer Engineering

Naval Postgraduate School

Monterey, CA 93943-5121

jknorr@nps.navy.mil

11. CSA Engineering, Inc.

Mountain View, CA

eric.flint@csaengineering.com